UNIVERSITY OF CAPE TOWN
IYUNIVESITHI YASEKAPA • UNIVERSITEIT VAN KAAPSTAD

BEHAVIOR OF RC BEAMS PATCH REPAIRED AND STRENGTHENED WITH FRP COMPOSITES:

A NUMERICAL STUDY

By

Salathiel MUNDELI

Submitted in partial fulfillment of the requirements for the degree of

Master of Science in Civil Engineering

DEPARTMENT OF CIVIL ENGINEERING

FACULTY OF ENGINEERING AND THE BUILT ENVIRONMENT

Supervisor: Prof. Pilate MOYO

May, 2014

DECLARATION

I know the meaning of plagiarism and declare that all the work in the document, save for that which is properly acknowledged, is my own. It is being submitted for the degree of Master of Science in Civil Engineering in the University of Cape Town, South Africa. I also confirm that no part of this work has been submitted to any university or other academic institutions for the award of any degree.

Signed by candidate

Salathiel MUNDELI

Date: 2/05/2014

Abstract

Reinforced concrete (RC) beams get deteriorated and become deficient mainly due to corrosion of steel reinforcements, poor maintenance and design, earthquakes and aging. Patch repair and structural strengthening using fiber reinforced polymers (FRP) have been increasingly adopted all over the world as an economical solution to upgrade the load carrying capacity of such beams. However, the failure modes of such repaired and strengthened RC beams are governed by brittle and sudden premature debonding which involves separation of external reinforcement; i.e. FRP and RC beam. Different researchers have used different approaches including experimental, analytical and numerical to investigate the behavior of patch repaired and FRP strengthened RC beams. It is noteworthy that there are no such numerical studies that investigated the effect of patch repair.

In this study, a numerical investigation was carried out using the commercial finite elements analysis software ABAQUS with the aim of investigating the overall behavior of RC beams patch repaired and strengthened with FRP plates including the failure mechanisms. One control RC beam and four patch repaired and FRP strengthened RC beams with varying degrees of damage were investigated. In this respect, the length of the patch material was 450, 800, 1300 and 1800mm. All beams were rectangular in cross section. Furthermore, corrosion was simulated by reducing tensile steel cross section by 10% over the length of the patch. To describe the behavior of such RC beams, different material models were used. Concrete damaged plasticity model was used for both concrete and repair material; a linear elastic perfectly plastic model was used for both longitudinal and transversal reinforcing steel while a linear elastic isotropic model was used for FRP material. The interface between concrete and FRP was modeled using a cohesive bond model.

Results from numerical investigations show that the proposed FE model is able to describe the overall behavior of reinforced concrete beams patch repaired and strengthened with FRP in terms of crack pattern, load deflection curves, yielding of steel and failure mechanisms as compared to experimental findings obtained from the same specimens. The mode of failure was intermediate crack induced debonding that was initiated at critical cracks under the loading points and propagated towards the plate ends. In addition to that, increasing the patch length increased the energy required for overall damage.

Generally, results show that numerical approach can be used to investigate deeply the behavior of RC beams patch repaired and strengthened with FRP strips. It was also observed that the approach is able to capture parameters such as damage energy and strain distribution in FRP, which are not easily captured experimentally or analytically.

DEDICATION

To Almighty God

To my parents, brothers and sisters

ACKNOWLEDGEMENT

I would like to extend my appreciation and sincere gratitude to my supervisor Professor Pilate MOYO for his kind guidance and positive criticisms throughout this work. Without his devotion, this research would not have come to its end. I would also like to thank the Concrete Materials and Structural Integrity Research Unit (CoMSIRU) for providing necessary equipment.

The author would like to extend his special thanks to the Government of Rwanda for providing the necessary financial support through Rwanda Education Board (REB) for his master‟s studies at the University of Cape Town. The financial support is highly acknowledged. I also thank the management of Kigali Institute of Science and Technology (KIST) for allowing me to pursue my postgraduate studies and for their follow up of my studies.

My thanks also go to Mrs. Elly Yelverton for her motherly welcome when I arrived at UCT.

I would like to thank Mr. Hellmut and Dr. Greg Mitchel from the Finite Elements Analysis Services (FEAS) for their assistance in using ABAQUS software. I also thank Mr. Matongo KABANI, a PhD student for his assistance in reviewing my work and making corrections.

Lastly, I would like to thank my fellow students in CoMSIRU for being brothers and sisters. God bless you all.

Contents

List of Figures

List of Tables

Chapter 1

INTRODUCTION

1.1. Background

Reinforced concrete (RC) structures are commonly used around the world in civil infrastructures such as highway bridges, tall buildings, marine structures, stadiums; due to their ability to resist flexure, vibrations, high temperatures, corrosion if well protected and their reduced cost of maintenance. However, these structures deteriorate with time and lose their load carrying capacities and durability due to a number of reasons. Some of the causes of such losses include aging, overloading, corrosion of steel reinforcement, errors during design and construction stages, inadequate selection of materials, poor maintenance and natural disasters such as earthquakes. The corrosion of reinforcing steel in concrete is a major problem facing civil engineers and surveyors today as they maintain aging reinforced concrete structures in general (Broomfield, 2003:1). Corrosion results in steel cross section reduction and hence loss of strength.

The upgrade of load carrying capacity and life extension of deteriorated reinforced concrete structures may be achieved via appropriate repair and strengthening techniques. Traditionally, different methods of strengthening with different degrees of success have been used to upgrade the load carrying capacity of reinforced concrete structures. They include among others bonding of steel plates, external post-tensioned cables bonded to the tension face, cross section enlargement, addition of new steel members and reduction of span length with steel bonding being mostly used (Supaviriyakit *et al.* 2004) and more recently the use of Fiber Reinforced Polymer (FRP) composites. Lee and Hausmann (2004) reported some drawbacks associated with bonding steel plates to existing reinforced concrete structures such as higher cost of installation, increased weight of the structure and corrosion of the plate that could adversely affect the bond strength between the plate and the concrete and consequently reduce the effectiveness of the strengthened member.

Owing to the disadvantages of the use of steel plates for strengthening of RC structures, fiber reinforced polymer composites (FRP) have been used increasingly in the last decades. The FRP composites used in RC strengthening are made up of matrix and fibers that may be unidirectional

or multidirectional. The fibers are embedded in a matrix that protect them against environmental attacks and ensures stress transfer. Polyester, vinylester and epoxy are the most commonly used polymeric materials used with high performance reinforcing fibres (Taljsten, 2006).

The advantages of FRPs include high strength, low weight, high durability, versatility, and ease of installation (Rabinovitch, 2008). FRP composites of different types can be bonded to structures by means of the adhesives as shown in Figure 1.1 to form a composite on the existing structure.

Figure 1.1: Typical application of FRP plates on RC beam (Motavalli & Czaderski, 2007)

They can be used to strengthen different RC structural elements including beams, slabs, columns, and walls to improve their stiffness and their response to static and dynamic loadings. FRP composites may be used in the form of plates, sheets and rods. Even though bonding FRPs to RC structures improves their load carrying capacity, strengthened RC beams are prone to different types of failure some of which are common to all reinforced concrete beams, others being special to FRP strengthened RC concrete structures.

Since the advent of FRP composites usage in construction industry and particularly in strengthening of civil infrastructures, intensive studies including experimental, analytical and numerical; have been carried out to understand the behavior of reinforced concrete beams that are strengthened with such composites.

Au & Büyüköztürk (2006) reported five possible modes of failures of FRP strengthened RC structures, three of which are related to decohesion in different materials making up the system and two interface separations between FRP and concrete or between adhesive and concrete substrate as shown in 1.2. It should be noted that special failures associated with FRP strengthened reinforced concrete beams which involve loss of composite action are brittle as opposed to failure of conventional RC beams, which in most cases are ductile depending on the design.

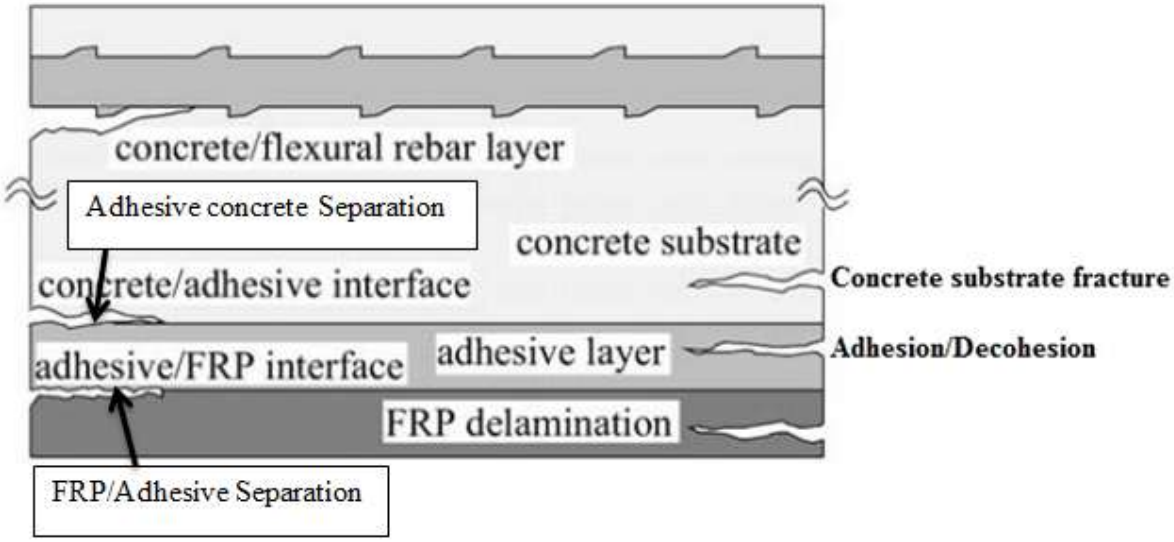

Figure 1.2: Failure modes in FRP strengthened RC beams.

In addition to failure modes shown in Figure 1.2, FRP strengthened RC beams may fail by concrete crushing before yielding of the reinforcing steel, steel yielding followed by FRP rupture, steel yielding followed by concrete crushing and shear failure. Except FRP rupture, other modes of failure stated above may also be found in conventional reinforced concrete beams. The particular premature mode of failure associated with FRP strengthened beams is called debonding. Debonding may initiate at flexural or flexural-shear crack in the high moment region and propagates towards one of the plate ends inducing the so called intermediate crack induced debonding as reported by Yao & Teng (2007) in their experimental work.

The authors also reported that debonding may also occur at or near the plate end due to critical diagonal crack or due to plate cut-off.

Debonding failure whether it is intermediate crack induced or triggered at the plate end, prevents the FRP to be fully utilized and thus reduce the effectiveness of structural strengthening.

Several other researchers conducted experimental investigations to study the behavior, modes of failure and ultimate load carrying capacity of strengthened RC beams and hence to develop design guidelines and models to predict the premature failure of debonding (Matthys, 2000; Obaidat *et al*, 2010 and Camata *et al*. 2006). In their studies, they found that debonding was intermediate crack induced.

Besides experimental studies, analytical studies based on strength of materials to determine the shear and normal interfacial stress concentration and hence compare the principle stress to that of the weakest material to predict the debonding load have also been done by different researchers. (Roberts, 1988; Malek *et al*. 1998; and Smith & Teng, 2001). Fracture mechanics that is based on energy approach has also been used by different researchers (Au & Büyüköztürk, 2006; Rabinovitch & Frosting, 2001 and Günes *et al*. 2009). In this approach a comparison between the energy required to create new surfaces and the toughness of the material or interface is done to predict crack growth and hence failure.

With the development in computer technology and in the use of finite element methods to solve complex engineering problems, numerical approaches have also been used in discretizing and analyzing reinforced concrete beams strengthened with FRP composites. The general procedure in numerical studies is to select appropriate material constitutive models and analysis procedures. Strengthened reinforced concrete beams can be analyzed in both 2D and 3D spaces. Numerical approaches also consider that debonding is largely influenced by concrete cracking. There are two approaches in modeling the cracking behavior of concrete: smeared crack approach and discrete crack approach. The smeared crack approach treats cracked concrete as a continuum and captures the deterioration process of cracked concrete using constitutive relationship and hence smears the crack over the continuum whereas discrete crack approach considers cracking in concrete as geometrical discontinuity and thus it is physically modeled (Chen *et al*. 2011). Modeling concrete using one of the above approaches and choosing proper constitutive relationships for interfaces and for other materials like steel and FRP has proven to be a powerful method in investigating the ultimate load capacity and modes of failure of reinforced concrete beams strengthened with fiber-reinforced polymers (FRP).

In this regard, a number of studies have been reported in the literature (Lu *et al*. 2007; Rami *et al*. 2012; Obaidat *et al*. 2010, Baldvin, 2011 and Niu & Wu, 2005).

It should be noted that, despite the fact that a lot of experimental and analytical works have been done on the behavior of reinforced concrete beams strengthened with FRP composites, few studies have considered the effect of the patch repair.

Repair consists of removing damaged concrete and replacing it with new layer, this situation was not considered in the numerical investigations. Mojabeng (2010) carried out experimental studies on reinforced concrete beams patch repaired and strengthened with carbon fiber reinforced polymers (CFRP). The author found that patch repairs and CFRP strengthening have a positive effect on the structural capabilities of improving the load carrying capacity of the reinforced concrete beams, reinstating durability and protecting reinforcement from corrosion.

While experimental studies have been done on patch repaired and FRP strengthened reinforced concrete beams (Mojabeng, 2010; Malumbela, 2010; Rio et al. 2005), no numerical studies on patch repaired and FRP strengthened RC beams; to the author‟s knowledge; have been reported yet. Practically, before the application of FRP, the damaged concrete has to be removed and replaced by a repair material, which often has a higher strength than the existing concrete. Thus, for a close up analysis of such situation a numerical study is necessary. This gap pushed the author to undertake a numerical study to investigate the behavior of reinforced concrete beams patch-repaired and strengthened with FRP laminates.

1.2. Objectives of the project

1.2.1. Main objective

The main objective of this research is to investigate numerically the behavior of reinforced concrete beams patch repaired and strengthened with carbon fiber reinforced polymers (CFRP) plates. The focus of the research is to develop a finite element model that will be used to investigate the effect of repair mortar and the application of the CFRP on the ultimate load capacity and modes of failure for reinforced concrete beams that are damaged due to corrosion. Since premature debonding failure is the main failure and is caused by cracks which propagate horizontally in concrete, cracking must be investigated closely to assess its effect on overall failure of the beams.

1.2.2. Specific objectives

i) Develop a finite element model to study the effect of patch repairs on the flexural behavior and failure mechanisms of FRP-strengthened RC beams by varying in length the damaged area.

ii) To simulate corrosion of reinforcement by reducing the cross sectional area of steel reinforcement in the damaged area and investigate the effect of corrosion on the flexural behavior and ultimate moment capacity of reinforced concrete beams.

iii) Compare the results from numerical modeling with experimental findings on the same beams for validation. Key points to consider are the modes of failure, load deflection relations, crack pattern and ultimate loads.

1.3. Scope of the project

The current research project is limited on the numerical study of reinforced concrete beams patch repaired and strengthened with CFRP plates. The study doesn‟t consider any other structural elements such as columns, slabs, etc. The investigated beams are rectangular in cross section. Strengthening is done using one plate bonded at the bottom of the beam and in the middle of the width. The commercial finite element analysis software ABAQUS will be used to develop finite element models for reinforced concrete beams and for their analysis. The beam is shown in Figure 1.3.1. 3D modeling space will be used. Each material involved will be modeled using appropriate constitutive models. The only interface considered is that between concrete and CFRP. Full bond is assumed between concrete and steel reinforcement and perfect bond between concrete and patch repair is also assumed.

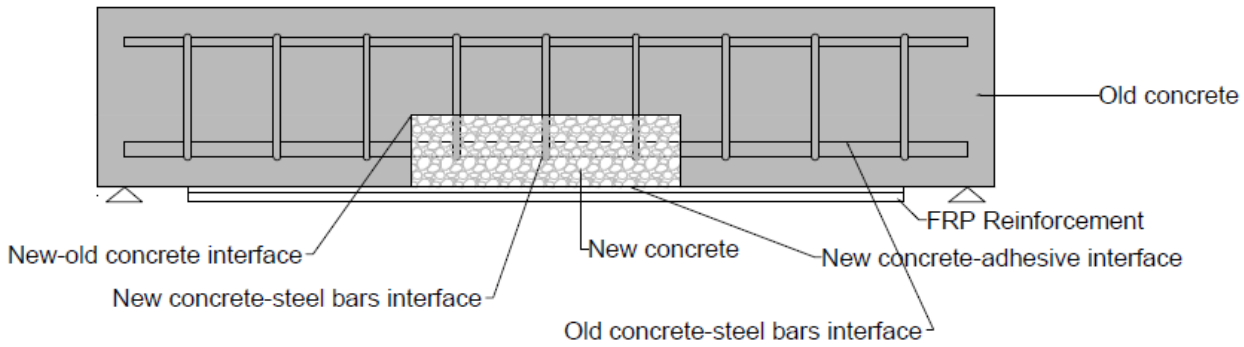

Fig.1.3: Repaired and CFRP strengthened reinforced concrete beam.

1.4. Outline of Thesis

This thesis consists of six chapters:

Chapter one gives the general background to the research by addressing the problem, research objectives and scope.

Chapter two reviews the repair and strengthening of reinforced concrete beams, modes of failure, failure prediction approaches and models.

Chapter three describes the numerical modeling of reinforced concrete beams focusing on the behavior of materials involved and constitutive models used for numerical investigations. Previous studies on modeling RC beams will be reviewed.

Different approaches used to model the behavior of concrete, steel, CFRP and epoxy/interface will be discussed. A choice of appropriate modeling procedures that will be used for patch repaired and CFRP strengthened RC beams will be done for each material involved.

Chapter four presents the procedures followed for the development of the finite element model of reinforced concrete beams patch repaired and strengthened with CFRP plates in Abaqus software. Base features, element types for different materials, assembly of different parts, boundary conditions and interactions are described in details.

Chapter five presents the results of modeling work, comparison with experimental findings along with discussion of results.

Chapter six summarizes the work, draws conclusions and gives recommendations for future work.

Chapter 2

LITERATURE REVIEW

2.1. Introduction

Although hundreds of thousands of successful reinforced concrete structures are annually constructed worldwide, there are large numbers of concrete structures that deteriorate or become unsafe due to inadequacy of design detailing, construction and lack of adequate maintenance, overloading, chemical attacks, corrosion of rebar, foundation settlement, abrasion, fatigue effects, atmospheric effects, changes in use, changes in configuration, and natural disasters such as earthquake (Jumaat *et al. 2006*). The serviceability and durability then become compromised. Therefore, it is necessary to keep these structures serviceable. Even though complete replacement of deteriorated or damaged structures may be an option, repair and strengthening is often a more economic choice. However, it is also a challenging and expensive task, which usually does not receive proper attention it deserves due to different reasons such as budgetary constraints, political decisions, insufficient knowledge and neglect (Gunes, 2004).

While different methods of repair and strengthening are available, patch repair and fiber reinforced polymers strengthening are increasingly used all over the world for retrofitting of deficient reinforced concrete structures. However, there are premature debonding failures that are associated with FRP strengthened RC beams and which prevent the full utilization of this technique previously used in aerospace industry. Several experimental and theoretical studies have been done to study the behavior predict the failure loads and hence keep the structures safe and serviceable. This chapter discusses the principles of patch repair, structural strengthening, modes of failure of FRP strengthened RC beams and failure prediction approaches.

2.2. Repair and strengthening of reinforced concrete structures

2.2.1. Repair of concrete structures

Concrete repair is not a “band-aid” to a structure in trouble; it is a complex engineering task (Vaysburd, 2006). Currently, the dominant cause of reinforced concrete deterioration is corrosion of reinforcing bars.

Corrosion is caused by carbon dioxide and chloride ions entering in concrete and damaging the passive layer that protects steel reinforcement through concrete alkalinity reduction or just breaking down the layer. Carbon dioxide comes from the atmosphere and in presence of moisture it forms carbonic acid, which reduces the alkalinity of concrete, and hence the protection of concrete to steel bars and when there is enough oxygen and moisture corrosion will initiate.

Chloride induced corrosion is due to chloride ions from sea water and de-icing salts that penetrate the concrete cover and breakdown the protective oxide layer around steel reinforcement, thus depassivating the steel and permitting corrosion and reduce its alkalinity and hence its protection to steel (Jumaat *et al. 2006*).

Corrosion results in cracking and concrete spalling. One method of restoring the integrity of damaged concrete structures is to repair locally the damaged areas by replacing the weak concrete with one of a wide range of repair material materials. This process is known as patch repair. The durability of repair greatly depends on both its adherence to the substrate concrete and the protection it can provide to the steel reinforcement against corrosion (Nounu and Chauhdary, 1999). Therefore, it must have physical and chemical properties which are compatible with the substrate concrete, design and the use of the structure to which it are applied.

Compatibility in concrete repair systems refers to a balance of physical, chemical, and electromechanical properties and deformation between the repair and substrate that ensures the system as a whole withstands stresses induced by restrained volume changes, chemical and electrochemical effects without premature deterioration or distress over a design period of time (Vaysburd, 2006). Poor compatibility may result in shrinkage of the patch repair as a result of moisture loss which builds-up of stresses in both repair and the concrete substrate (Mojabeng, 2010). The main failure modes in concrete patch repair have been identified by Rahman *et al*. (2000) as tensile cracking through the thickness of the patch layer, shearing of the substrate concrete below the interface of the repair and the substrate concrete and finally as peeling failure of interface between repair layer and substrate concrete due to transverse tension. Adequate preparation of the concrete substrate is therefore important for the achievement of a durable repair. Thus, the damaged concrete must be saw cut and removed.

The damaged concrete should be cut according to figure 2.1 (C & CI) to avoid cuts meeting at acute angles. The surface must be cleaned properly prior to patch application to ensure good adhesion of the repair material.

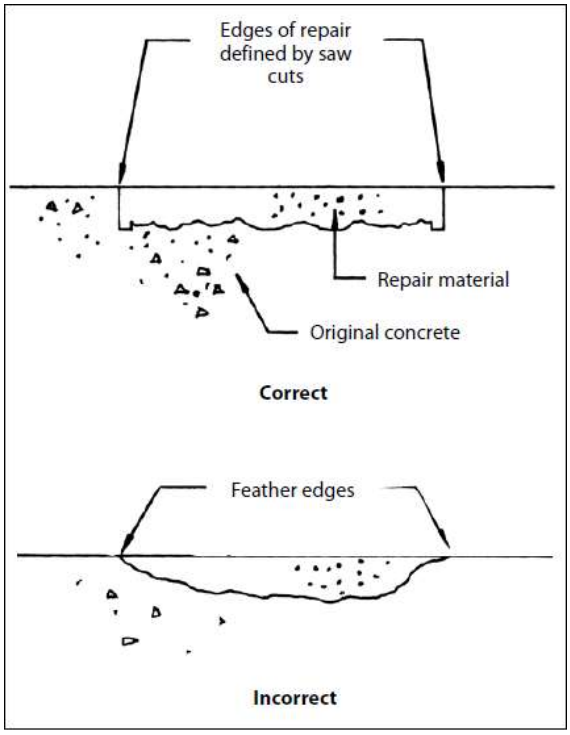

Figure 2.1: Substrate preparation for repair application.

In terms of repair material applications, the US Bureau of reclamation (1997) suggests that hand applied mortar or concrete should be used for patching of relatively small and isolated areas and for a depth of repair that exceeds 150mm. It should be noted that a bonding agent has to be applied after surface preparation and before the application of the repair material to improve its cohesion with concrete substrate. Repair may also be done using shortcreting where concrete or mortar is applied with high speed.

2.2.2. Structural strengthening of reinforced concrete structures.

In actual life of concrete structures, there are different situation in which they need to be strengthened. They may include seismic retrofit to satisfy current code requirements, upgraded loading requirements; damage caused by accidents and environmental conditions, initial design flaws and change of use (Motavalli & Czaderski, 2007).

The strengthening or retrofitting of existing reinforced concrete structures to resist higher design loads, correct deterioration related-damage or increase ductility and stiffness has traditionally been accomplished using conventional materials and construction techniques and include externally bonded steel plates and external post-tensioning on horizontal members such as beams and slabs and steel or concrete jackets on vertical structural members such as columns, figures 2.2 and 2.3.

(a) (b)

Figure 2.2: Traditional methods of strengthening: (a) concrete jacket, (b) steel plate bonding. (Y. Chhabra, 2013).

Composite materials made of fibers in a polymeric resin also known as fiber reinforced polymers (FRP) have emerged as an alternative to traditional materials and techniques due to their lightweight and noncorrosive properties, in addition to their availability in different forms ranging from factory-made laminates to dry fiber sheets that can be wrapped to conform to the geometry of a structure (ACI 440.2R-02). They also exhibit high tensile strength. According to Motavalli and Czaderski (2007), the overall cost of the whole strengthening job using FRP materials can be as competitive as using conventional materials, in addition to being quick and easy to handle on site with minimum interruption to use of facility.

FRP materials are used for strengthening of different structural component as shown on figure 2.3 in which the additional material in black represents the FRP composites.

This research covers only strengthening for bending using laminates. The laminate system consists of a flat plate with a typical size of 1.2 x100mm and is most suitable for flat surfaces such as beams, walls and slabs (Taljsten, 2006).

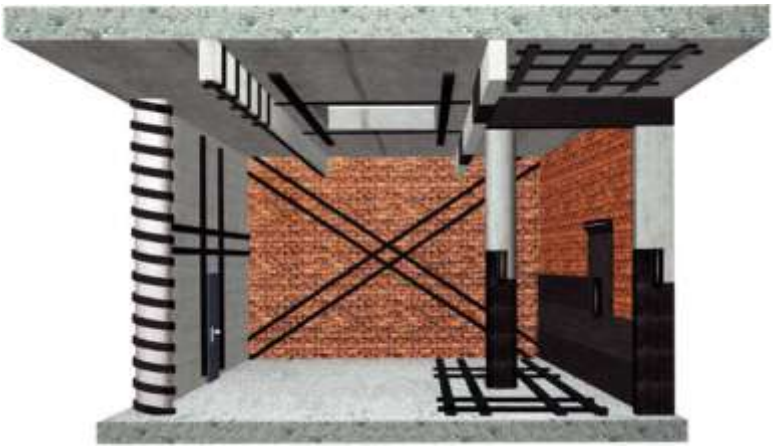

Figure 2.3: Typical structural elements strengthened with FRP materials (Sika)

As for the application of repair material, it is necessary to prepare either mechanically or chemically the concrete substrate before the application of the primer or epoxy followed by FRP plate. Improper preparation can result in delamination of the plate before it achieves its intended use of transferring stresses. The epoxy is the matrix creating a strong bond but also subjecting the fibers to debonding stresses with uneven concrete surface (Buyokozturk and Hearing, 1999). For this reason, ACI 440.2R-02 recommends that the concrete or the repaired surface to which FRP system is to be applied should be freshly exposed and free of loose or unsound materials.

2.3. Modes of failure of strengthened RC beams

The use of FRP in structural strengthening is a recognized all over the world as a potential solution. However, there are design problems that need to be addressed. From structural mechanics point of view, an important concern regarding the effectiveness and safety of this method is the potential of brittle debonding failures (Gunes, 2004). Failure of FRP strengthened concrete beams can take place through several mechanisms depending on the beam geometry and strengthening parameters as have been observed by different researchers in their

experimental observations; (Buyukozturk et al. 2004; Camata et al. 2004; Teng & Chen, 2009; Gao et al. 2004; Yao & Teng, 2007).

It should be noted from extensive experimental studies done that, some failure modes are similar to what can happen in conventional beams i.e. unstrengthened RC beams. These failure modes include concrete crushing in the compression zone and shear failure according to Camata et al. (2004) and they can be easily predicted using current design code. It is worth to note that a common point to all researchers is that debonding failure initiates from flexural or flexural shear crack which propagates horizontally towards the end of the FRP ends and trigger separation of the FRP from the concrete substrate. This separation most often takes place in the concrete cover.

Debonding may also initiate from the FRP end due to high stress concentration at that location. Generally, for flexurally strengthened beams, Teng and Chen (2009) classified the failure modes into flexural failure when the composite action between the bonded plate and the RC beam is maintained up to failure, figure 2.4, and into debonding failure which involves loss of composite action and generally occur in the concrete.

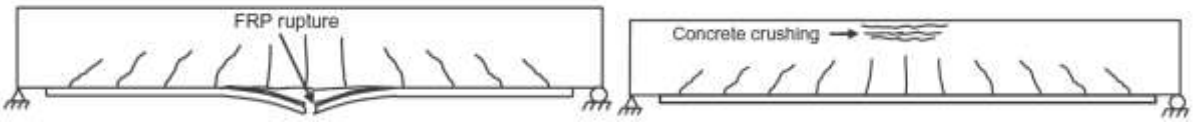

Figure 2.4: Conventional flexural failure modes for FRP strengthened RC beams

Another type of failure reported by Teng and Chen (2009) is intermediate crack induced debonding. In their investigations they found that this type of failure is caused by large local strain at the location of the flexural or shear crack which causes local debonding to be formed and the tensile force that is released by the cracked concrete creates high stress concentration when it is being transferred to FRP and to steel reinforcement. This causes the debonding to propagate to the nearer end and hence induce complete separation. This mode of failure is shown in figure 2.5.

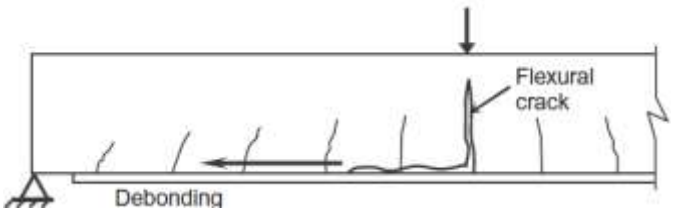

Figure 2.5: Intermediate crack induced debonding

Gao *et al*. (2004) and Teng and Chen (2009) reported another type of debonding failure which is frequently encountered in FRP strengthened beams which is called concrete cover separation. This failure is due to a crack forming near the plate end due to stress concentration and then propagating horizontally at the level of reinforcement resulting in the separation of the concrete cover. The intermediate crack induced debonding failure is believed to be particularly important for relatively slender members and members strengthened with relatively thin FRP plate or sheet and is attracting increasing attention as an important mode of failure (Teng *et al*. 2003). Different modes of concrete cover separation are shown on figure 2.6 below.

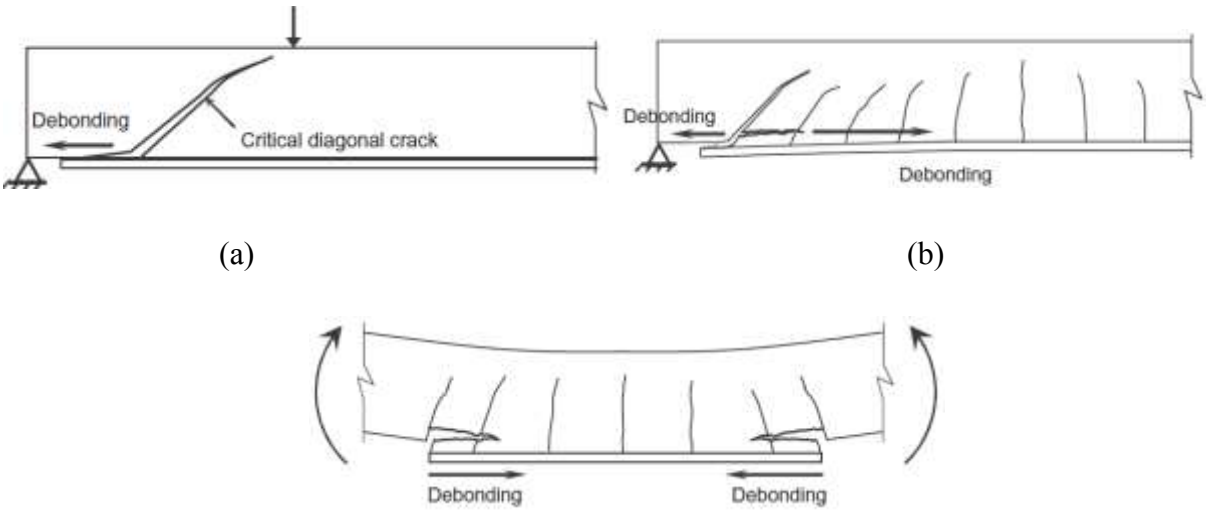

Figure 2.6: Concrete cover separation: (a) critical diagonal crack debonding, (b) concrete cover separation, (c) concrete cover separation under pure bending.

The effective use of FRP in structural strengthening of reinforced concrete beams will not be achieved unless good understanding of the behavior and failure mechanisms are put in place.

It must be noted that debonding failure may also be influenced by poor workmanship and use of inferior adhesive in addition to small unevenness of the concrete substrate that may cause localized debonding of the FRP (Teng and Chen, 2009). Such failures must be adequately considered in the design process; otherwise they may reduce significantly the effectiveness of strengthening (Buyukozturk *et al*., 2004).

2.4. Debonding failure prediction

Reinforced concrete structures that are subjected to external loads tend to fail under the action of these loads. If they are not completely collapsed they can be repaired and strengthened to extend their life service. However, their performance is mainly governed by the bond mechanism between concrete and external reinforcement. Many researchers have reported premature debonding as the main failure of FRP strengthened RC beams. Thus, it is of good practice to limit the applied load to avoid such premature failure associated with strengthened structures and predict when debonding will take place. Debonding like any other failure mode is related to the performance of materials working together with FRP. Over the last decades, several researches have been done in an effort of understanding the causes and mechanisms of debonding failures through theoretical, experimental and numerical approaches (Buyokoztruk & Yang, 2006). (Buyokoztruk & Yang, 2006) further classified debonding prediction approaches into strength of materials and fracture mechanics in addition to semi-empirical and empirical relationship established to predict the debonding failure.

Empirical and semi-empirical models are relatively simple models that do not require complex stress and fracture analyses and may be elaborated from experimental observations. They can be easily implemented in design calculations. However, empirical and semi-empirical are limited by the experimental set up and loading arrangement used during their development. Strength of materials and fracture mechanics approaches are critically discussed in the following sections.

2.4.1. Strength of materials approach

Prediction of debonding failures through strength of material approach involves determination of the interfacial or bond stress distribution in FRP strengthened members based on properties of the material making up the system. Calculated stresses, i.e. normal and shear are compared to the

ultimate strength of materials and interface to predict the mechanisms and load level of debonding failure (Buyukozturk et al, 2004). All materials are assumed linear elastic, perfect bond between concrete and FRP and linear strain distribution assumptions are made although concrete cracking is considered (Buyukozturk et al, 2004). Figure 2.7 shows the distribution of interfacial stresses around the cracks and at the FRP plate end.

The figure also shows the variation of both interfacial shear and normal stress over the bond length. It is useful to note that cracks and FRP plate end introduce material and geometrical discontinuities respectively. Those discontinuities are the source of stress concentrations as illustrated in figure 2.7.

When interfacial shear and normal stress across the adhesive are assumed to be constant approximate solutions are obtained and higher order solutions are obtained when interfacial stresses vary across the adhesive layer.

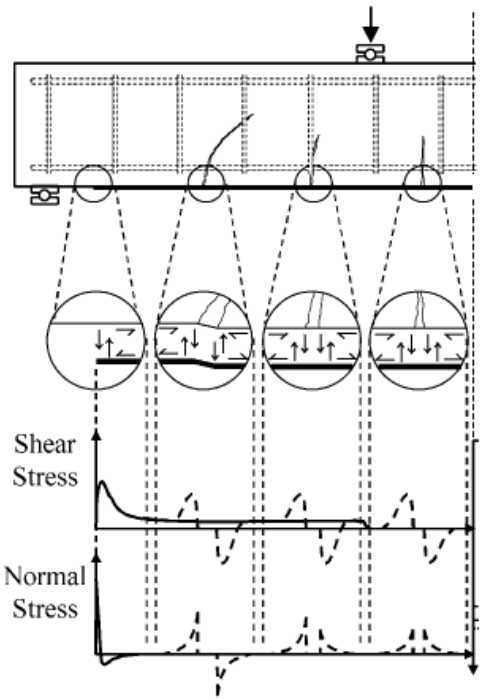

Figure 2.7: Distribution of interfacial stresses at material and geometrical discontinuities.

Strength of materials approach derives its models based on the stress distribution depicted in Figure 2.8 in which number 1 and 2 stands for concrete beam and FRP plate respectively. The magnitude of interfacial stresses at the material and geometrical discontinuities are calculated based on the usual theory of stress analysis and quite often based on the theory of liner elasticity.

Calculated stresses are compared with the ultimate strength of materials or with the strength of the interface and hence compared to a failure criterion. From this approach different failure criteria were followed such as biaxial failure of concrete (Malek et al, 1999), Mohr-Coulomb failure criterion (Varastehpour & Hamalen, 1997) and maximum value set for shear and normal stresses (Roberts, 1989). Some of the strength of materials based models for debonding prediction are reviewed below.

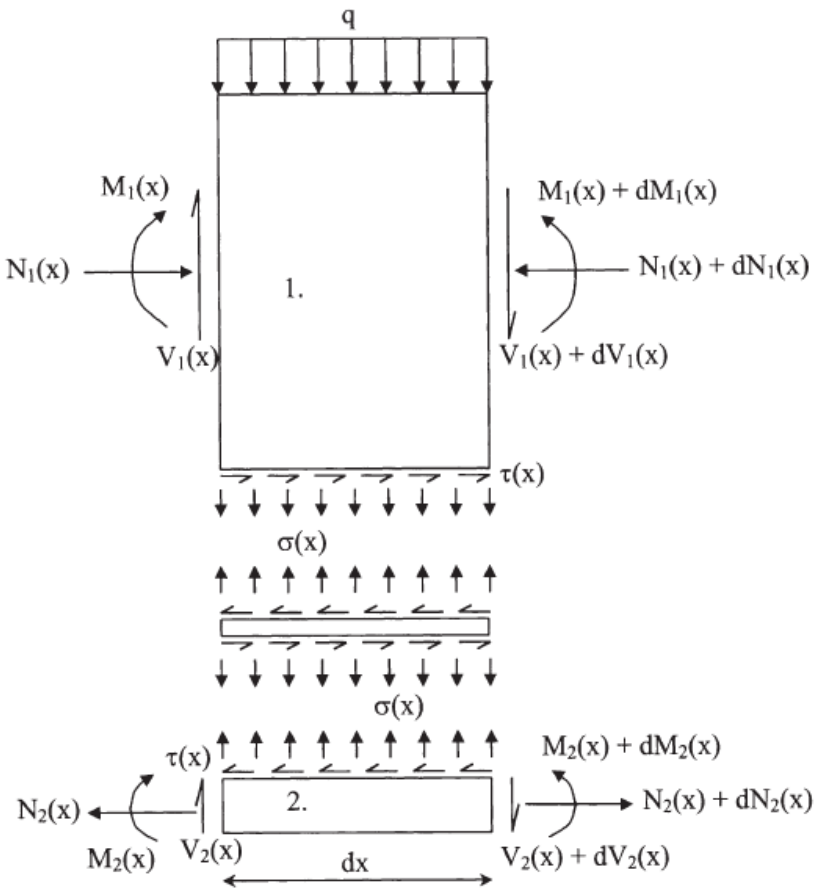

Figure 2.8**:** Interfacial shear and normal stress distribution (Smith and Teng, 2001)

Strength of material approach generates relatively simple models that can be easily applied in practical design. The approach may also be suitable for different types of plates provided that material and geometrical properties are well included. In addition, accurate but relatively complicated models were developed, but these are difficult to apply in design. Though the approach has a number of advantages, it also has limitations. In fact, the approach fails to investigate the failure modes observed in experimental investigation such as horizontal propagation of debonding from regions of high stress concentrations. The approach is also not accurate for small zones at the interface ends.

Another shortcoming of the approach is the versatility of failure criteria making difficulty to apply. Different criteria were developed by different researchers and include maximum normal and shear stresses (Pareek et al. 1999, Quantril et al 1996), splitting tensile strength of concrete (Malek et al. 1998), modulus of rupture of concrete (Tumialan et al. 1999) and Mohr-Coulomb criterion (Wu et al. 1997, Ziraba et al. 1994). It is clear now that strength of materials based models do not address debonding phenomenon, which may take place at the interface, they only consider debonding in different constituent materials making the strengthening system. As reported by Rabinovitch and Frostig (2001), stress criterion is valid for ductile elastoplastic materials and yields inaccurate results in cases of cracking, crack propagation and collapse for brittle materials. From the above discussion, it is necessary to look for models, which will include nonlinearity of materials and interfaces, horizontal propagation of debonding failures, and generating models that can be easily applied in the design of strengthening systems.

2.4.2. Fracture Mechanics Approach

Debonding is a general term used to describe a significant decrease in member capacity due to initiation or propagation of a major crack in the vicinity of the interface region and may follow two possible paths: within the constituent element or at the interfaces of the materials involved in the strengthening system (Au & Büyüköztürk, 2006). In the fracture mechanics approach, the debonding failure is treated as a crack propagation promoted by local stress intensities around the crack tip. The formation and propagation of a crack necessitates certain energy per unit area of the crack plane. The approach uses the fracture mechanics concepts and principles to predict the failure load of retrofitted beams.

In this approach stress intensity factors or energetic criteria such as energy release rate are used to predict the onset and propagation of cracks and hence debonding failure (Rabinovitch and Frostig, 2001).

The common assumption made bay various researchers is the consideration of different mechanisms of energy dissipation in FRP strengthened RC beams under loading (Gunes et al. 2009, Au & Buyukozturk, 2006 , Achinta & Burgoyne, 2012). For debonding to take place, the energy release rate which is the energy available for fracture should be greater than or equal to the total energy dissipated or fracture energy. Fracture energy represents the energy required for fracture. Different models were developed to determine the energy dissipated considering different mechanisms such as cracking and crushing of concrete, yielding of steel reinforcement and debonding. Like for strength of materials based models, fracture mechanics models reported in the literature are based on elastic properties of materials and interfaces. Fracture mechanics is able to consider the mixed mode delamination which may occur as a result of combination of normal and shear stresses. Pure fracture modes are shown in figure 2.9 below. These are mode I or opening mode, mode II and III or shear modes.

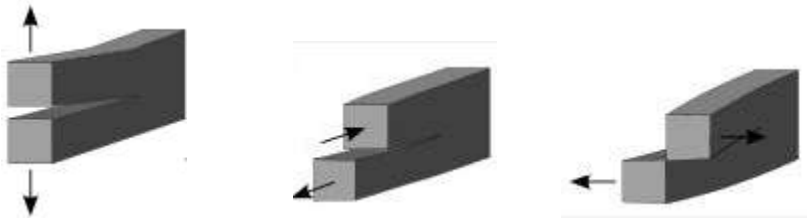

(a) (b) (c)

Figure 2.9: Fracture modes: (a) Opening, (b) In-plane shear, (c) Out-of-plane shear.

Although fracture mechanics based models are able to investigate both interfacial and material debonding, they fail to consider nonlinear behavior of materials. The other challenge with such models is the difficulty in the determination of fracture energy of various materials and interfaces as well as for failure modes and the determination of crack tip stress fields. Thus, there is a need of a coupled approach that will consider strength of materials and fracture mechanics to capture debonding failure that may take place in the materials or at the interface.

Several other researchers such as Hearing (2000), Taljsten (1996), Rabinovitch (2008) and Gunes (2004) used principles of fracture mechanics to develop their models despite the limations stated above.

2.5. Summary.

The most common and critical failure mode of FRP strengthened beams is the debonding. This failure is still preventing the wide use of this attractive solution of life extension of existing concrete structures. All attempts that have been done on the behavior of such systems reported this model of failure and due to its complexity; its complete understanding has not been achieved yet. However, it is agreed by numerous researchers that this failure takes place at the locations of the strengthened beams where there are material discontinuities (cracked regions) and where there are geometrical discontinuities (at the plate end). A common understanding to all researchers is that debonding is initiated by the formation of a crack at those locations due to high shear and normal interfacial stress concentrations with shear dominating. Once a crack forms in the concrete at or near the plate end or in the constant bending moment region, the crack may propagate horizontally at the level of the tension reinforcement as it also propagates towards the neutral axis. The horizontal propagation of the crack induces debonding (Smith and Teng, 2002).

As agreed upon by different researchers, for debonding to occur a certain material limit must be reached. Some researchers called this limit critical principal stress or any other failure criterion as mentioned in 2.4.1 and others called it maximum energy release rate. This has led to studying debonding problem under two main approaches: Strength of materials and fractures mechanics. Although strength of material models are based on well-known theory of elasticity, they fail to capture nonlinearity of concrete and steel and only considers localized debonding in materials. In addition, they fail to address debonding that may take place at the interfaces between materials making the strengthening system.

Fracture mechanics on the other hand being able to address both material and interface debonding is limited by its complexity and difficulties in measuring concrete and interface‟s toughness or fracture energy.

Like strength of materials, fracture mechanics models reported in the literature do not take into consideration nonlinear behavior of materials. They are based on elastic and fracture properties of material and interface. Thus, it is necessary for better understanding of the behavior of patch repaired and FRP strengthened RC beams to take into consideration both strength of materials and fracture mechanics as well as nonlinear behavior of materials. Therefore, further researches are needed to improve the existing knowledge. One way of achieving this is the use of numerical methods in which the combinations of approaches can be done and nonlinear behavior easily introduced. However, material constitutive relationships and interaction between different materials are always approximated.

Although many experimental and analytical studies have been published by numerous researchers on the behavior of reinforced concrete beams patch repaired and strengthened beams, not many numerical studies have been reported to the author‟s knowledge to investigate the behavior of reinforced concrete with repair material taken into account. From that fact, this research project is aimed at investigating numerically the behavior of reinforced concrete beams patch repaired and strengthened with FRP plate with different degrees of damage.

Chapter 3

NUMERICAL MODELING OF REINFORCED CONCRETE BEAMS

3.1. Introduction

The analysis and design of reinforced concrete structures has often been done based on analytical approaches to determine with relatively high accuracy the stresses and state of deformations in the structures assuming linear elasticity behavior of materials. However, the analytical approach faces some problems, which prevent it to be a simple and accurate tool of analysis. Some of the issues include among others (Buyukozturk, 1975):

i) Nonlinear load-deformation response of concrete and difficulty in forming suitable constitutive relationship under combined stresses,

ii) Progressive cracking of concrete under increasing load and the complexity in the formulation of the failure behavior for various stress states,

iii) Steel and its interaction with concrete and

iv) Time dependent effects such as creep and shrinkage of concrete.

Since the advent of modern computational techniques using finite elements methods, it has been found that it is even possible to determine the stress and deformation fields for more complex structures. However, this requires a good understanding of the behavior of materials involved, thus the requirements of accurate material constitutive relationships. The complexity in the behavior and failure mechanisms of reinforced concrete beams retrofitted with fiber reinforced polymers has led researchers to resort to the use of finite element methods and a substantial work has been done so far. In order to simulate any structure, it is necessary to have a good understanding of its physical behavior and response to various loading conditions because otherwise the numerical analysis will be limited. For reinforced concrete, the material behavior and the interaction between them are crucial. Finite element method improves the experimental and analytical findings and has an added advantage of investigating local failures and determine quantities that cannot be easily determined from the laboratory and analytical investigations.

Cracking, tension softening, non-linear multiaxial material properties, complex steel concrete interface behavior and other effects previously ignored or treated in a very approximate way can now be modeled rationally with the help of finite elements methods (Amgad, 1998).

In finite element modeling of reinforced concrete beams much attention has been put on the behavior of concrete since it is the main component of the system and hence affects its overall behavior.

Finite element methods have been found to be robust and reliable numerical approaches to solve a wide range of civil engineering problems and give accurate and realistic results. This chapter discusses the modeling aspects of different materials involved in the present study and presents the constitutive models adopted for the present study. The chapter also highlights some authors who used the same material models in their researches.

3.2. Material constitutive models

3.2.1. Concrete

Concrete is a composite material obtained by mixing aggregates and binder with water. The mixture develops its strength and other properties over time as it hardens. The behavior of the paste and aggregate is linear; however, the resulting mixture is nonlinear. This is because of the weak interface that exists between the paste or matrix and the aggregate called interface transition zone (ITZ). The other reason of concrete nonlinearity may be attributed to its porosity that causes non uniform stress distribution when concrete is loaded. Thus, its behavior largely depends on the microstructure properties.

Even though it exhibits nonlinearities and difficulties in modeling its behavior, concrete has become a popular material used all over the world due to its low cost, the availability of its ingredients and advances in its technology made over the last decades. For the purpose of this study, it is important to remember that concrete cracking affects the debonding failure and that concrete behaves differently in compression and in tension, which makes it a complex material. Therefore, it is necessary to have a good understanding of its behavior when in service. Concrete under uniaxial compression behaves in a nonlinear manner following a small linear portion, according to the curve shown in figure 3.1 (Baldvin, 2011) and figure 3.2. The figures illustrate different stages that concrete undergoes as the load increases in compression.

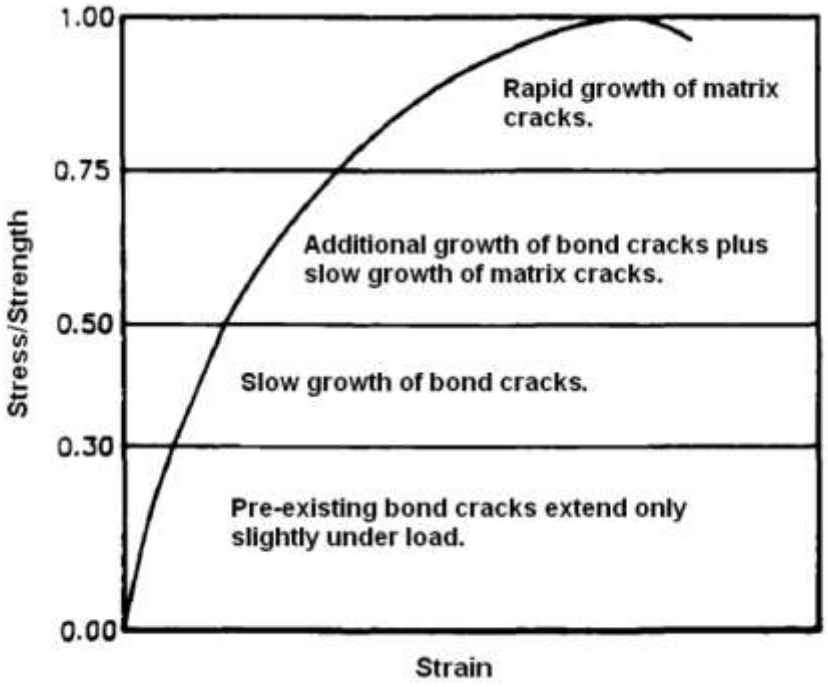

Figure 3.1: The compressive stress-strain curve for concrete

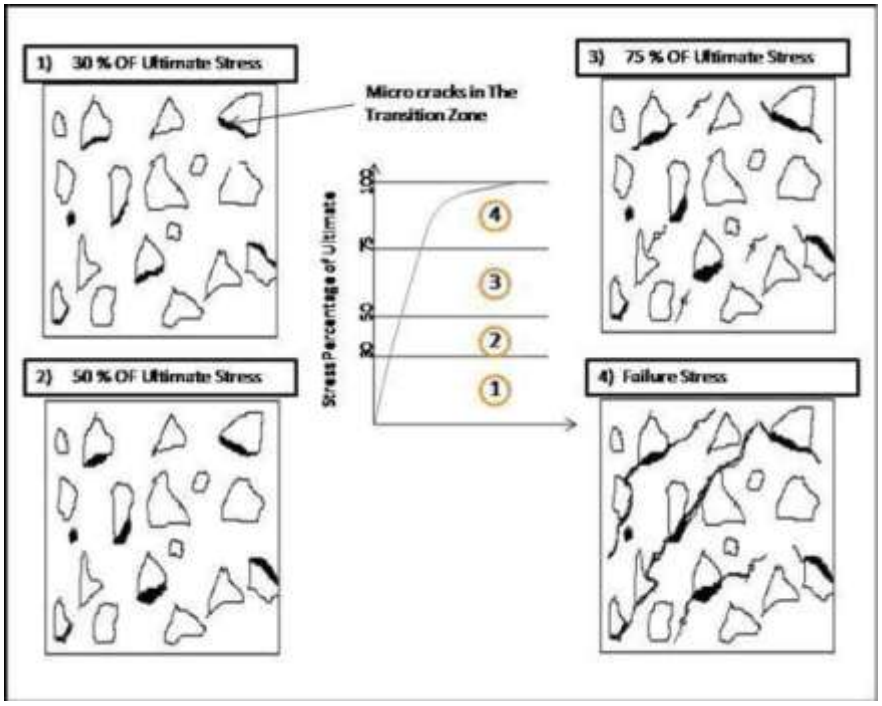

Figure 3.2: Development of concrete cracking under uniaxial compression (**www.theconcreteportal.com, accessed on 24/11/2013**)

The micro cracks that appear before macro cracks (visible) in concrete are caused by segregation, shrinkage or thermal expansion in the paste and therefore exist even before any load has been applied (Simonelli, 2005). Even though finite element method is believed to be a reliable tool for the analysis of complex engineering problems, it doesn‟t capture the above causes of micro cracks, thus there are always slight differences between experimental and numerical results.

The increased use of concrete as a primary structural material in the construction of different types of complex structures such as reactor vessels, dams, bridges, etc., has attracted attention of many researchers to develop sophisticated material models for concrete to predict its response to a variety of loading situations (Babu *et al*. 2005). Such models were developed for both compression and tension. It is important to note that the shape of the curve for concrete under tension is more or less similar to that in compression with different values of peak stresses.

3.2.1.1. Concrete material constitutive relationships.

While the stress strain relationship in figure 3.1 represents the uniaxial stress state, concrete in actual structures is subjected to multiaxial stress state. Thus, both uniaxial and multiaxial stress states must be considered for proper representation of the behavior of concrete. Buyukozturk and Shareef (1985) classified approaches used to determine the stress-strain relationships under various stress states for concrete into five categories, namely:

(i)Linear and nonlinear elasticity theories;

(ii) Elastic perfectly plastic models;

(iii) Elastic strain hardening plasticity models;

(iv) Plastic damage (fracturing)-type models;

(v) Endochronic theory of inelasticity.

Chen (1982) classified the approaches into (1) representation of given stress-strain curves by using curve fitting methods, interpolation, or mathematical functions; (2) linear and non-linear

elasticity theories; (3) perfect- and work-hardening-plasticity theories; and (4) Endochronic theory of plasticity.

Theoretical and experimental investigations have showed that most of engineering materials including concrete initially respond elastically, which means that the deformation is fully recoverable at the removal of the load. However, once the load exceeds certain limit called yield load, the deformation is no longer fully recoverable. Part of the deformation can be recovered while another part remains permanent. In this case, the response is nonlinear and there is a need of plasticity to treat the non-recoverable deformation along with elasticity to deal with recoverable deformation. As concrete gets deformed it also undergoes certain damage. Concrete plasticity and damage modeling are dealt with in details in subsequent sections.

3.2.1.1.1. Linear and nonlinear behavior of concrete.

Models based on linear elasticity are the simplest models treating concrete as a linear elastic material until its failure. The model are more accurate in tension since the failure strength is small and from the fact that concrete is linear up to about 30% of its ultimate strength. These models do not capture the nonlinearity of concrete observed in experiments. In numerical analysis elastic models for concrete were used by Zhang &Teng (2009) in their study to determine the interfacial stresses in steel plated RC beams. Even though these models are widely used in numerical implementation, they fail to model the inelastic deformations of concrete especially when concrete undergoes unloading as found from experiments.

Buyukozturk & Shareef (1985) further classified approaches used to develop nonlinear elasticity models into hypoelastic and hyperelastic depending on whether the formulation accounts for loading history or not, respectively. The nonlinear elasticity model is based on the concept of variable moduli where concrete is assumed to be incrementally elastic and thus its response can be simulated by a piecewise linear elastic model with variable moduli as shown in figure 3.3 (Kwak and Filip, 1990).

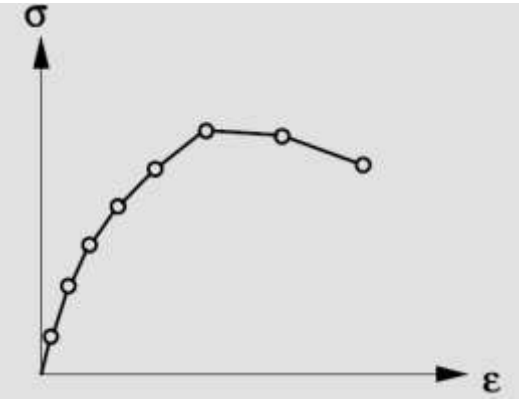

Figure 3.3: Nonlinear relationship based on variable moduli

In compression various uniaxial stress strain relationships have been developed. It is important to stress that concrete under biaxial compression exhibits higher strength than in uniaxial. At an equal biaxial compression state ($\sigma_1 / \sigma_2 = 1$) there is an increase in strength of about 16% in which case concrete compressive strength is approximately 1.16 f_c with f_c being the uniaxial compressive strength and an increase of 25% when ($\sigma_1 / \sigma_2 = 0.5$); however , the strength decreases almost linearly as the applied tensile is increased for the case of biaxial compression-tension (Amgad, 1998).

The behavior of concrete in tension is similar to that in compression. When concrete is considered as a continuum, its stress-strain relation comprises the pre and post peak regions. When a concrete specimen is subjected to uniaxial tension, it first responds elastically up to the peak load. Over this pre-peak region, stresses and strains are uniformly distributed over the specimen. At peak load, the strains start to localize within a narrow zone of micro-cracks called process zone or softening zone; which occurs at the weakest section of the specimen; after which macro-cracks will develop and propagate (Dirk Arend, 1991). As for compression, in the softening zone the load that can be transferred decreases with an increase in deformation which results in unloading of the concrete outside the process zone as illustrated by line II in figure 3.4 according to Dirk Arend (1991).

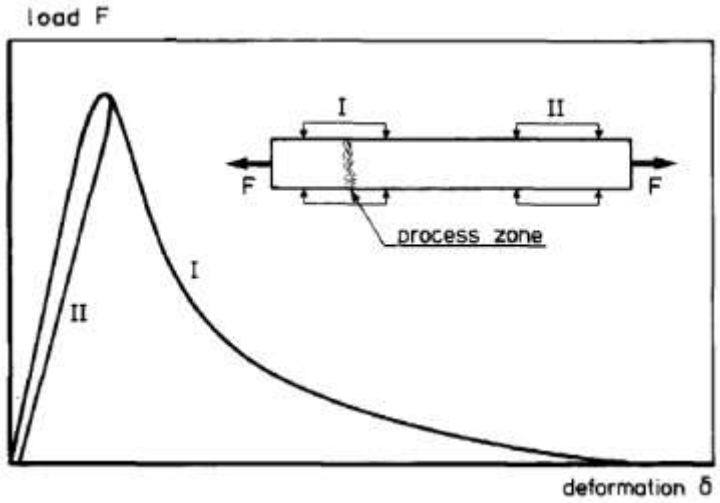

Figure 3.4: Load deformation relation for concrete under tension.

In tension, the crack is assumed to occur when the principal stress in concrete element exceeds a limiting value, which in most case is the tensile strength of concrete. The crack propagates in the direction perpendicular to the direction of the principal stress and that crack direction is fixed for all subsequent cracks. It is also important to note that cracking reduces the stiffness of the concrete which is known as tensile damage.

Various uniaxial and biaxial stress-strain relationships are reported in the literature for both compression and tension. Some of them are described below:

*i).*The stress strain relationship proposed by Saenz (1964)

$$\sigma_c = \frac{E_c \varepsilon_c}{1 + (R_1 + R_E - 2)\left(\frac{\varepsilon_c}{\varepsilon_0}\right) - (2R - 1)\left(\frac{\varepsilon_c}{\varepsilon_0}\right)^2 + R\left(\frac{\varepsilon_c}{\varepsilon_0}\right)^3} \tag{3.1}$$

where $R = \frac{R_E(R_\sigma - 1)}{(R_\varepsilon - 1)^2} - \frac{1}{R_\varepsilon}$, $R_E = \frac{E_c}{E_0}$, $E_0 = \frac{f_c^{'}}{\varepsilon_0}$, $R_\varepsilon = \frac{\varepsilon_c}{\varepsilon_0}$ and $\varepsilon_0 = 0.0025$, $R_\varepsilon = 4$, $R_\sigma = 4$, R is the ratio relation, R_E is the modular ratio, R_ε is the strain ratio and E_0 is the secant modulus. The above relationship is an equivalent stress-strain that can be used to represent both biaxial and triaxial stress state.

These models was used by a number of researchers in their numerical studies to model concrete in uniaxial compression and include Obaidat *et al.* (2010), Chen *et al*. (2011), and Chen *et al.(*2008)

*ii).*Desayi and Krishan (1964) stress-strain formula:

$$\sigma = \frac{E\varepsilon}{1+\left(\frac{\varepsilon}{\varepsilon_P}\right)^2}, \tag{3.2}$$

with σ, ε are the stress and strain tensor, E is the Young"s modulus and ε_p is the strain at peak stress.

*iii).*The non-linear compressive response of concrete proposed by BS EN 1992-1-1 (Eurocode 2, 2004: 33, 3.1.5) in the following form:

$$\sigma_c = \frac{k\eta - \eta^2}{1+(k-2)\eta} f_{cm} \tag{3.3}$$

where $\eta = \frac{\varepsilon_c}{\varepsilon_{c1}}$ with ε_{c1} the strain at peak stress and given by $\varepsilon_{c1} = 0.7 f_{cm}^{0.31} \leq 2.8‰$ with f_{cm} is the mean value of concrete cylinder compressive strength.

$$k = 1.05E_{cm}\frac{|\varepsilon_{c1}|}{f_{cm}}.$$

This model was used by (Baldvin, 2011) in his finite element analysis of concrete cracking using concrete damaged plasticity model that will be explained later and it will be used in the present study because of its simplicity and representation of uniaxial compression concrete behavior.

In tension, Carreira and Chu (1986) proposed the following stress-strain relation:

$$\frac{\sigma_t}{\sigma'_t} = \frac{\beta\left(\frac{\varepsilon}{\varepsilon'}\right)}{\beta - 1 + \left(\frac{\varepsilon}{\varepsilon'_t}\right)^{\beta}} \tag{3.3}$$

where σ_t is the stress corresponding to the strain ε, σ'_t is the point of maximum stress, ε'_t strain corresponding to maximum stress and β is a parameter that depends on the shape of the stress-strain diagram.

For concrete under uniaxial tension, Dirk Arend (1991) proposed the following tension-softening curve based on extensive tensile tests on concrete.

$$\frac{\sigma_t}{f_t} = \left[1 + \left(c_1 \frac{w_t}{w_{cr}}\right)^3\right] e^{-c_2 \frac{w_t}{w_{cr}}} - \frac{w_t}{w_{cr}}\left(1 + c_1^3\right) e^{-c_2} \tag{3.4}$$

with $w_{cr} = 5.14 \frac{G_F}{f_t}$

where w_t is the crack opening displacement, w_{cr} crack opening displacement at the complete release of stress, σ_t is the tensile stress normal to the crack direction, f_t uniaxial tensile strength and G_F is the fracture energy required to create a stress-free crack over a unit area. $c_1 = 3.0$ and $c_2 = 6.93$ are constants determined from tensile tests on concrete. It is well known that concrete tensile strength can be estimated from its compressive strength since it is difficult to measure directly tensile strength. The fracture energy can be estimated according to

$G_F = \left(0.0469 d_a^2 - 0.5 d_a\right)\left(\frac{f'_c}{10}\right)^{0.7}$ as reported by Chen et al.(2011) where d_a in mm stands for the maximum aggregate size and f'_c for the cylinder compressive strength in MPa. Note that Chen et al. (2011) and Chen et al. (2008) to model concrete in tension in their numerical analysis of reinforced concrete used above model developed by Dirk Arend (1991).

Wang and Hsu (2001) also developed the average (or smeared) stress-strain curve of concrete in tension for both the ascending and descending branches of the stress-strain relation according to the following equations respectively:

$$\sigma_1 = E_c \varepsilon_1 \text{ for } \varepsilon_1 \leq \varepsilon_{cr} \tag{3.5}$$

$$\sigma_1 = f_{cr}\left(\frac{\varepsilon_{cr}}{\varepsilon_1}\right)^{0.4} \text{ for } \varepsilon_1 \succ \varepsilon_{cr}$$

According to Abaqus 6.10 user manual, it is reasonable for relatively heavily reinforced concrete structures to assume that the strain softening after failure reduces stress linearly to zero at a total strain of about 10 times the strain at failure. The strain at failure in standard concrete is typically 10^{-4} which suggests that tension stiffening that reduces the stress to zero at a total strain of about 10^{-3} is reasonable. This approach will be used in the current research project. Note that tension stiffening is, in a cracked section, is that mechanism between adjacent cracks that allows tensile forces to be transmitted from the steel to the surrounding concrete by bond forces and thus concrete may be considered to increase the stiffness of steel reinforcement (CEB-FIP, 1993). The above models however do not consider the multiaxial stress state that is acting on concrete in actual structures.

3.2.1.1.2. Concrete Plasticity

Concrete when loaded in compression exhibits different responses under various stress states, i.e. uniaxial, biaxial and triaxial stress states. Plasticity models were found adequate due to their ability to directly represent multiaxial stress states. In plasticity, it is convenient to assume that the total deformation comprises of recoverable and non-recoverable or plastic deformations. This is illustrated in figure 3.5, which represents the uniaxial stress strain curve for plain concrete up to tensile and compressive failure. It is clear that for tensile failure, the response is linear elastic up to failure and no plastic strains occur. However, for concrete in compression, after point A i.e. the elastic limit, the response is nonlinear caused by the progressive micro cracking up to point D. According to Chen (1982), zone AC and CD correspond exactly to the behavior of a work hardening elastoplastic and elastic perfectly plastic solids respectively.

He also defined perfectly plastic or work hardening material as that material which does or does not admit changes of permanent strain under constant stress respectively.

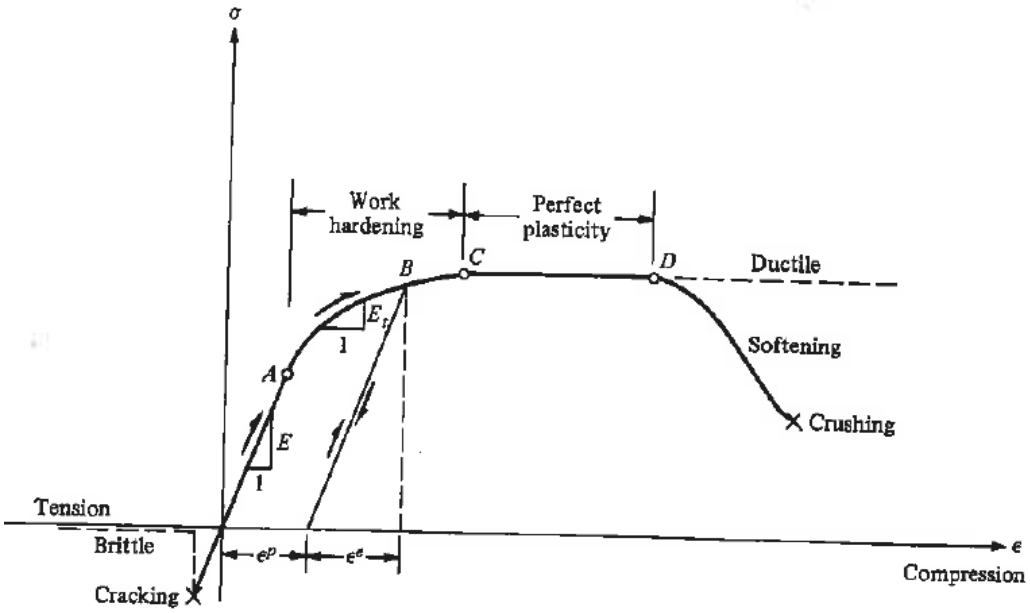

Figure 3.5: Uniaxial stress strain curve, pre and postfailure regime (Chen, 1982).

Therefore, for concrete, the current practice is to assume that it is an elastic perfectly plastic material under compression as illustrated in figure 3.6 and an elastic brittle material in tension.

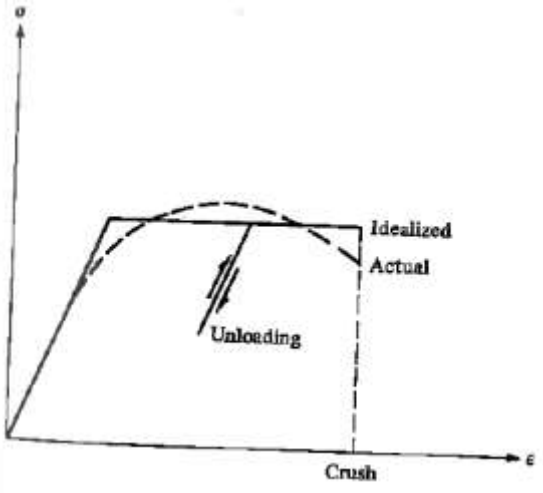

Figure 3.6: Elastic perfectly plastic idealization for concrete in compression (Chen, 1982).

Thus, a yield criterion for compression plasticity and the maximum-normal stress criterion for tension cutoff are generally required to approximate the failure surface of concrete. In addition, it is necessary to account for the ability of concrete to flow like a ductile material before reaching its crushing strain when subjected to a triaxial compression. All these aspects are considered by adopting a perfectly plasticity model shown in figure 3.6.

Three statements are necessary to define the general behavior of concrete under a complex stress state (Chen 1982):

i) The material is elastic until it reaches the yield limit, i.e. until a certain function of the stress components reaches a certain value. This is known as the yield function and is denoted as

$$f\left(\sigma_{ij}\right)=k\,, \tag{3.6}$$

ii) The plastic deformation takes place without limit. For the plastic flow to continue, the state of the stress must remain on the yield surface. This is known as the criterion for loading; that it is

$$df=\frac{\partial f}{\partial \sigma_{ij}}d\sigma_{ij}=0 \tag{3.7}$$

and finally,

iii) This flow strain is permanent, i.e. it remains when the stresses are removed or when the stress intensity drops below the yield value. This known as the criterion for unloading,

$$df=\frac{\partial f}{\partial \sigma_{ij}}d\sigma_{ij}\prec 0 \tag{3.8}$$

The yield function was interpreted and represented as a failure surface by various researchers for isotropic materials, i.e. those materials in which only principle stresses σ_1,σ_2 and σ_3 are considered in the development of the failure criterion. Thus for a perfect plastic material, we can write $f\left(\sigma_1,\sigma_2,\sigma_3\right)=k$ which is a fixed surface in the stress space and where each point inside it represents an elastic state of stress and each point on it a plastic state (Chen 1982). Thus, the failure surface represents the boundary of elastic behavior of concrete.

This surface will be referred to as yield criterion in the remaining of this thesis. It is also necessary to note that since the magnitude of the plastic strain ε_{ij}^{p} is unlimited during flow, we must think in terms of the strain rates or infinitesimal changes of strain, or strain increments, $d\varepsilon_{ij}$ keeping in mind that this strain increment is the sum of the elastic and plastic staring increments (Chen, 1982).

$$d\varepsilon_{ij} = d\varepsilon_{ij}^{e} + d\varepsilon_{ij}^{p} \tag{3.9}$$

Generally, concrete plasticity models are based on the same principles of plasticity for metals with some modifications to account for particular properties of concrete. The key aspects of a plasticity model include the yield surface defined above (initial and subsequent yield surfaces), the flow rule and the hardening/softening rule (Yu *et al*.2010a). The initial yield surface determines the onset of plastic deformation; the flow rule determines the direction of plastic deformation; and the hardening/softening rule defines how the yield surface evolves with plastic deformation.

Many yield criteria were developed in an effort to defining the failure criterion for concrete subjected to multiaxial stress states, which cannot be predicted using a simple tensile or compressive stress. According to Chen (1982) the failure criterion may be yielding, initiation of cracking, load carrying capacity and extent of deformation. The criterion for concrete the failure may be tensile which is defined by the formation of cracks and loss of tensile strength in the direction normal to the direction of crack or it may be compressive which is defined by the development of many cracks and concrete loses most of its strength. Tensile failure may be considered as brittle while compressive failure may be considered as ductile.

Chen (1982) classified the yield functions into:

i) One parameter models (for example maximum tensile stress criterion by Rankine; Shearing stress criteria by Tresca and von Mises);

ii) Two-parameter models (Mohr Coulomb criterion; Drucker-Prager criterion);

iii) Three-parameters models (Brester-Pister criterion; William-Warnke criterion);

iv) Four-parameters models like Ottosen criterion; and

v) Five-parameters model for example the refinement of the William-Warnke criterion by adding two additional degrees of freedom.

For concrete plastic models to be useful, they should be defined independently of the coordinate system by which the stresses are defined so that they will not change once stress coordinates change. Those coordinate independent combinations of principal stresses are called stress invariants and are independent of properties of a specific material. The stress invariant are the first, second and third invariants of stress tensor; I_1, I_2 and I_3; and first, second and third invariant of deviatoric stress tensor; J_1, J_2 and J_3. They are defined below in terms of principal stresses:

$$I_1 = \sigma_1 + \sigma_2 + \sigma_3;\ I_2 = \sigma_1\sigma_2 + \sigma_2\sigma_3 + \sigma_3\sigma_1;\ I_3 = \sigma_1\sigma_2\sigma_3 \tag{3.10}$$

$$J_1 = (\sigma_1 - \sigma_2) + (\sigma_2 - \sigma_3) + (\sigma_3 - \sigma_1) \tag{3.11}$$

$$J_2 = \frac{1}{6}\left[(\sigma_1 - \sigma_2)^2 + (\sigma_2 - \sigma_3)^2 + (\sigma_3 - \sigma_1)^2\right] \tag{3.12}$$

$$J_{3\,?} = \begin{bmatrix} \sigma_1 - \frac{1}{3}I_1 & \sigma_{12} & \sigma_{13} \\ \sigma_{21} & \sigma_2 - \frac{1}{3}I_3 & \sigma_{23} \\ \sigma_{31} & \sigma_{32} & \sigma_3 - \frac{1}{3}I_1 \end{bmatrix} \tag{3.13}$$

It is necessary to note that the principal stress coordinate system corresponds to the orientation in which the material has no shear. Among the various yield criteria that are in use, the Drucker-Prager has been extensively used to model concrete because of its simplicity (involving only two parameters) and its capability to capture shear strength increase as a result of increase in hydrostatic pressure. The general expression of the Drucker-Prager yield criterion is the extended von Mises criterion to include the effect of hydrostatic pressure on the shearing resistance of the material. It has the following form:

$$f = \sqrt{J_2} + \theta I_1 = k \tag{3.14}$$

where θ and k are positive material constants, I_1 the first invariant of the stress tensor and J_2 the second invariant of the deviatoric stress tensor. θ and k represent a measure of internal material friction and cohesion, respectively and may be expressed using uniaxial tensile and compressive strength values (Salari &Saeb, 2004) as:

$$\alpha = \frac{1}{\sqrt{3}} \frac{f_c - f_t}{f_c + f_t}, \quad k = \frac{2}{\sqrt{3}} \frac{f_c f_t}{f_c + f_t} \tag{3.15}$$

Note that plastic deformation is accompanied by an increase in volume which is known as dilatancy and is the consequence of dependency of yield function on hydrostatic pressure (Chen 1982).

The flow rule can be associated or non-associated depending on whether it is connected or not with the yield function, i.e. they have the same shape or not. The associated flow rule implies that the plastic flow vector is directed along the normal to the surface of plastic potential. Experimental data, however, have shown that the associated flow may not be the most appropriate option to characterize the response of concrete. Therefore, non-associated flow rule will be used in this study even if it results in material stiffness matrix that is not symmetric. However, Abaqus 6.10 is promising; it switches itself to unsymmetric matrix storage once non-associated flow rule is used. For perfectly plastic material, the simplest work hardening rule is to assume that the yield surface expands uniformly without distortion as plastic flow occurs (Chen, 1982).

3.2.1.1.3. Plasticity and Damage Models for Concrete

Several plasticity models for concrete were developed over the past years. The key characteristics for any plastic model are the yield criterion, the flow rule and the hardening rule as stated in the previous section. The parameters included in these rules are the basic differences between plasticity models. A summary of plastic models developed based on the Drucker-Prager yield criterion; equation 3.10 can be found in Yu et al. (2010).

Yu et al. (2010) for example modified the Drucker-Prager yield criterion to account for the shear strength ratio and confining pressure for materials under biaxial and triaxial stress states. The modified yield criterion becomes:

$$F = \sqrt{J_2} - K\theta I_1 - Kk \tag{3.16}$$

where K represents the shear strength ratio. The representation in $I_2 - \sqrt{J_2}$ plane is shown below:

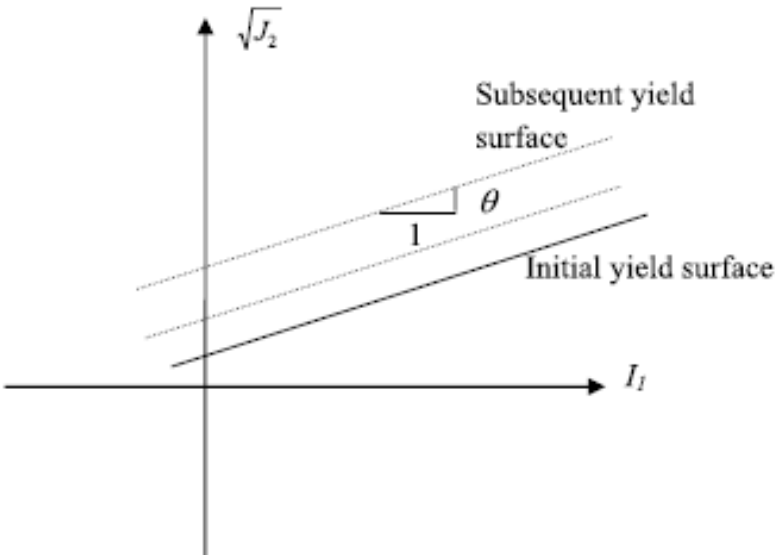

Figure 3.7: Yield criterion in $I_1 - \sqrt{J_2}$ plane

The hardening rule to account for confining pressure is a function of both confining pressure and plastic deformation as

$$k = k\left(\sigma l, \varepsilon_p\right) \tag{3.17}$$

where σl is the confining pressure Finally, the non-associated flow rule with a potential function parameter β related to plastic deformation, the confining pressure and the rate of confinement increment:

$$\beta = \beta\left(\sigma I, \frac{\Delta \sigma I}{\Delta \varepsilon I}, \varepsilon_p \right) \tag{3.18}$$

Plasticity based models have been used with considerable accuracy to predict the behavior of concrete under multiaxial stress states. However, it has been reported that concrete undergoes stiffness degradation due to cracking.

Plasticity based models are incapable of capturing such degradation caused by strain softening. In their studies, Mazars and Cabot (1989) concluded that damage; which is the propagation and coalescence of micro-cracks; appears after a threshold and is mostly located in the interface transition zone which they called interface halo, and in the cement matrix.

They further reported that two types of damage exist in connection with the stress state and history: (1) The collapse of the microporous structure of the cement matrix which is attributed to the hydrostatic pressure applied to the material and that may lead to consolidation, and (2) the propagation of micro-cracks that are mostly located in the cement matrix. This fact has led researchers to develop models based on continuum damage theory to account for stiffness degradation and strength of concrete under increasing load.

Degradation of concrete is modeled based on degradation variables in both compression and tension which may be scalar for isotropic formulation or tensorial for anisotropic formulation. In fact the degradation is anisotropic which means that the micro-cracks are direction dependent, however, due to difficulties in numerical implementation, the isotropic damage has been used extensively by adopting two independent scalar damage parameters one for tension and one for compression. The simplest form of the transformation function for isotropic damage developed by Kachanov (1958) and reported by Lucioni et al. (1996) is of the following form:

$$f(\beta) = (1 - d) \tag{3.19}$$

where $\beta = d$ is the inner damage variable and is such that

$d = 0$ for the undamaged virgin material

$d = 1$ for completely damaged material.

Equation 3.19 forms the basis of concrete damage models.

For example, Mazars and Cabot (1989) developed a scalar damage model based on the thermodynamics of irreversible process, in which they defined the stress tensor and the damage energy release rate as:

$$\sigma = \Lambda_0 (1 - D) : \varepsilon^e \text{ and } Y = \frac{1}{2} \Lambda_0 : \varepsilon^e : \varepsilon^e$$

where Λ_0 is the initial stiffness matrix. The equations were developed assuming that damage affects only the elastic properties. To distinguish between the response in tension and compression, they coupled two types of damage D_t and D_c measured in uniaxial tension and uniaxial compression, respectively. The total damage was then the weighted sum expressed as

$$D = \alpha_t D_t + \alpha_c D_c \tag{3.20}$$

where α_t and α_c which are related to strains, define the contribution of each type of damage for general loading and for uniaxial tension $\alpha_t = 1$, $\alpha_c = 0$, $D_t = D$ and vice versa for uniaxial compression. They further defined the evolution of damage according to $D_t = F_t\left(\bar{\varepsilon}\right)$ and $D_c = F_c\left(\bar{\varepsilon}\right)$,

with $F_i\left(\bar{\varepsilon}\right) = 1 - \frac{(1 - A_i)K_0}{\bar{\varepsilon}} - \frac{A_i}{\exp\left[B_i\left(\varepsilon - \bar{K}_0\right)\right]}$, $(i=t, c)$, $\bar{\varepsilon}$ is the equivalent strain.

K_0, A_i and B_i are identified independently from compression tests on cylinders and bending tests on beams.

Luccioni et al. (1996) based on the principles of thermodynamics developed a damage model where the total energy was considered to be a sum of elastic and plastic parts. The degradation variable was obtained by normalizing the energy dissipated by damage to unit as:

$$\kappa^d = \left[\frac{r}{g_t^{*d}} + \frac{(1-r)}{g_c^{*d}}\right] m_0 \psi^e d \tag{3.21}$$

where $\psi^e = (1-d)\psi^0$ is the elastic part of the free energy with ψ^0 elastic energy of the undamaged material and m_0 density of the material. The multiaxial stress weight factor r, generally used to convert uniaxial condition to multiaxial is given by the following expression:

$$r = \frac{\sum_{i=1}^{3} \langle \sigma_i \rangle}{\sum_{i=1}^{3} |\sigma_i|} \text{ and } g_t^{*d} = \frac{\sum_{i=1}^{3} |\sigma_i|}{\bar{\sigma}} g_t^d, \quad g_c^{*d} = \frac{\sum_{i=1}^{3} |\sigma_i|}{\bar{\sigma}} g_c^d$$

g_t^d and g_c^d are the maximum energy densities dissipated in uniaxial tension and compression processes, respectively and σ_i the principal stress. The equivalent damage threshold evolution law that accounts for both tension and compression damages was then defined as:

$$f(\sigma_{ij}, \kappa^d) = r\sigma_t(\kappa^d) + (1-r)\sigma_c(\kappa^d) \tag{3.22}$$

The same threshold evolution law was developed by normalizing the energy dissipated by the plastic process to unity as

$$K(\sigma_{ij}, \kappa^p) = r\sigma_t(\kappa^p) + (1+r)\sigma_c(\kappa^p) \tag{3.23}$$

where $\sigma_t(\kappa^p)$ and $\sigma_c(\kappa^p)$ define the evolution of the yielding threshold in uniaxial tension and compression tests, respectively.

κ^p is the plastic damage variable given by

$$\kappa^d = \left[\frac{r}{g_f^{*p}} + \frac{(1-r)}{g_c^{*p}}\right] \sigma_{ij} \dot{\varepsilon}_{ij}^p \tag{3.24}$$

In which, $g_f^{*p} = \frac{\sum_{i=1}^{3} |\sigma_i| R^{op}}{\bar{\sigma}} g_f^p$ and $g_c^{*p} = \frac{\sum_{i=1}^{3} |\sigma_i|}{f(\sigma_{ij})} g_c^p$

g_f^p and g_c^p are the maximum energy densities dissipated by the plastic process in uniaxial tension and compression, respectively and they are given by $g_f^p = \frac{G_f}{l_c}$ and $g_c^p = \frac{G_c}{l_c}$ where G_f and G_c are the fracture and crushing energies, respectively and l_c is an external parameter related to the size of the finite element.

It has been noted that plasticity models when used alone are incapable of capturing the stiffness degradation observed in experiments and on the other hand, damage models alone are not suitable to describe both irreversible deformation and volumetric expansion observed in compression. Since both irreversible deformations and stiffness degradation occur simultaneously and both contribute to the nonlinear response of concrete when it is loaded by multiaxial stress states, it is convenient to adopt models that encompass both plasticity and damage. To this end, a huge number of studies have been done in an effort to couple plasticity and damage to develop plastic damage models for concrete failure prediction.

Combinations of plasticity and damage usually consider plasticity with isotropic hardening and enrich it by either isotropic or anisotropic damage (Grassl &Jirasek, 2006). We have already indicated the disadvantages associated with the anisotropic damage in terms of numerical implementation. Plasticity and damage can be combined with plasticity formulated in the effective stress space, i.e. the effective stress meant as the average micro-level stress acting on the undamaged material and is defined as force divided by the undamaged part of the area. The combination can also be done with plasticity formulated in the nominal stress space, which is meant as the macro-level stress defined as force divided by the total area according to (Grassl &Jirasek, 2006). Different researchers did different combinations so far. For example, Lee and Fenves (1998) and Jason et al. (2012) used effective stress space while Lubliner et al. (1989) and Imran and Pantazopouli (2001) used nominal stress space.

For the purpose of this study, the combination done by Lubliner et al. (1989) and later modified by Lee and Fenves (1999) is discussed. The reason is that the combination of plasticity and damage in Abaqus 6.10 is based on this model and hence will be used to model the behavior of concrete in both tension and compression. The plasticity is formulated in the effective stress space since for damaged material only the effective area carries the external applied load.

The model is since now referred to as concrete damaged plasticity (CDP) which is a continuum, plasticity-based, damage model for concrete able to capture its plastic behavior and stiffness degradation.

3.2.1.1.4. Concrete Damaged Plasticity Model

The model assumes that concrete mainly fails in tension by cracking and in compression by crushing. The model is derived by decoupling the total strain increment into elastic and plastic components such that:

$$\varepsilon = \varepsilon^e + \varepsilon^p \text{ and } \sigma = E : \left(\varepsilon - \varepsilon^p\right) \tag{3.25}$$

where σ is the stress tensor and E is the tensor elastic stiffness. This is known as incremental plasticity model. Introducing the scalar damage for stiffness degradation,

$$E = (1-D)E_0 \tag{3.26}$$

where E_0 is the initial elastic stiffness (undamaged material),

E is the degraded elastic stiffness and *D* is the damage variable which varies from zero for undamaged material to one for completely damaged material. Combination of equation 3.25 and 3.26 leads to the following general stress strain relationship:

$$\sigma = (1-D)E_0 : \left(\varepsilon - \varepsilon^p\right) \tag{3.27}$$

Or for uniaxial tension and uniaxial compression $\sigma_t = (1-D_t)E_0 : \left(\varepsilon_t - \varepsilon_t^p\right)$

and $\sigma_c = (1-D_c)E_0 : \left(\varepsilon_c - \varepsilon_c^p\right)$ respectively.

Denoting the effective stress as $\bar{\sigma} = E_0 : \left(\varepsilon - \varepsilon^p\right)$ the general stress strain relationship becomes:

$$\sigma = (1-D)\bar{\sigma} \tag{3.28}$$

In this plastic-damage model, stiffness degradation based on the concept of effective stress is embedded in plasticity model (Lee & Fenves, 1989). Therefore, it must satisfy the three key points of a plastic model, i.e. yield criterion, flow rule and hardening rule.

In the framework of this model, the yield criterion proposed by Lubliner et al. (1989) and modified by Lee and Fenves (1999) is adopted and is having the following form in the effective stress space:

$$F(\sigma,\varepsilon^p)=\frac{1}{1-\alpha}\left[q-3\alpha p+\beta(\varepsilon^p)\langle\sigma_{\max}\rangle-\gamma\langle-\sigma_{\max}\rangle\right]-\sigma_c(\varepsilon^p)\le 0 \tag{3.29}$$

where $\bar{p}=\frac{1}{3}\bar{\sigma}:I$ is the effective hydrostatic pressure, $\bar{q}=\sqrt{\frac{3}{2}\bar{S}:\bar{S}}$ is the Mises equivalent effective stress with $\bar{S}=\bar{p}\,I+\bar{\sigma}$ the deviatoric part of the effective stress tensor, $\hat{\bar{\sigma}}_{\max}$ is the algebraically maximum eigenvalue of the effective stress tensor.

The function $\beta\left(\bar{\varepsilon}^p\right)$ was modified into a function of two plastic damage parameters as

$$\beta\left(\bar{\varepsilon}^p\right)=\frac{f_{co}}{f_{to}}(1-\alpha)-(1+\alpha) \tag{3.30}$$

The coefficient α can be determined from the initial equibiaxial and uniaxial compressive yield stress σ_{b0} and σ_{co} as $\alpha=\frac{\sigma_{b0}-\sigma_{c0}}{2\sigma_{bo}-\sigma_{c0}}$ and

$$\bar{\sigma}_t=\frac{\sigma_t}{(1-D_t)}=E_0\left(\bar{\varepsilon}_t^p\right)$$

$$\bar{\sigma}_c=\frac{\sigma_c}{(1-D_c)}=E_0\left(\bar{\varepsilon}_c^p\right)$$

are the effective uniaxial cohesion stresses that determine the size of the yield criterion. f_{co} and f_{to} are the uniaxial initial yield compressive and tensile stresses respectively. The coefficient γ is only significant for triaxial compression stress states and is determined from the following equation:

$$\gamma=\frac{3(1-K_c)}{2K_c-1} \tag{3.31}$$

where K_c is the ratio of the second stress invariant on the tensile meridian (TM) to that on the compressive meridian (CM) at initial yield for any given value of the pressure invariant *p* such that the maximum principal stress is negative. It must satisfy the condition $0.5 \prec K_c \prec 1$. This parameter governs the shape of the yield criterion which doesn"t need to be always a circle as in the initial Drucker-Prager formulation as shown in figure 3.8.

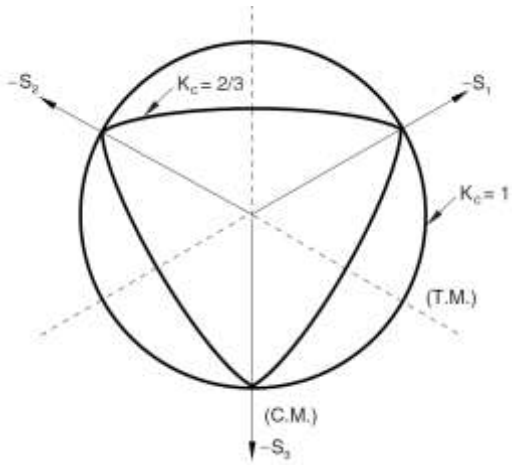

Figure3.8: Yield surfaces in the deviatoric plane corresponding to different values of K_c

The plastic damage model makes use of non-associated flow rule in which the strain increment is

$$\dot{\varepsilon}^{p} = \dot{\lambda}\frac{\partial G\left(\bar{\sigma}\right)}{\partial\left(\bar{\sigma}\right)} \tag{3.32}$$

With the flow potential *G* defined as the Drucker-Prager hyperbolic function given by:

$$G = \sqrt{\left(\in \sigma_{t0} \tan\psi\right) + \bar{q}^{2}} - \bar{p}\tan\psi \tag{3.33}$$

where ψ is the dilatation angle measured in the $p-q$ plane at high confining pressure; which physically means concrete angle of internal friction, σ_{t0} is the uniaxial tensile stress at failure and $\in$ is referred to as the eccentricity that defines the rate at which the function approaches the asymptote, i.e. the flow potential tends to a straight line as the eccentricity approaches zero as

shown on figure. $\dot{\lambda}$ is a positive scalar factor of proportionality which is non-zero only when plastic deformation occurs. In addition to dilatation angle, eccentricity, parameter K_c, there are other two parameters that define also the behavior of concrete under multiaxial stress states. These are the ratio of the strength in biaxial state to the strength in uniaxial strength, which shows the point in which concrete undergoes failure under biaxial compression; and the viscosity parameter that helps to overcome convergence difficulties associated with material models exhibiting softening and stiffness degradation.

The hardening rule is characterized by two independent variables $\bar{\varepsilon}_t^{\,p}$ and $\bar{\varepsilon}_c^{\,p}$ which are referred to as equivalent plastic strain in tension and in compression, respectively. That is:

$$\varepsilon^{p} = \begin{bmatrix} \bar{\varepsilon}_t^{p} \\ \bar{\varepsilon}_c^{p} \end{bmatrix}$$

The hardening parameters are state variables and control the evolution of the yield criterion and the degradation of the elastic stiffness; thus they control micro cracking and crushing of concrete. The response of concrete is characterized by damaged plasticity in both tension and compression. The strain stress response is initially linear in tension up to the failure stress σ_{to} which shows the onset of cracking beyond which the formation of micro cracks is represented macroscopically with a softening strain response as shown in figure.

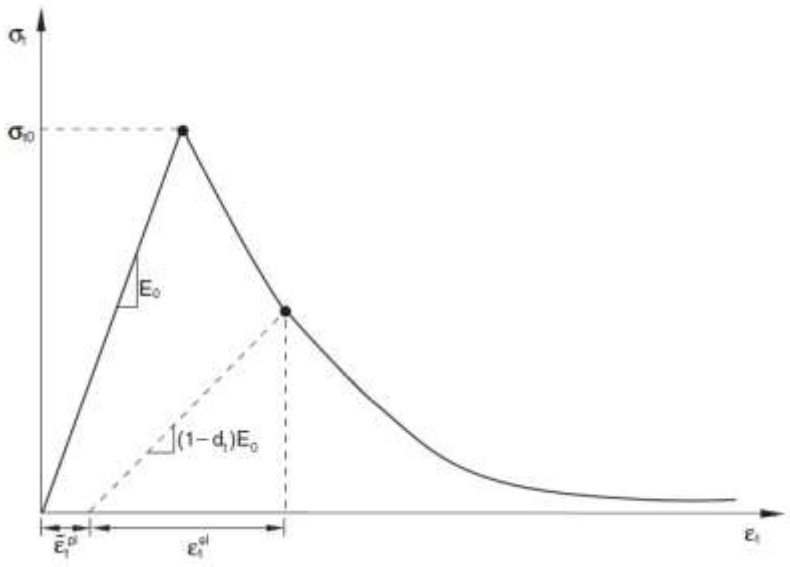

Figure 3.9: Response of concrete to uniaxial tension (Abaqus, 2010)

Figure 3.9 shows that unloading from any point from the softening curve, i.e. in the post-peak region, one can see that the elastic stiffness has been degraded and the level of degradation depends on the magnitude of the plastic strains.

Under uniaxial compression, the response is also linear up to a certain stress level as already mentioned in the previous sections. The stress at the elastic limit is called yield stress, σ_{co} followed by a plastic regime response characterized by stress hardening up to ultimate stress, σ_{cu} beyond which the response is strain softening. As mentioned before, the degraded response of concrete is characterized by two independent uniaxial damage variables, D_t and D_c varying from zero for undamaged concrete to one for fully damaged concrete.

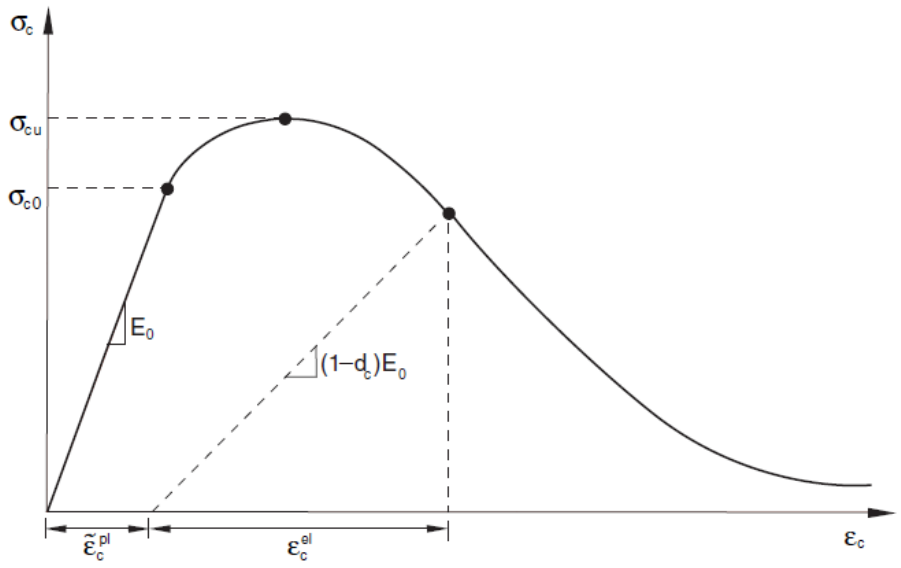

Figure 3.10: Response of concrete to uniaxial compression (Abaqus, 2010)

In tension uniaxial data are supplied to Abaqus for the softening regime in terms of stress as a function of cracking strain. The stress strain behavior of concrete in uniaxial compression is defined in Abaqus for the region outside of the elastic limit. The yield stress is a function of inelastic strain. In compression, the unloading data are supplied in terms of compressive damage curves. Abaqus converts both inelastic and cracking strains into corresponding plastic strains, which are compatible with the present model. Therefore, it is necessary to separate the total tensile strain into cracking strain $\bar{\varepsilon}_t^{ck}$ and elastic strain corresponding to undamaged material ε_{ot}^{el} corresponding to undamaged material in tension.

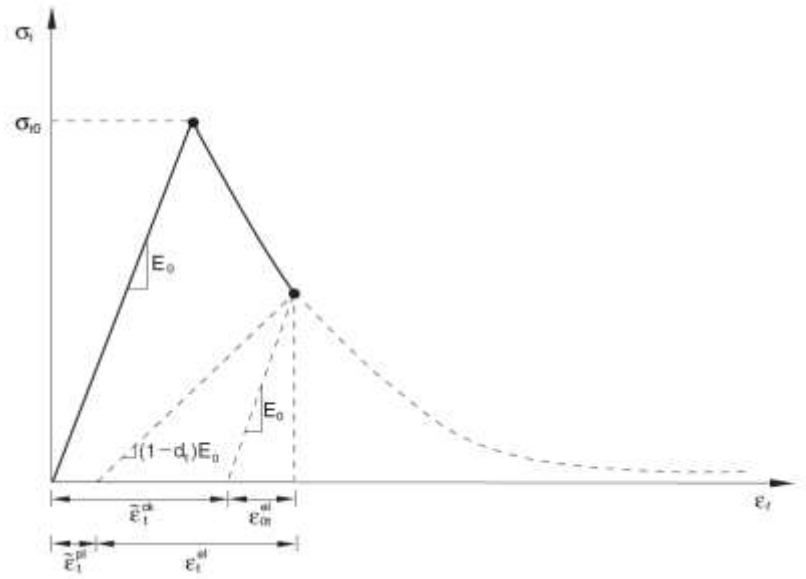

Figure 3.11: Definition of tension stiffening data (Abaqus, 2010)

Similarly, the total compressive stress is divided into inelastic strain $\bar{\varepsilon}_c^{in}$ and elastic strain corresponding to undamaged material ε_{oc}^{el} according to figure 3.12.

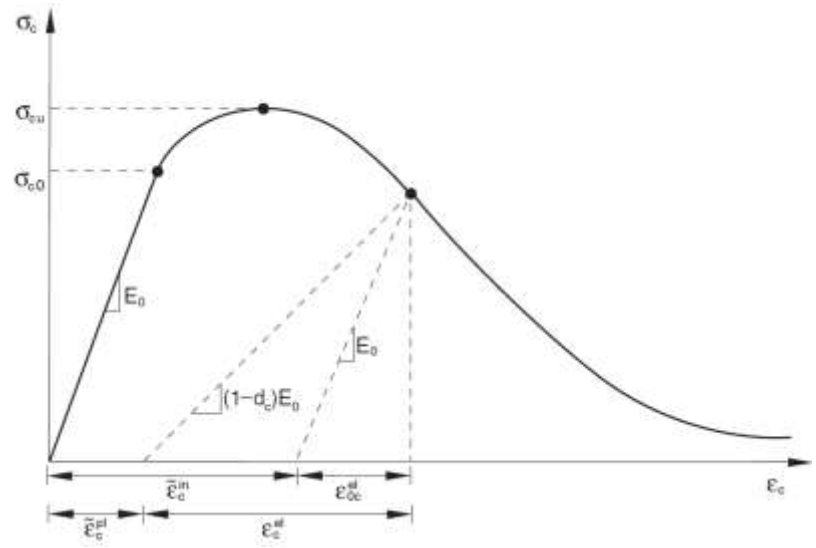

Figure 3.12: Definition of compression hardening data (Abaqus, 2010)

In summary, the implementation of concrete damaged plasticity model in Abaqus requires a sound provision of the parameters that define the behavior of concrete under multiaxial stress state and the description of concrete in uniaxial compression and tension.

A number of researchers including among others Obaidat *et al*. (2010), Baldivin (2010), Chaudhari & Chakrabarti (2012), Omidi and Lotfi (2010) and Shastri (2010), have implemented concrete damaged plasticity model in Abaqus and the results of their studies were in good agreement with experimental findings showing the capability of the model to represent the nonlinear behavior of concrete. Therefore, the model could be extended to reinforced concrete beams patch repaired and strengthened with FRP. This is done in this study. It is useful to note that none of the above researchers considered the effect of patch repair as another additional material.

3.2.1.1.5. Concrete cracking modeling

Concrete material is characterized by its high compressive strength and low tensile strength which, when it is exceeded results in concrete cracking leading to complete collapse. Thus, concrete cracking is a crucial aspect to be considered carefully in any design related to reinforced concrete structures. Concrete cracking is a design limiting factor in some structures like liquid retaining structures. It has been noted in the previous sections that concrete cracking is caused by damage which promotes the propagation and coalescence of micro cracks that already exist in concrete even before the application of external loading. From numerical point of view, cracking of concrete introduces discontinuities in the FE mesh.

Currently, cracking of concrete in finite element can be modeled through discrete crack or fictitious crack approach and smeared crack approach. It is important to note at this stage that the smeared crack may be fixed or rotating in the sense that its direction may be fixed just at the onset of cracking or may change the direction as the principle strain direction changes.

Discrete crack approach

In the discrete crack approach, it is assumed that cracking occurs by separation of nodal points initially occupying the same position and thus cracks are formed along the element boundaries as shown in figure 3.13a (Cevera and Chiumenti, 2006). Therefore the crack geometry strongly depends on the mesh. Discrete crack may be defined as a discontinuity in the displacement field. It is also necessary to note that discrete crack cerates mesh bias as seen in figure 3.13 (a&b).

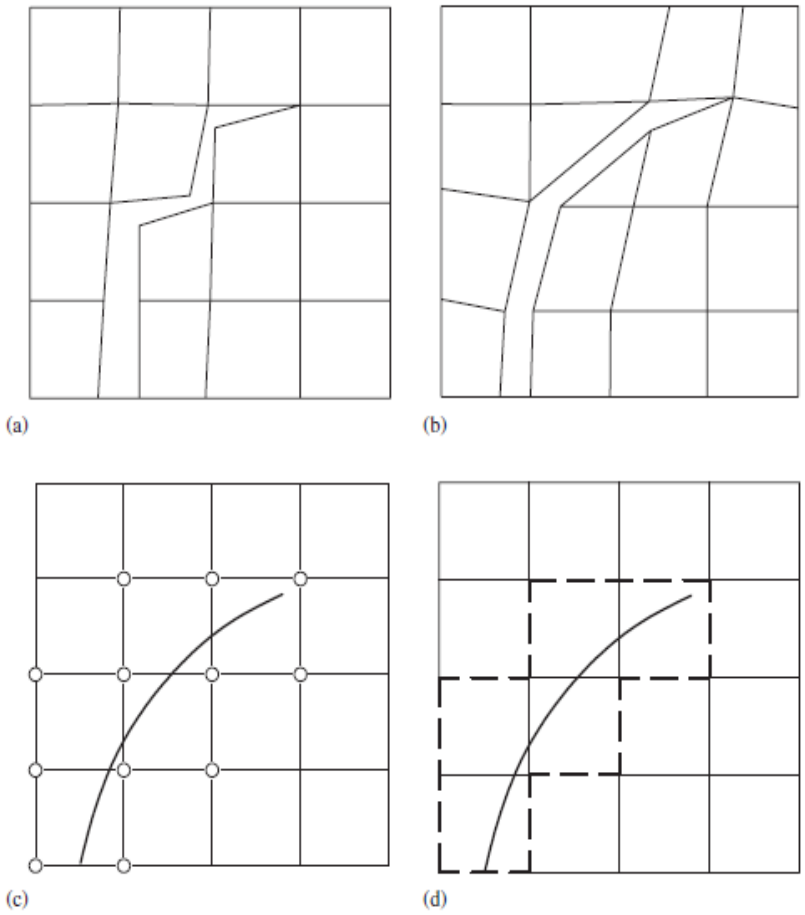

Figure 3.13: Discrete crack approaches to crack propagation (Cevera & Chiumenti, 2006)

By refining the mesh, i.e. introducing new elements that lie in the direction of crack, a better representation may be found (3.13b). However, remeshing is a tedious work in numerical implementation.

Belyschko and Black (1999) introduced a new method of modeling discrete crack independent of the mesh, i.e. without remeshing at the crack tip. They called the method extended Finite Element Method (XFEM) and can model both stationary and moving cracks. The method allows the presence of discontinuities, i.e. cracks in an element by enriching the degrees of freedom with special functions to capture the singularity around the crack tip and the jumps in the displacement field across the crack surface. See figure 3.13c and d. Discrete crack approach is suitable for problems that involve few dominant cracks to represent strain discontinuities (Kwak and Filippou, 1990).

Smeared crack approach

The approach considers cracked concrete as a continuum and captures the deterioration process by using a constitutive relationship and hence smears cracks over the continuum. Smeared crack represents many finely spaced cracks over the affected elements rather than representing a single crack as shown in figure 3.14.

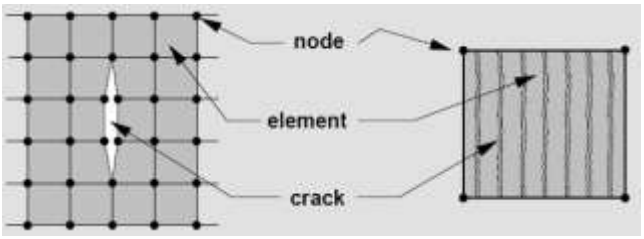

Figure3.14: Crack approaches: Discrete (left), Smeared (right) (Kwak &Filippou, 1990:25).

Smeared crack approach doesn‟t account for progressive cracking caused by the coalescence of micro cracks resulting in crack opening and hence concrete material doesn‟t remain as a continuum as initially assumed in smeared crack approach. Smeared crack models therefore do not account for discontinuities in the topology of the FE mesh (Cevera &Chiumenti, 2006).

In modeling concrete cracking, it is possible to represent the generation of discontinuities without touching the element by introducing discontinuities in it but rather operating at the material level. This is achieved by defining constitutive laws in the post failure regime, i.e. in the strain softening that will allow stresses over the affected elements to be released (Simonelli, 2005).

According to Asferg (2006) what is important for cracking in a concrete structure is not how cracking is initiated but how it will propagate. The growth of any crack requires the consumption of a certain amount of energy, thus, the crack propagation can only be studied through an energy based criterion. In this study the energy required to open a unit area crack, G_f as defined by Hillerborg et al. (1976) will be used. This energy is a material parameter. The model will assume a linear loss of strength after cracking as shown in figure 3.15.

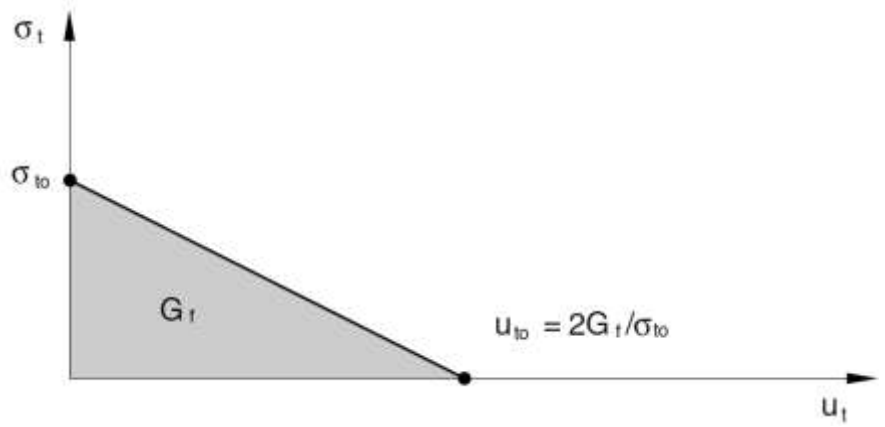

Figure 3.15: Post-failure stress energy curve (Abaqus, 2010)

3.2.2. Steel Reinforcement

Steel reinforcement used together with concrete is of small cross section as compared to the cross section of concrete, and can therefore be assumed to have only axial stiffness. Steel carries both tensile and compressive stresses. In a cracked concrete section, steel alone carries tensile stresses. On finite element analysis, steel is assumed to have the same response in both tension and compression, see figure 3.16 (Kwak &Filippou, 1990:36). Normally, a steel specimen under uniaxial tensile test exhibits initially a linear elastic portion, a yield plateau, a strain hardening range in which stress again increases with strain and finally, a range stress drops off until failure.

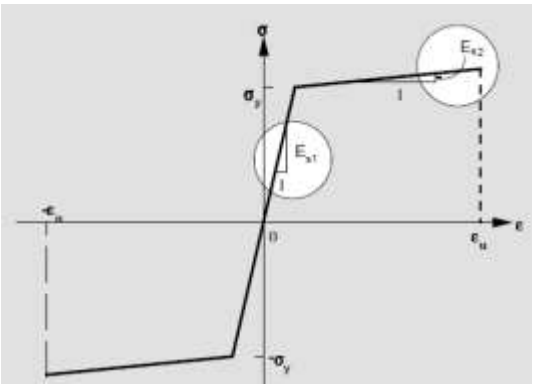

Figure 3.16: Bilinear stress strain curve of steel reinforcement.

However, in most studies this relation has been reduced to elastic-perfectly plastic as shown in figure 3.17.

This idealization was used by a substantial number of researchers in their finite element analyses (Chen et al. 2008; Hu et al. 2004; Chen et al.2011 and Obaidat et al. 2010). Linear elastic perfectly plastic model for steel is used in the present research project.

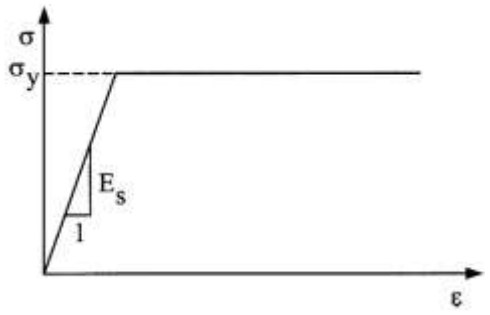

Figure 3.17: Elastic perfectly plastic model for steel reinforcement.

Representation of steel in finite element analysis of reinforced concrete structures has been done in three distinct ways: Discrete, embedded and distributed.

In discrete representation, steel reinforcement is modeled a separate element using one dimensional truss elements without rotational degrees of freedom; i.e. with only axial force carrying capacity. The compatibility of the displacements of the concrete and the steel is assured through the coincidence of steel elements with the boundaries of the concrete elements leading to the same order for the shape functions of concrete elements and truss elements (Simonelli, 2005). Bond slip and dowel action may be disregarded or considered implicitly by modifying the constitutive relations of concrete or steel.

One method of doing so in finite element is to define the tension stiffening through strain softening behavior of cracked concrete either by stress-strain relation or by applying a fracture energy cracking criterion. The discrete approach allows accounting for bond slip and dowel action directly, however it requires great effort for the discretization of the structure since each bar in the finite element has to be considered individually (Simonelli, 2005).

Alternatively, steel reinforcement can be embedded in concrete, i.e. incorporation of one dimensional element into two- or three-dimensional element. The embedded reinforcement elements are then superimposed onto the corresponding concrete elements (Simonelli, 2005).

This approach ensures a perfect bond between concrete and steel which is mostly assumed in the actual design of reinforced concrete structures. This method of modeling is adopted in this study.

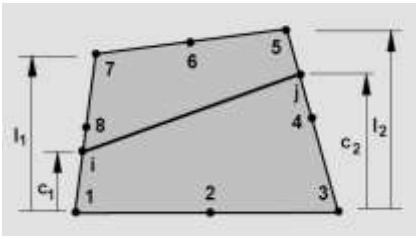

Figure 3.18: Embedded steel element *i-j* in 8-noded concrete element.

It can be seen from the figure that in embedded approach, reinforcing bars may pass through the concrete elements in arbitrary fashion.

Finally, steel reinforcement may be represented in a distribute way, whereby it is smeared over an element that is superimposed onto the main concrete element. For example, membrane elements with an eccentricity can be superimposed onto shell elements to model a layer of reinforcement.

3.2.3. Adhesive: Concrete/FRP Interface

The interface between concrete and FRP plates is usually made of an epoxy adhesive. The adhesive bonds the two adherents, i.e. concrete and FRP in order to develop full composite action and resists their separation up to its ultimate strength. Therefore, necessary amount of force will be applied before complete separation of the adherents. The epoxy is obtained by refinement of petroleum and when mixed with a hardener it results in epoxy adhesive widely used in FRP structural strengthening (Taljsten, 2006). The bond behavior between FRP and concrete is a key issue in the design of FRP strengthened reinforced concrete structures since in most of the cases the premature failure of debonding occurs in this interface. Therefore, it is necessary to understand its mechanical behavior and accurately predict its failure in order to capture the overall failure of the strengthened beam. From modeling point of view, this interface may be modeled as a perfect bond or it can be modeled based on cohesive zone model. In the present research project, the author will make use of cohesive zone model for the interface between concrete and FRP plate.

The modeling of epoxy adhesive for concrete/FRP interface should capture its mechanical behavior by considering its axial and shear stiffness. Cohesive elements available in Abaqus are used for this purpose. A cohesive element is thought as being composed of two faces separated by a thickness in which the relative motion of both faces along the thickness direction represents opening or closing of the interface and the relative change in position of bottom and top faces measured in the plane orthogonal to the thickness represents the transverse shear behavior of the cohesive element. See figure 3.19 below.

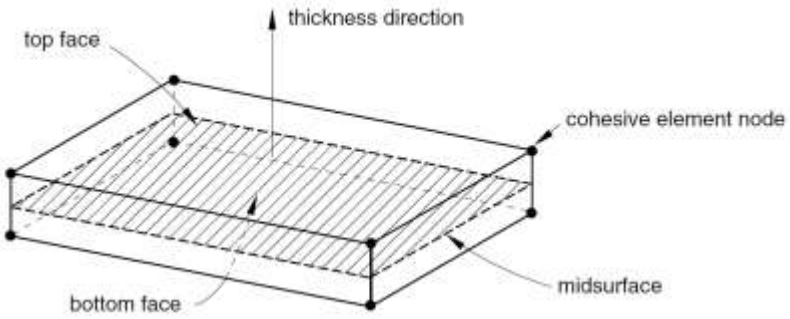

Figure 3.19: Spatial representation of a 3-D cohesive element (Abaqus, 2010)

The response of cohesive elements may be continuum if the thickness is finite where the macroscopic material properties such as stiffness and strength of cohesive elements can be used or traction at the interface versus relative motion across the interface. The latter will be used in the present research project since the thickness of the adhesive is relatively small. The response of cohesive elements in terms of traction separation assumes a linear elastic traction separation law prior to damage and a damage evolution law after peak.

The failure of the cohesive zone is characterized by a progressive stiffness degradation driven by a damage process. As discussed by Joannes and Renard (2009), the adhesive layer may be thought as an idealized interfacial surface material consisting of an upper and lower surface connected by a continuous distribution of normal and tangential springs and possible failure types are shown in figure 3.20.

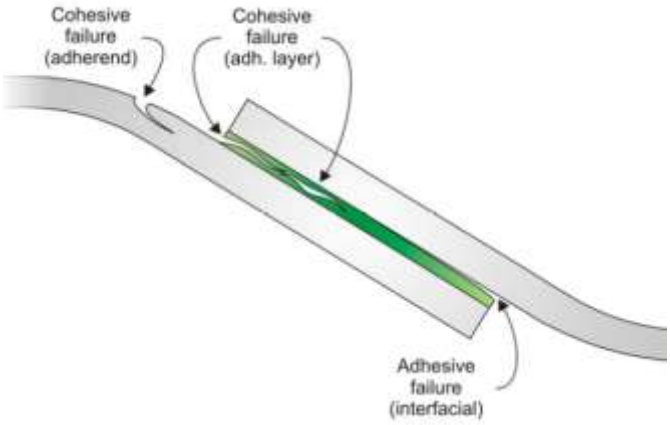

Figure 3.20: Fracture types of an adhesive joint.

The general framework for modeling of cohesive elements requires the definition of a damage initiation criterion, a damage evolution law and a choice of element removal or deletion upon reaching a completely damaged state, see figure 3.21. In the elastic traction separation approach, the elastic behavior is represented by the following relationship according to Abaqus user manual (2010):

$$t = \begin{Bmatrix} t_n \\ t_s \\ t_t \end{Bmatrix} = \begin{bmatrix} K_{nn} & K_{ns} & K_{nt} \\ K_{ns} & K_{ss} & K_{st} \\ K_{nt} & K_{st} & K_{tt} \end{bmatrix} \begin{Bmatrix} \varepsilon_n \\ \varepsilon_s \\ \varepsilon_t \end{Bmatrix} = K\varepsilon \qquad (3.34)$$

where t is the traction stress vector consisting of three components representing a normal and two shear tractions and ε is a strain vector. K represents the interface stiffness and is determined as the ratio of the modulus of elasticity of the adhesive material and its thickness in the respective direction. According to Daudeville *et al.* (1994), the interface stiffness will reduce to zero for complete debonding and will be equal to infinity for perfect bond.

The relationship represented by expression 3.34 stands for fully coupled behavior between normal and shear components. For uncoupled behavior, the off-diagonal terms must be set to zero.

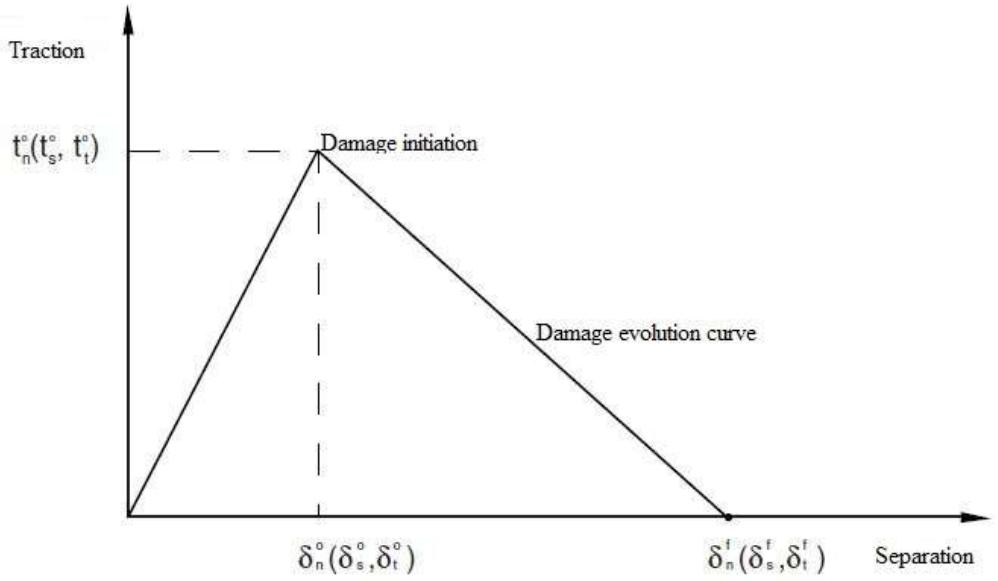

Figure 3.21: Bilinear traction separation law.

The initiation of damage in Abaqus may be defined based on a number of criteria including maximum nominal stress criterion, maximum nominal strain criterion, quadratic nominal stress criterion, and quadratic nominal strain criterion.

In the present study, the maximum nominal stress criterion will be used. It states that damage initiates when the maximum nominal stress ratio reaches a value of one and it is written as (Abaqus, 2010):

$$\max\left\{\frac{\langle t_n\rangle}{t_n^o},\frac{t_s}{t_s^o},\frac{t_t}{t_t^o}\right\}=1 \tag{3.35}$$

The Macaulay bracket $\langle\ \rangle$, has its usual meaning of describing rump functions, t_n^o, t_s^o and t_t^o represent the peak values of the nominal stress when the deformation is either purely in normal or purely in the first or second shear direction. Damage evolution for cohesive elements, i.e. the rate at which the degradation of stiffness occurs in Abaqus is modeled using mesh-independent measures such as plastic displacement and physical energy dissipation. The damage is governed by a damage parameter *D* which is equal to zero for undamaged material and equal to one for completely damaged material and considers normal and two shear directions. Thus, it is useful to consider interaction between normal and shear directions.

In Abaqus, two approaches are used for such interaction and include energy and traction approaches. For the purpose of the present study, the traction approach will be used to account for both normal and shear deformations.

According to Abaqus user manual (2010), two ingredients are of great importance in the definition of damage evolution in Abaqus software. Those are effective displacement at complete failure and energy dissipated due to failure of cohesive elements. Here the energy dissipated due to failure will be used. It can be defined in terms of linear or exponential softening laws or in terms of the damage parameter D defined directly as a tabular function of the effective displacement relative to the effective displacement at damage initiation. Linear softening type will be used.

3.2.4. Fiber Reinforced Polymer material

Fiber Reinforced Polymers (FRP) composites are made of high strength fibers embedded in a polymer resin also called the matrix. FRP material is a composite material defined according to Hull & Clyne (1996) as a material containing two or more integrated constituent materials with each material keeping its own identity. There is a distinct interface between the fibers and the matrix which makes each constituent to retain its physical and chemical identity, but they produce a combination of properties that cannot be achieved with either of the constituents alone (Gunes, 1994). Fibers are the main stress carrying components while matrix binds them together and protects them in addition to carrying stresses in the transverse direction. There are basically three types of fibers that are currently in use. They include glass, aramid and carbon fibers. The matrix may be polyester, vinyl ester and epoxy. The epoxy is mostly used due to its better mechanical properties and durability (Taljsten, 2006).

The arrangement of fibers may be random within the material but it is also possible to arrange them so that they are oriented in the directions expected to have the highest stresses and in such case the composite is termed as anisotropic, i.e. with different properties in different direction. When fibers are oriented only in one direction, the composite is termed as isotropic which are more suitable for use in strengthening for bending since the strength in longitudinal direction is of interest.

FRP materials behave in a linear elastic-brittle manner, i.e. the behavior is linear elastic up to failure and figure below compares the stress strain relationship for different types of carbon fiber reinforced polymers (CFRP) manufactured by Sika.

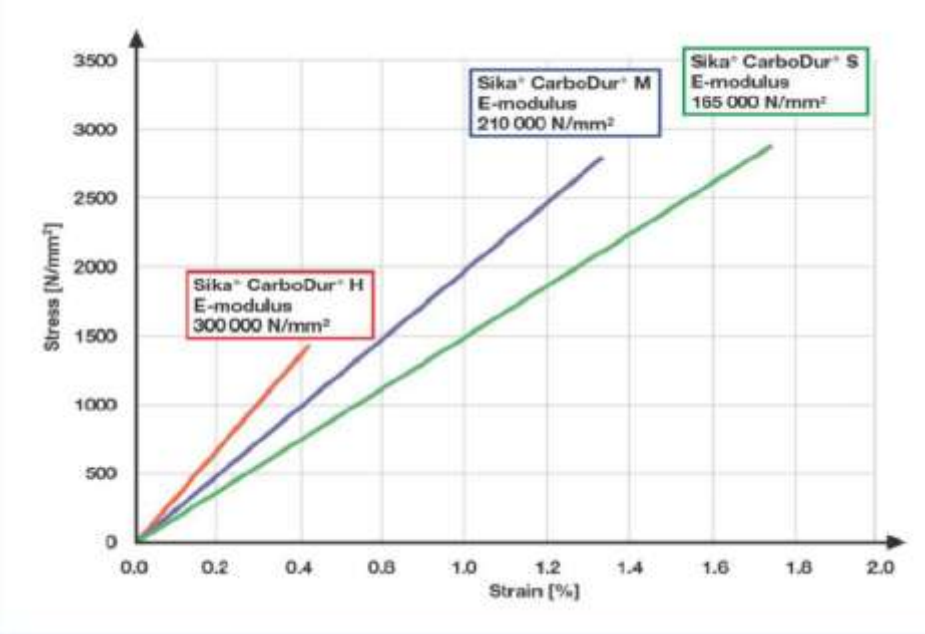

Figure 3.22: Stress strain relation for CFRP (Sika)

In case of isotropic composite like those used in the present study (Sika CarboDur S), the stiffness in the fiber direction is obtained using the rule of moisture (Roylance, 2000) as:

$$E = V_f E_f + V_m E_m \tag{3.36}$$

with V_m matrix volume fraction, V_f volume fraction of fibers and E_m and E_f the corresponding modulus of elasticity. It is clear that the properties of the FRP composite largely depend on the proportion of the constituents and the relationship between them.

3.3. Summary

Finite elements method is among different numerical methods used to solve a wide range of complex engineering problems. It consists of subdividing a complex structure or components into finite elements and solves for each element to find the response field of interest with relatively high accuracy.

However, for the method to be successful, it is necessary for the user to have a thorough understanding of the behavior of different materials involved in the physical problem and the interaction between them. This chapter presents the nonlinear response of concrete and its cracking mechanisms. Plasticity concepts are also considered in an effort of capturing the behavior of concrete in compression under multiaxial stress state. The behavior of reinforcing steel is idealized as elastic perfectly plastic and methods of modeling its interaction with concrete are reviewed.

The interface between concrete and FRP composite constitutes a major component in the overall behavior of reinforced concrete strengthened with fiber reinforced polymer materials in terms of premature debonding that was found to take place in the adhesive layer, at the bond line between the adhesive and FRP or even in the concrete cover along the rebar. Techniques of capturing debonding mechanisms are discussed. Lastly, consideration is given to the linear elastic brittle response of the FRP material. The above material behavior and interactions between them constitute a basis for finite element modeling of reinforced concrete beams patch repaired and strengthened with fiber reinforced polymers as fully discussed in chapter three of this thesis.

Chapter 4

METHODOLOGY: FINITE ELEMENT MODELING

4.1. Introduction

Bonding fiber reinforced polymer plates bonded to the tension face of deteriorated and deficient reinforced concrete beams is a promising method of restoring the load carrying capacity of such beams. While a large number experimental tests have been done by various researchers over the past decades to investigate the behavior and modes of failure of reinforced concrete beams strengthened with FRP composites, numerical studies are still lacking. Numerical methods for the analysis of reinforced beams retrofitted with FRP materials is done based on commercially available finite element software packages such as ABAQUS, ANSY, LUSAS, etc. ABAQUS was used in this project. The modeling space in Abaqus may be 1D, 2D, or 3D. The strengthened reinforced concrete beams under this investigation were modeled in three dimensional space though some components like steel reinforcements were modeled in one dimensional space.

Finite elements methods consist of discretizing the actual geometry of the structure into a collection of finite elements where each finite element represents a discrete portion of the physical structure. In Abaqus finite elements are joined by shared nodes and a collection of such nodes and finite elements constitutes the mesh. It is important to note at this stage that the user can discretize the geometry into finer mesh with a relatively high number of elements or coarse mesh when he makes use of fewer elements and this affects the accuracy of the solution. After assigning material properties to finite elements, the solution consists of finding quantities of interest at the nodes, then for the whole element and finally for the whole structure. In this study, nodal displacements are of interest from which stresses and strains for each element can be obtained and hence the overall behavior of the beam can be predicted. In the present study a number of assumptions for materials and interactions between them will be made.

In this research project, different finite element models were developed for control beam, i.e. unrepaired and unstrengthened and for various patch repair lengths such as 450mm, 800mm, 1300mm and 1800mm. The following diagram describes different steps that were followed from model development to visualization of analysis outputs.

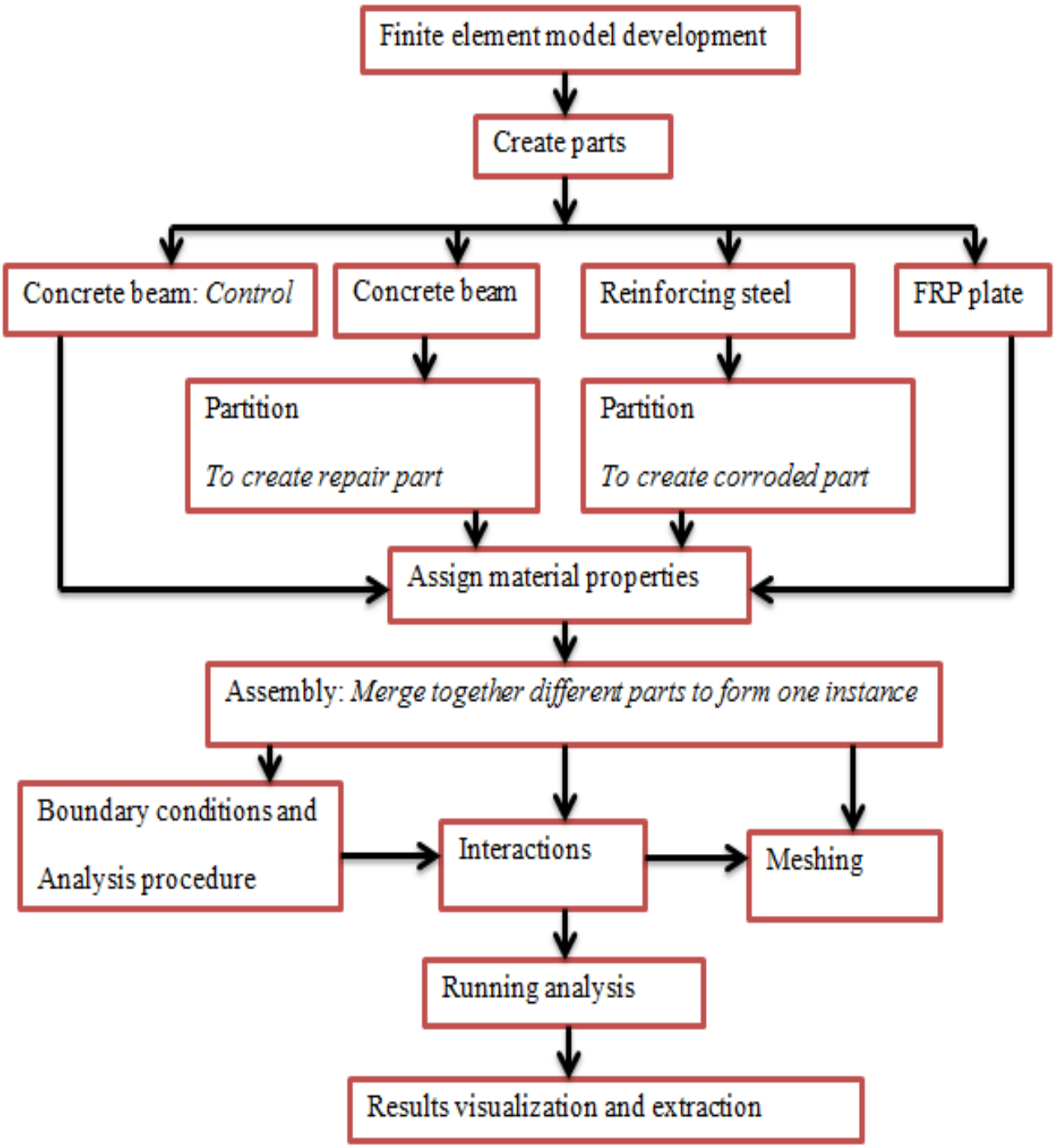

Figure 4.1: Finite element models development.

4.2. Reinforced concrete beam geometry and model construction

The main objective of this study is to investigate numerically the behavior of reinforced concrete beams patch repaired and strengthened with FRP plates. The geometry of the beam ($2000mm * 155mm * 254mm$) for which finite elements models are developed is shown in figure 4.1. The figure also shows the reinforcement details.

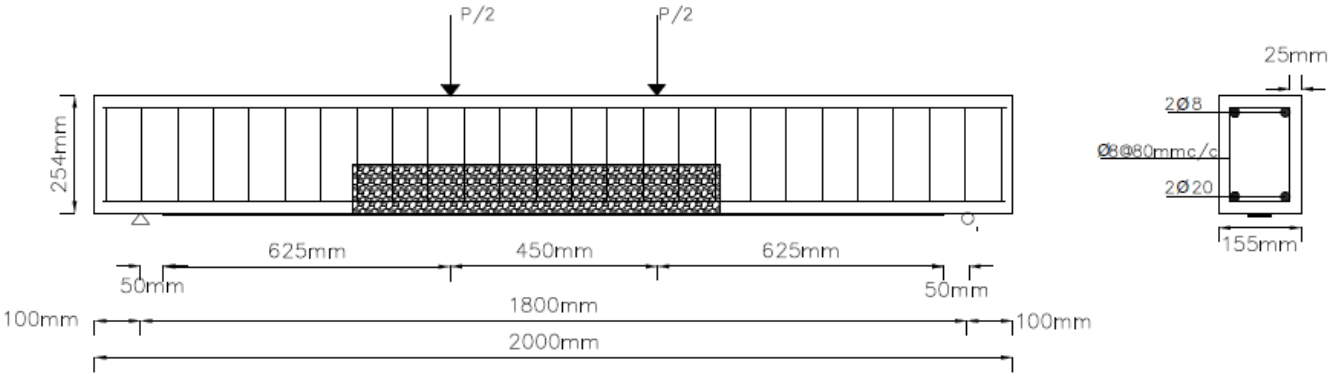

Figure 4.2: Geometry and reinforcement details of the modeled beam.

All parts making up the model were created in Abaqus CAE, which is the graphical user interface in which we create models, submit jobs, monitor the analysis and evaluate the results. Any part in Abaqus was created from a particular base feature, which contains geometry information and any rules governing the behavior of the geometry. That means that all parts created were native parts, i.e. they were not imported from other pre-processing softwares. In Abaqus, the beam geometry was created as a 3D deformable solid part and is shown in figure 4.2. The figure shows the beam with 450mm patch repair. Since there is a perfect bond between concrete and epoxy, the beam was partitioned at its bottom to create the adhesive part. This will in addition ensure mesh continuity between concrete and adhesive. The beam was again portioned to create a region representing the patch repair. However, for the control beam the partition was only done for the definition of the loading area.

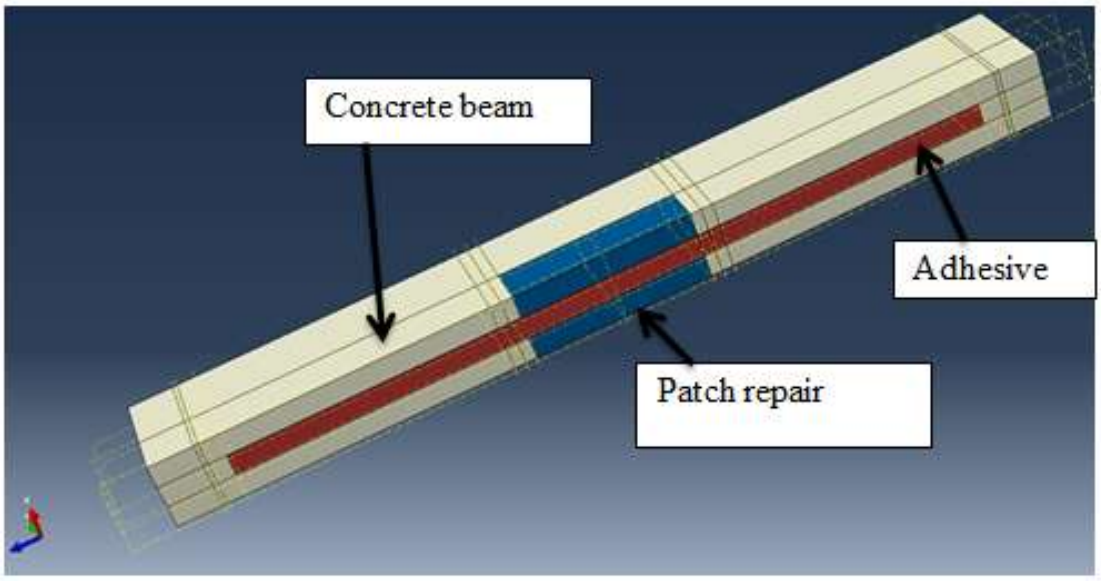

Figure 4.3: Concrete beam created and partitioned in Abaqus.

In a similar way, concrete beams with various patch repair lengths were created. Those were having patch length of 800mm Figure 4.3(a), 1300mm, Figure 4.3(b) and 1800mm, Figure 4.3(c); all shown in 2D for the purpose of localizing the patched area. To complete the model construction steel reinforcing bars were also created using wire features and FRP plate was created using solid feature. The created parts are shown in figure 4.3(d), for compression steel; 4.3(e) for portioned tension steel, 4.3(f) for vertical stirrup and 4.3(g) for FRP plate. It is useful to note that tension steel was partitioned to model the reduction in the steel cross section due to corrosion. Thus, steel was portioned to a length equal to the patch repair length for each case. Different portions thus created will be assigned different cross sections.

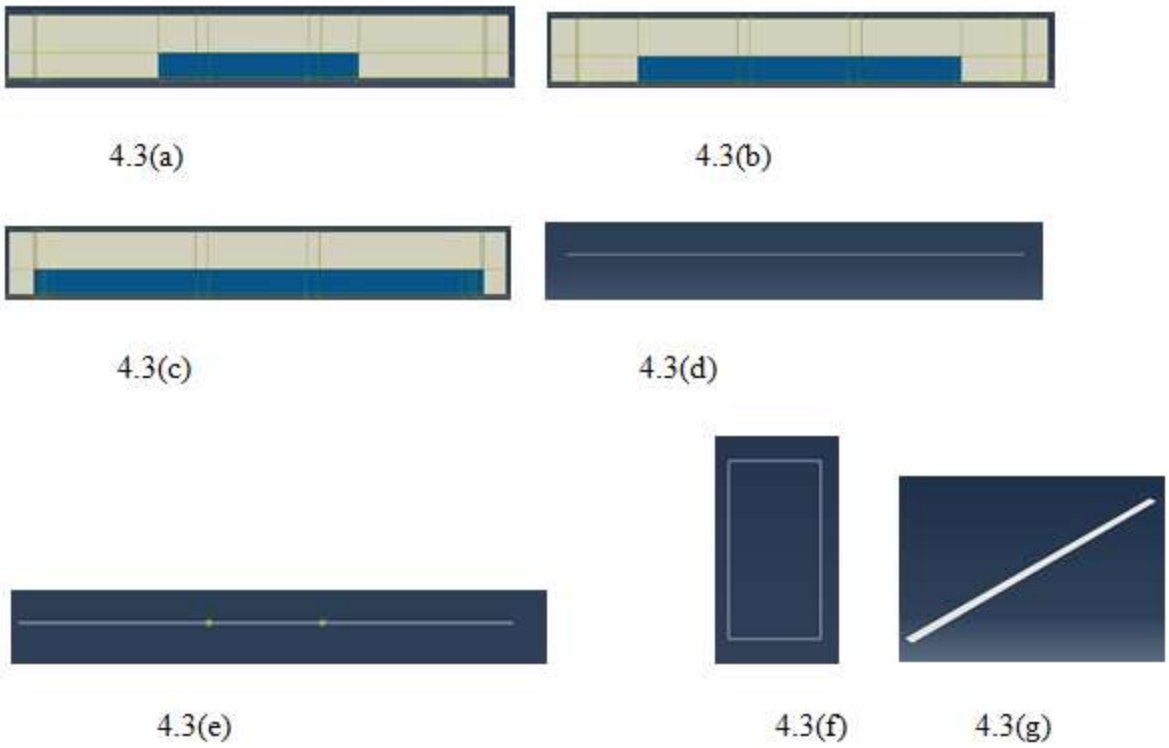

Figure 4.4: Parts created in Abaqus.

4.3. Material properties definition and assignment.

For a finite element model to be successful, it is necessary that material behavior be predicted as accurate as possible. This requires a sound selection of the constitutive relations. In this section, various constitutive relationships that were used to get the necessary input data for each material involved are presented.

4.3.1. Concrete

As discussed in section 3.2.1.1.4, concrete behaves as a plastic material when it is subjected to multiaxial stress state. At the same time, its elastic properties get damaged due to concrete cracking and crushing which leads to stiffness degradation. From these reasons, in this study the constitutive behavior of concrete was done using concrete damaged plasticity model in Abaqus.

The implementation of this model in Abaqus requires the definition of the behavior of concrete in both uniaxial tension and compression from which damage parameters can be derived.

4.3.1.1. Constitutive behavior of concrete in compression

Concrete used in this research was tested in the lab and was found to have cube strength after 28 days of 50MPa. Similarly, the patch material was having cube strength of 70MPa. The following other properties were also defined for both concrete and patch material:

Table 4.1: Concrete and repair material properties.

Property name	**Concrete**	**Repair material**
Compressive strength ($f_{ck,cube}$)	50MPa	70MPa
Mean compressive strength(f_{cm})	48Mpa	65MPa
Secant modulus of elasticity(E_{cm})	35000MPa	38400MPa
Mean tensile strength (f_{tm})	3.5MPa	4.3MPa
Fracture energy (G_f)	0.08N/mm	0.15N/mm
Poisson‟s ratio (υ)	0.2	0.2

Except the compressive strength that was measured in the lab, the fracture energy taken in the interval above and assumed Poisson‟s ratio; other properties were derived according to BS EN 1992-1-1 (Eurocode 2, 2004: 33, 3.1.5). The nonlinear response of both concrete and repair material shown in figure 4.4 and 4.5 was determined using the relationship given in BS EN 1992-1-1 (Eurocode 2, 2004: 33, 3.1.5) as discussed in section 3.2.1.1.1 and rewritten here for convenience as:

$$\frac{\sigma_c}{f_{cm}} = \frac{k\eta - \eta^2}{1+(k-2)} \qquad (4.1)$$

where $\eta = \frac{\varepsilon_c}{\varepsilon_{c1}}$, with ε_{c1} the strain at peak stress and given by $\varepsilon_{c1} = 0.7 f_{cm}^{0.31} \leq 2.8‰$. The strain in concrete is ε_c and $k = 1.05 \frac{|\varepsilon_{c1}|}{f_{cm}}$. This expression provides the basis for input data in Abaqus to describe the compressive behavior of both concrete and repair material.

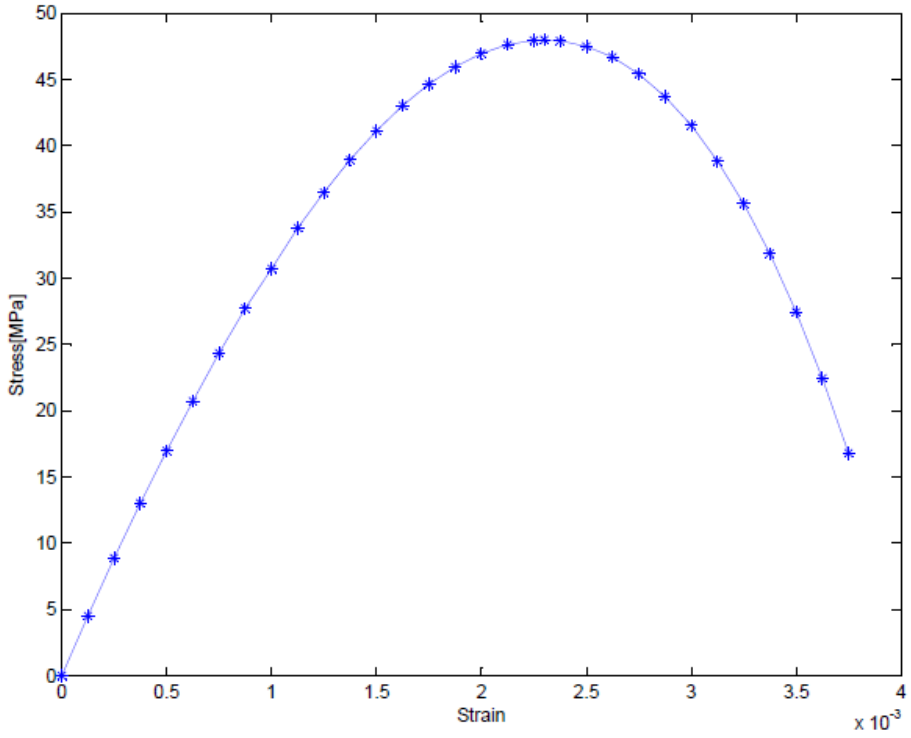

Figure 4.5: Nonlinear response of concrete under uniaxial compression.

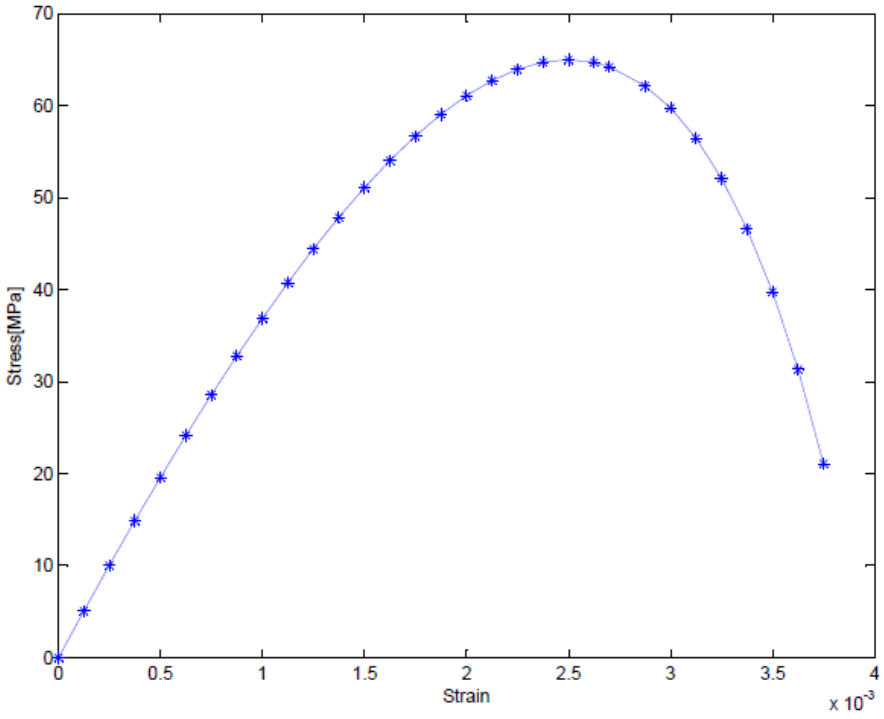

Figure 4.6: Nonlinear response of repair material under uniaxial compression.

The implementation of concrete damaged plasticity requires the inelastic strains to describe the compressive behavior of concrete. The inelastic strains were calculated for both concrete and repair material from the star values of figures 4.4 (a) and (b) as the total strain minus the elastic strain corresponding to the undamaged material according to (Abaqus, 2010):

$$\varepsilon^{in} = \varepsilon_c - \frac{\sigma_c}{E_0} \tag{4.2}$$

where E_0 is the undamaged modulus of elasticity of concrete and repair material. According to the above expression, the values that were used as input in Abaqus are shown in table 4.2.

Abaqus will convert the inelastic strains into plastic strains that are compatible with the present model. Thus, the uniaxial relationships will provide the hardening variables which are needed in this model as previously discussed in section 3.2.1.1.4.

Table 4.2: Stress strain values used as input in Abaqus for compressive behavior.

(a) Concrete

Yield stress[MPa]	Inelastic strain
19.2	0.00E+00
20.72	3.30E-05
24.35	5.43E-05
27.71	8.33E-05
30.72	1.22E-04
33.81	1.59E-04
36.48	2.08E-04
38.95	2.62E-04
41.13	3.25E-04
43.04	3.95E-04
44.65	4.74E-04
45.96	5.62E-04
46.98	6.58E-04
47.64	7.64E-04
47.96	8.80E-04
48.00	9.29E-04
47.93	1.01E-03
47.51	1.14E-03
46.71	1.29E-03
45.42	1.45E-03
43.72	1.63E-03
41.56	1.81E-03
38.84	2.02E-03
35.64	2.23E-03
31.88	2.46E-03
27.44	2.72E-03
22.45	2.98E-03
16.79	3.27E-03

(b) Repair material

Yield stress[MPa]	Inelastic strain
26	0.00E+00
28.56	6.25E-06
32.8	2.08E-05
36.87	3.98E-05
40.75	6.38E-05
44.43	9.30E-05
47.88	1.28E-04
51.09	1.70E-04
54.05	2.17E-04
56.71	2.73E-04
59.07	3.37E-04
61.08	4.09E-04
62.73	4.91E-04
63.95	5.85E-04
64.73	6.89E-04
65.00	8.07E-04
64.71	9.40E-04
64.24	1.03E-03
62.17	1.26E-03
59.76	1.44E-03
56.45	1.65E-03
52.11	1.89E-03
46.61	2.16E-03
39.75	2.46E-03
31.34	2.81E-03
21.08	3.20E-03

The calculated plastic strains must not be negative and or decreasing with increasing inelastic strains; otherwise Abaqus will issue an error message. Abaqus converts inelastic strains into plastic strain according to the following formula given in Abaqus user manual (2010):

$$\varepsilon^{p} = \varepsilon^{in} - \frac{D_c}{(1-D_c)}\frac{\sigma_c}{E_0} \tag{4.3}$$

where σ_c is concrete compressive strength and D_c is a scalar stiffness degradation variable in compression. The characterization of the post-peak behavior, i.e. beyond the ultimate stress (48MPa for concrete and 65MPa for repair material) in compression was done in terms of inelastic strains and stiffness degradation variable in compression. This was aimed at describing the irreversible damage that would occur during strain softening. The compressive scalar degradation variables D_c along the descending portion of the stress-strain curve were calculated according to: $D_c = 1 - \frac{\sigma_c}{f_c}$ (4.4)

where σ_c the stress on the descending portion of the curve and f_c is the peak compressive stress. Table 4.3 gives the tabular form of data that served as input in Abaqus for the strain softening regime.

Table 4.3: Concrete compression damage input data.

(a) Concrete

Damage Parameter	Inelastic strain
0.00E+00	0.00E+00
1.46E-03	1.01E-03
1.02E-02	1.14E-03
2.69E-02	1.29E-03
5.38E-02	1.45E-03
8.92E-02	1.63E-03
1.34E-01	1.81E-03
1.91E-01	2.02E-03
2.58E-01	2.23E-03
3.36E-01	2.46E-03
4.28E-01	2.72E-03
5.32E-01	2.98E-03
6.50E-01	3.27E-03

(b) Repair material

Damage Parameter	Inelastic strain
0.00E+00	0.00E+00
4.46E-03	9.40E-04
1.17E-02	1.03E-03
4.35E-02	1.26E-03
8.06E-02	1.44E-03
1.32E-01	1.65E-03
1.98E-01	1.89E-03
2.83E-01	2.16E-03
3.88E-01	2.46E-03
5.18E-01	2.81E-03
6.76E-01	3.20E-03

4.3.1.2. Constitutive behavior of concrete in tension

The behavior of concrete under uniaxial tension was described by a linear elastic response prior to cracking; that is before the ultimate tensile strength of concrete was reached

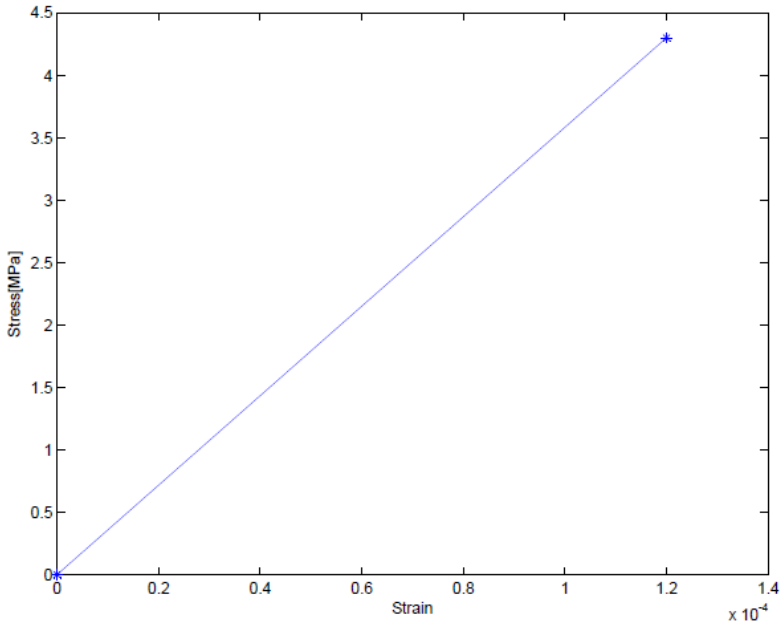

Figure 4.7: Response of concrete under uniaxial tension.

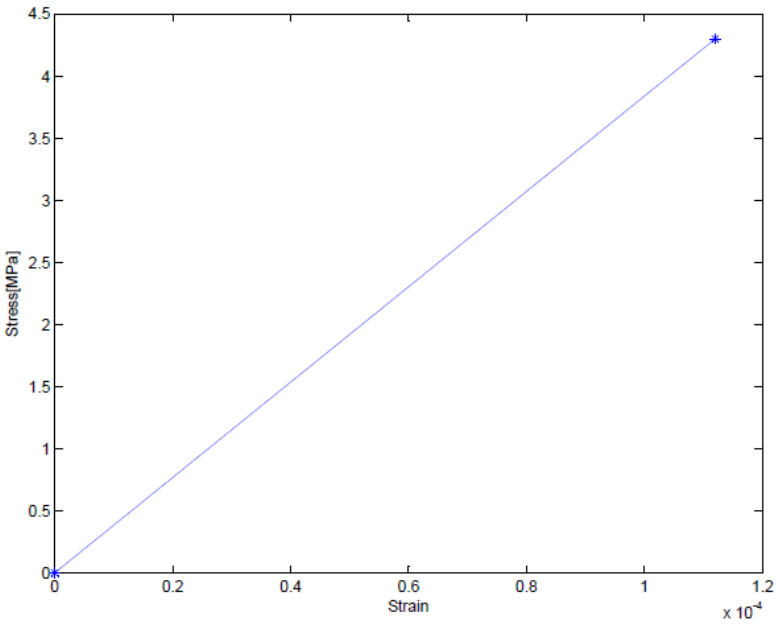

Figure 4.8: Response of repair material under uniaxial tension.

Figure 4.6 and 4.7 show the linear elastic behavior for both concrete and repair material and the values that were used as input for tensile behavior in Abaqus.

However, Abaqus requires the cracking strain versus yield stress. Therefore, those data were provided knowing that the cracking strain at the onset of cracking is zero and that the total strain is $\varepsilon_{cr} = f_{tm}/E = 0.0001$ for concrete and 0.00012 for repair material. Table 4.4 shows the values that were used as input in Abaqus for the description of the tensile behavior of concrete and repair material. In the present constitutive model for both concrete and repair material under uniaxial tension, the post-cracking behavior was described as a function of stress and cracking strain. As for the case of uniaxial compression, cracking strain was found by taking the total strain minus the elastic strain corresponding to undamaged material (Abaqus, 2010). Formula 4.2 was again used but replacing compressive strain and stress by tensile strain and tensile stress respectively.

Table 4.4: Stress strain values used as input in Abaqus for tensile behavior.

(a) Concrete

Yield stress[MPa]	**Cracking strain**
3.50	0.00E+00
3.11	1.11E-04
2.72	2.22E-04
2.33	3.33E-04
1.95	4.44E-04
1.56	5.55E-04
1.17	6.67E-04
0.78	7.78E-04
0.39	8.89E-04
0.00	1.00E-03

(b) Repair material

Yield stress[MPa]	**Cracking strain**
4.30	0.00E+00
3.91	9.82E-05
3.42	2.11E-04
2.93	3.24E-04
2.44	4.36E-04
1.95	5.49E-04
1.46	6.62E-04
0.98	7.74E-04
0.49	8.87E-04
0.00	1.00E-03

The strain softening behavior presented in table 4.4 is also known as tension stiffening effect for cracked concrete. The strain type of stiffening was used in this study. One of the methods used to describe tension stiffening as used here is to assume that the strain softening after failure reduces the stress linearly to zero at a total strain of about ten times the strain at failure (Abaqus 2010).

In this study, a total strain of 0.001 when stress reduces to zero was adopted as can be seen in table 4.4.

It was said before that the elastic stiffness of concrete get degraded due to both compression and tension. However, the effect is less for the case of compression since cracking runs in a direction parallel to the principal compressive stress. Stiffness degradation in tension was described in the same way as for compression. Tensile damage variables were calculated using equation 4.4 by replacing the compressive stresses by tensile stresses. Thus, the data for concrete tensile damage were provided in terms of tensile damage parameter and cracking strain as presented in table 4.5.

Table 4.5: Concrete tension damage input data.

(a) Concrete

Damage Parameter	Cracking strain
0.00E+00	0.00E+00
1.11E-01	1.11E-04
2.23E-01	2.22E-04
3.34E-01	3.33E-04
4.43E-01	4.44E-04
5.54E-01	5.55E-04
6.66E-01	6.67E-04
7.77E-01	7.78E-04
8.89E-01	8.89E-04

(b) Repair material

Damage Parameter	Cracking strain
0.00E+00	0.00E+00
9.07E-02	9.82E-05
2.05E-01	2.11E-04
3.19E-01	3.24E-04
4.33E-01	4.36E-04
5.47E-01	5.49E-04
6.60E-01	6.62E-04
7.72E-01	7.74E-04
8.86E-01	8.87E-04

The above data provided as input to Abaqus describe the uniaxial tensile and compressive behavior of concrete and repair material. However, those two materials as used in reinforced concrete beams are subjected to multiaxial stress states as discussed in the previous sections. To complete the definition of the concrete damaged plasticity taking into account multiaxial stress states, it was necessary to provide Abaqus with parameters that define the plasticity of concrete, i.e. the yield criterion and flow rule in the effective stress space. Hardening parameters will be determined by Abaqus according to equation 4.3. These parameters will account for multiaxial effective stress state for concrete in three dimension space. Generally, five parameters govern such a behavior for both concrete and repair material. The values assigned to those parameters are reported in table 4.6.

Table 4.6: Plasticity parameters for concrete and repair material

Parameter name	Assigned value
Dilatation angle (ψ)	37^0
Eccentricity $(\in)$	0.1
Ratio of initial equibiaxial yield stress to initial uniaxial compressive stress (f_{b0}/f_{c0})	1.16
Ratio of the second stress invariant on the tensile meridian to that of compressive meridian (K)	0.67
Viscosity parameter (μ)	0.01

Except the dilatation angle that was chosen according to Kmiecik & Kaminski (2011), other parameters were taken as default values as recommended by Abaqus user manual (2010). It is also important to remind at this stage that a perfect bond between concrete and repair material was assumed in the present finite element analysis.

The above material properties were assigned to concrete beam and repair through solid homogeneous section type that were created in the property module of Abaqus.

4.3.2. Reinforcing steel

As discussed in section 3.2.2, steel was modeled as a bilinear elastic perfectly plastic material embedded in concrete. The cross section of tensile steel reinforcement was reduced by 10% over a length equal to the patched length to emulate the loss in steel cross section that occurs due to corrosion over the damaged portion of the beam. Therefore, steel was portioned and the corroded portion was assigned a section $282.6mm^2$ whereas the non-corroded part was assigned a cross section of $314\,mm^2$.

The total length of steel was $1950mm$ accounting for a cover of $25mm$ on either end. The yield stress used for both tension and compression steel was $460MPa$, the modulus of elasticity was $200GPa$ while the Poisson"s ratio was taken as 0.3.

Steel stirrups were also modeled using the same constitutive relationship. No interaction was considered between longitudinal and transversal steel, instead both were embedded in concrete. While the elastic modulus and the Poisson"s ratio for stirrups were the same as for longitudinal steel, the yield stress used was $250MPa$. Truss section type under the beam category in the section menu of the property module was created through which the above properties were assigned to both longitudinal and transversal reinforcements.

4.3.3. Epoxy/Concrete FRP interface

The interface between concrete and FRP material was modeled using cohesive zone model. A layer of $1mm$ representing the epoxy was created by portioning the bottom of the beam which was created with a total depth of $255mm$ instead of $254mm$. The cohesive section type was used and traction separation response was selected. This type of response was discussed in details in section 3.2.3. The elastic-traction type was used to accommodate the traction separation response. The normal stiffness K_{nn} was determined as the ratio of the elastic modulus of elasticity and the thickness of the adhesive layer. Similarly in the two shear directions, the shear stiffness was determined as the ratio of shear modulus and the thickness. Thus the values used to define the elastic-traction type are shown in table 4.7.

The initiation of damage was defined in terms of nominal stresses where the nominal stress in normal direction was $4MPa$ equal to bond strength and the nominal stress in the first and second direction was $15MPa$ as specified by the manufacturer.

Table 4.7: Elastic-traction type for epoxy

E/K_{nn}	G_1/K_{ss}	G_2/K_{tt}
1	1	1

The damage evolution was described in terms of displacement with a linear softening.

4.3.4. FRP Material

Fiber reinforced polymer is a composite material that may be made of fibers oriented in different directions. Therefore FRP in Abaqus should be modeled as a linear elastic orthotropic material. However, for the case of strengthening of reinforced concrete beams, it is clear that the stresses are mainly tensile in the longitudinal fiber direction.

The FRP material considered in this study was unidirectional and the modulus of elasticity in the fiber direction was of great importance. Therefore, the carbon fiber reinforced polymer (CFRP) was modeled as a linear elastic isotropic material. Its modulus of elasticity was taken as $165GPa$ as specified by the manufacturer and the Poisson‟s ratio was taken as 0.3. These properties will ensure that CFRP behaves in a linear elastic manner up to rupture.

4.4. Model assembly.

Different parts created previously exist independently of each other in local coordinates system even though material properties were assigned to them. In Abaqus/CAE, each part is represented by what is known as part instance. For complete construction of the model it was necessary to assemble different part instances. This was done in the assembly module to position and orient different part instances relative to each other in the global coordinates system. Steel reinforcements were positioned in the beam with a cover of $25mm$ on all the sides. Strengthening was done by using one FRP plate applied in on the bottom center of the beam as was shown in figure 4.2.

Part instances created were concrete beam (including patch repair and adhesive layer), tension steel, compression steel, shear reinforcement and FRP plate. Since Abaqus/CAE allows the user to instance a part several times; tension steel was instanced twice and compression steel as well. Shear reinforcement was instanced twice and linear pattern option in the assembly module was used to arrange twenty four stirrups as shown in figure 4.8.

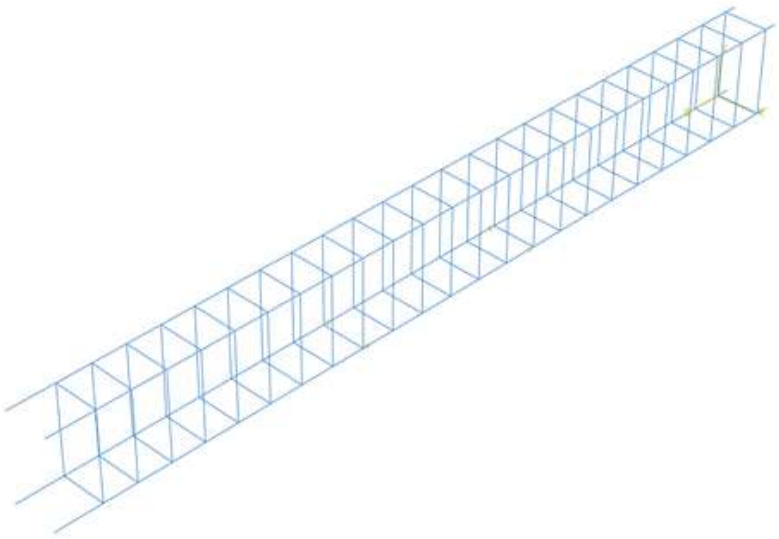

Figure 4.9: Reinforcement instances assembled in global coordinates system.

The assembly in figure 4.8 together with the remaining instances made up the whole model defined from different parts. Subsequent modeling tasks will be carried out on this assembly and hence on the whole model. Those include meshing, boundary condition definition, loading, requesting data output and the analysis itself.

Part instances created in the construction of the present finite element model were dependent instances as opposed to independent instances. A dependent instance is thought as a pointer to the original part it is representing. It only allows operations that do not change the geometry of the part to be performed. Since the present model comprised of 3D and 2D parts, dependent instances were chosen so that different parts could be meshed separately and different element types be assigned independently. In addition, dependent instances consume less memory and hence smaller input file (Abaqus, 2010). Other positioning tools that were used to bring together different part instances include the translate instance and rotate instance.

In the model definition two types of interactions were defined. The interaction between the FRP and the epoxy representing the interface was defined as a tie constraint. This will ensure that the two surfaces are bonded together permanently. Another constraint used was the embedded region to represent the interaction between concrete and reinforcing steel. This type of constraint ensures that there is no slip between the two materials, i.e. there is a perfect bond.

It removes the translational degrees of freedom of steel and makes them similar to those of concrete see figure 4.9. Figure also shows how reinforcements are embedded in concrete.

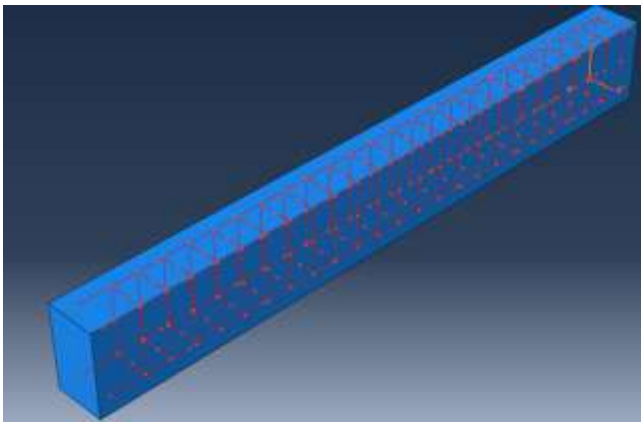

Figure 4.10: Embedded reinforcements.

The embedded constraint does not constrain rotational degrees of freedom, but fortunately reinforcing steel was modeled using truss elements with only translational degrees of freedom.

4.5. Loading and analysis procedure

Before load was applied to the model, it was necessary first to define steps in which both boundary conditions and loads will be active during the analysis. A step in Abaqus/CAE may be thought as functional unit which contains tools that were necessary for defining the history of the analysis. Aspects such as change in loading, requesting of output data and application of controls were performed under step. In this study only two steps were created. Initial step that is always created by default in Abaqus and one general analysis step. In this step the analysis procedure that was performed is static stress analysis. In this type of analysis, physical quantities such as inertia, creep and viscoelasticity were not considered. Step time as well as the necessary number of increments was specified since, the analysis is based on the Newton‟s method in solving nonlinear equilibrium equations. The direct linear equation solver using Gauss elimination method was adopted for the solution of the sets of nonlinear equations.

In the analysis step defined above two types of output data were requested and will be visualized later: filed output and history output. Field output data were requested for the model as a whole while history output data were requested for some parts or regions of the model.

History output data were for example support reaction, mid-span displacement and strain in FRP plate. However quantities such as damage energy release rate was requested for the whole model.

Boundary conditions that were applied to the present model consisted of two support reactions. One support reaction was pinned which will resist both vertical and horizontal forces but at the same allowing rotation. This was achieved by constraining all translational degrees of freedom, i.e. $u_1 = u_2 = u_3 = 0$. The other boundary condition was a roller support which was defined by only constraining translation in direction 1 and 3since the support itself allows horizontal translation, i.e. $u_1 = u_2 = 0$. To avoid concentrated deformations at the support, it was necessary apply the support at small area as shown in figure 4.10. The two boundary conditions were defined in the initial step.

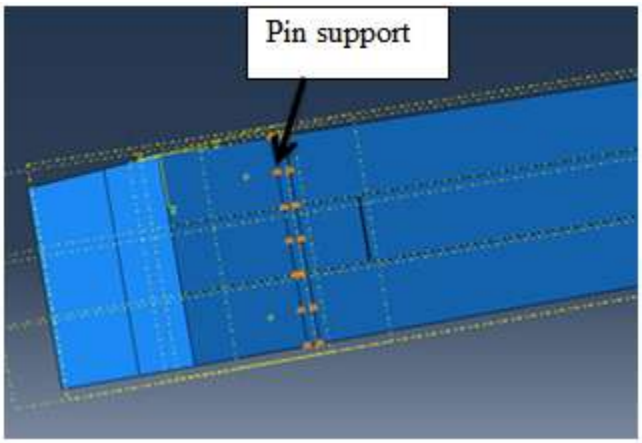

Figure 4.11: Typical support reaction.

In this model the load type was displacement control distributed over two loading areas that were $450mm$ apart. See figure 4.11. The displacement control was applied as a ramp which was applied with linear increments. Even though control displacement takes more time as compared to force control, it captures in good way the deformations and can go even beyond the peak load.

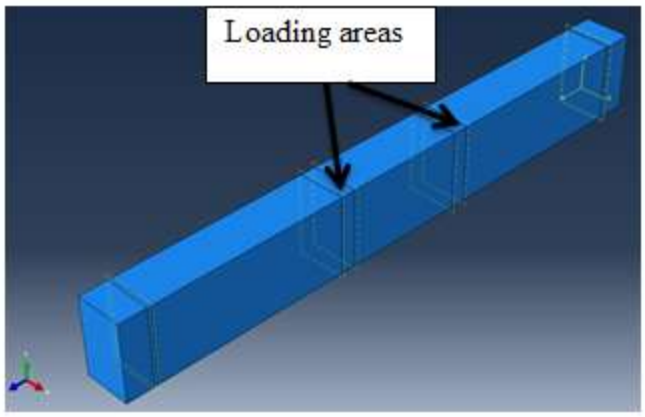

Figure 4.12: Loading pattern of the model.

4.6. Meshing

It was stated before that finite elements method consists of discretizing a given structure into a number of finite elements and solve for unknown quantities such as displacements at nodes for each element which will then be assembled in global coordinates system to obtain the response of the whole structure.

Meshing may therefore be defined as that process of dividing the structure into a number of small elements. This process is regarded as the key point in finite elements analysis since the accuracy of the solution depends on the number of elements.

The elements types used in the present model include solid elements used for discretization of concrete beam including the repair and for discretization of the FRP material. In Abaqus, solid elements may be first order using linear interpolation or second order using quadratic interpolation. Solid elements used here were C3D8R, i.e. linear 8 nodes isoparametric three dimensional brick elements with reduced integration. These were 3D stress elements. The level of integration refers to the number of Gauss points required for the integration of various quantities over the volume of each element. In this case two points in each direction are necessary as opposed to full integration where three points are required in each direction.

Full integration was not used here as for bending problems, it makes elements to be too stiff and hence the prediction of bending behavior may not be as accurate as was expected.

Cohesive elements were also used for meshing the interface between concrete beam and the FRP material. The elements were of the type COH3D8, i.e. 8 nodes three dimensional cohesive elements in Abaqus. Lastly, truss elements were used to discretize reinforcing steel. Truss elements are 3D elements having only axial stiffness and no bending stiffness. The elements used were T3D2, i.e. two node linear 3-D truss elements.

There are two types of methodologies for mesh generation in Abaqus: top-down and bottom-up. These methodologies are used differently depending on the modeling space and types of elements selected. Top-down was used here to discretize one and three dimensional geometries making up the model and was able to cope with different types of elements available. The control over mesh generation was done through partitioning. Top-down method of meshing was applied trough structured technique to generate mesh for concrete beam including patch repair. Always under top-down mesh generation method, free and sweep techniques were used to mesh steel reinforcement and cohesive zone respectively. They are distinguished by colors as shown in figure 4.13.

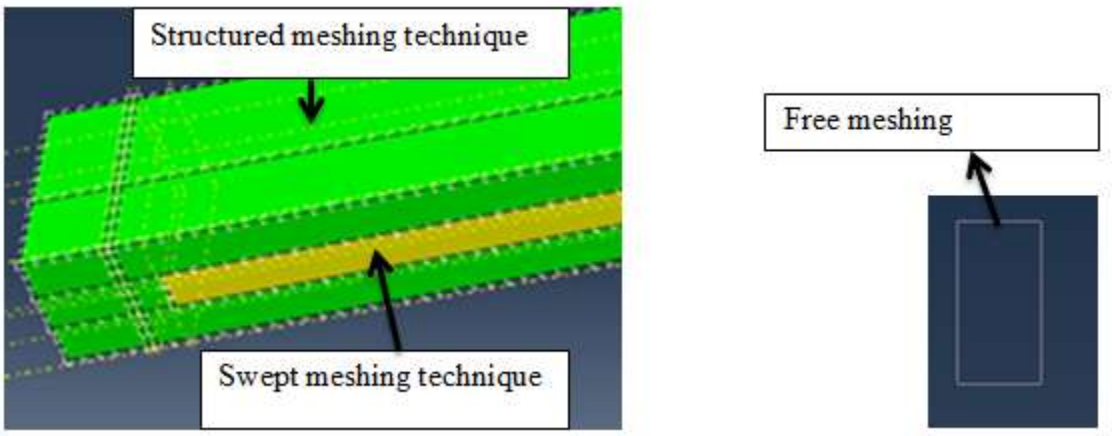

Figure 4.13: Meshing techniques.

Structured meshing follows pre-established mesh patterns trough seeding while swept meshing generates over one side or a region of the model known as the source and sweeps that mesh along a swept path to mesh the whole geometry (Abaqus, 2010). Free meshing as its name indicates doesn‟t needs pre-established mesh pattern, thus it gives greater flexibility. However, it gives the least control over the mesh.

Before meshing the density of the mesh must be specified through seeding of the edges of the model regions. Seeds are shown in figure 4.10 along the edges of the beam. The geometry of the beam was not complicated and hence seeding was applied uniformly with an approximate global size of 20mm. Figure 4.13 shows a typical meshed beam.

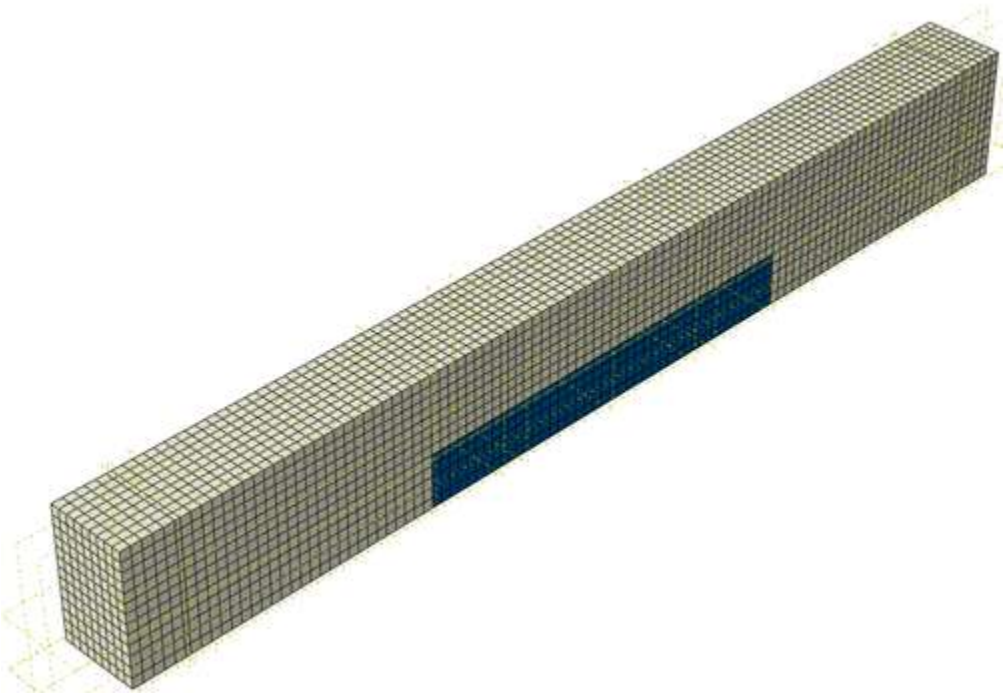

Figure 4.14: Typical meshed beam (800mm-Patch).

After all necessary tasks for building the model were done, the next step was to create a job and submit it for analysis. Monitoring of the analysis progress would also be done. The job type that was used is full analysis in which the input file associated to the model was written and the complete analysis was done. At the same time the results were written to the output database (ODB) for visualization.

4.7. Summary

This chapter discussed the methodology used for numerical investigation of reinforced concrete patch-repaired and strengthened with fiber composite materials (FRP). Different steps and procedures followed to define the geometry of the model were discussed. The mechanical properties assigned to each material involved were discussed and presented. The material properties were defined and applied to meet the behaviors discussed in chapter three.

The assembly of different components making up the structure was presented and the interactions between components are discussed. The interaction includes two constraints: tie and embedded region. The discretization of the whole structure into finite elements for analysis purposes was also looked at.

The chapter also presented the way in which boundary conditions were applied to the model, loading pattern and a method of specifying quantities that will be presented as out puts. Like any other type of analysis, this chapter discussed the analysis type that will be used for the present study which is static stress analysis type. Next chapter presents the results of numerical investigation done, discusses them and comparison with experimental results obtained from the same beams for validation of the model will also be done.

Chapter Five

RESULTS AND DISCUSSIONS

5.1. Introduction

This chapter presents and discusses the results obtained from finite element-based numerical investigation carried out on reinforced concrete beams patch repaired and strengthened with fiber reinforced polymer (FRP) plates. Five finite element models were built in Abaqus. They were control beam, 450mm-Patch repaired RC beam, 800mm-Patch repaired RC beam, 1300mm-Patch repaired RC beam and 1800mm-Patch repaired RC beam. It is useful to recap that for patch-repaired beams, tension steel reinforcements were ground over a length equal to that of the patch to simulate loss of cross section of 10% due to corrosion. The control beam on the other hand was not corroded.

As mentioned in the first chapter, the main objective of this study is to investigate the behavior of reinforced concrete beams patch repaired and strengthened with FRP plates. Thus, the effectiveness of repair and strengthening was investigated through variation of the damaged area. The variation of the damaged area was varied only in length while a height of 105mm was kept. In addition, the severity of damage and the extent of remedy that repair and strengthening may bring to reinforced concrete beams to upgrade the load carrying capacity were investigated.

The main failure mode of FRP strengthened reinforced concrete beams is debonding. It is characterized by a sudden separation of the FRP material from the main beam. Debonding failure is mainly caused by concrete cracking which induces stress concentrations around the cracks. When those stresses exceed the strength of the interface, debonding takes place. This type of failure was largely reported in the literature. Thus, the overall behavior of reinforced concrete patch repaired and strengthened with FRP plates bonded to their tension face was examined through concrete cracking, strain distribution in the FRP material and damage energy release rate. It is worth remembering that the word „damage" has also been defined at material level in constitutive relationships and should be distinguished from its use above. The chapter presents also a comparison of numerical results with experimental findings. However, it is necessary to note beforehand that, there will be eventual discrepancies between numerical and experimental results due to the assumptions made in finite element modeling.

5.2. Cracking behavior

It is well known that when reinforced concrete beams are subjected to bending, they are prone to cracking. Depending on the shear span ratio, we may expect flexural cracks, and or flexural-shear cracks or even purely shear cracks. Cracking in reinforced concrete beams is initiated when the maximum principal stress exceeds the tensile strength of concrete as discussed in chapter four. This is justified by the tensile stress distribution shown in figure 5.1 of the control beam. The maximum averaged tensile stress displayed was 3.7MPa, which exceeds the tensile strength of concrete. This value was taken after the first increment. However, not averaged value was probed as 3.6MPa, which was always greater than the tensile strength of concrete. This implies crack initiation at the first increment of load application.

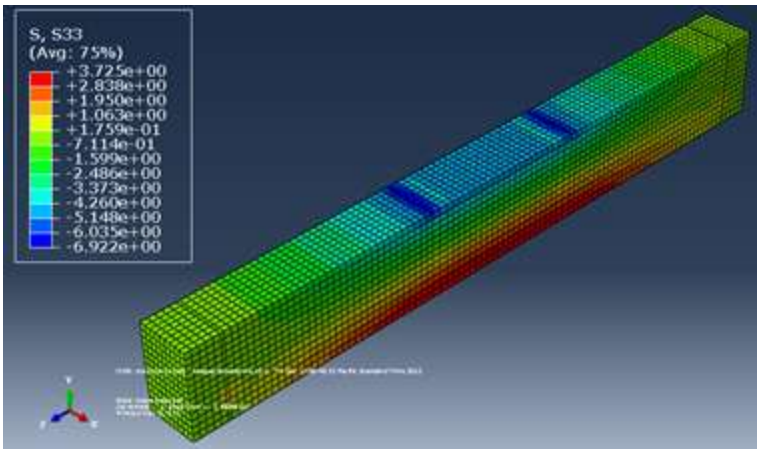

Figure 5.1: Tensile stress distribution in reinforced concrete beam (Control).

The tensile strength was set equal to $3.5MPa$ for concrete and $4.3MPa$ for the repair material. For patch-repaired RC beams, for example 1800mm-Patch, an averaged tensile stress of 4.4MPa was found at third increment. At the same time, not averaged tensile stress of 4.4 was probed in the bottom center. This value is greater than the tensile strength of the repair material and this involves cracking since tensile strength was exceeded. Tensile stress distribution for that RC beam is shown in figure 5.2.

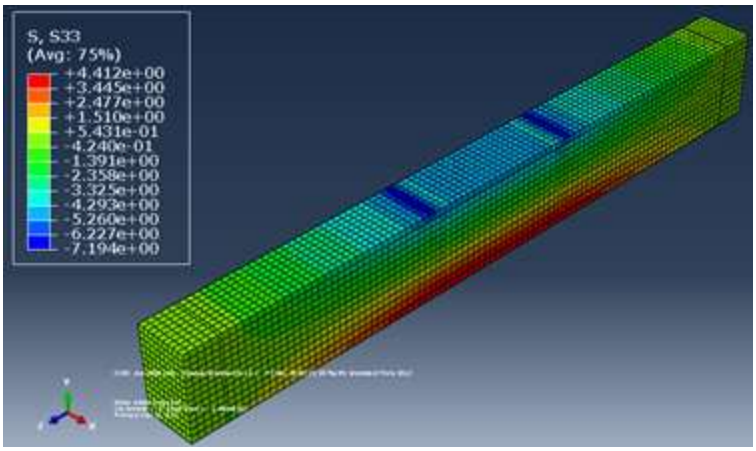

Figure 5.2: Tensile stress distribution in 1800mm-Patch repaired RC beam.

Concrete damaged plasticity model in Abaqus is a modification of the Drucker-Prager plasticity model done by Lubliner et al. (1998). According to the authors, cracking initiates at points where the tensile equivalent plastic strain is greater than zero and the maximum principal plastic strain is positive. Based on this concept, it was possible to visualize cracks, as it will be seen later in this chapter. That is, to display crack pattern, we had to switch to maximum principal equivalent plastic strain. Finite elements analysis carried out on control beam and on four patch-repaired and FRP-strengthened beams revealed that the initiation of cracking was not the same for all the beams as shown in figure 5.3. It is useful to note that the crack location was not known a priori.

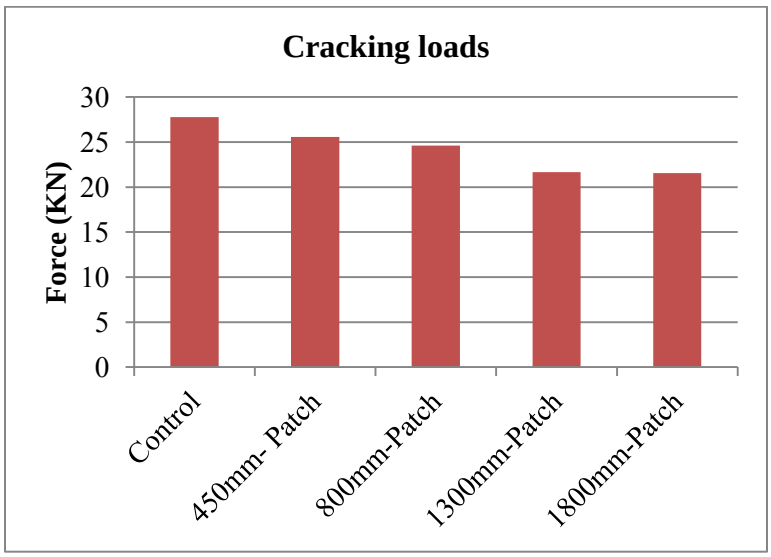

Figure 5.3: Cracking loads

As can be seen from the figure, crack initiated at a relatively higher load for control beam as compared to patch repaired and strengthened beam. As will be shown in the subsequent sections, the same was observed in the experiments, though patch repaired and strengthened beams were supposed to crack at higher loads due to high strength of the repair material. However, as it will be discussed later in terms of damage energy release rate, cracking of the control RC beam took place earlier, than the rest of the RC beams; though it took place at a higher load (27.79KN); as compared to patch repaired and FRP strengthened beams. This clearly showed that the addition of patch material delayed the cracking. (Appendix A).

Crack initiation always took place in the middle from the tension face of the beam and extended to the neutral surface; however, the propagation pattern was different for control and strengthened beams. As concrete was cracking, stresses in tension steel were increasing up to yield stress as shown in figure 5.4.

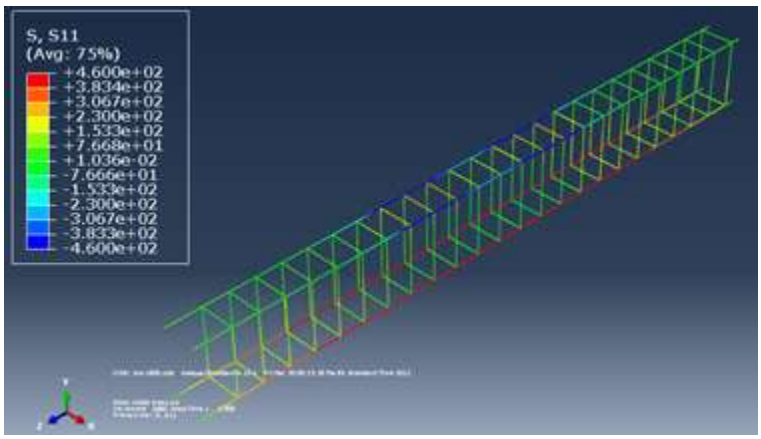

Figure 5.4: Stress distribution in steel reinforcement (1800mm-Patched RC beam)

It has been observed in this study that for proper crack pattern representation, it is useful to use force control. However, force control did not capture in a perfect manner the load displacement relationship and other failure mechanisms. This was because force control fails to capture the post peak behavior of the beams. Up to the ultimate load, all cracks will have formed before convergence issues arise, i.e. before the stiffness matrix becomes singular. This may be caused by numerical round off in the finite element models where bodies, which were supposed to be in contact, are not. This will result in rigid body motion. On the other hand, displacement control did a better representation of the load displacement relation, as it is able to consider the

descending part up to complete failure. Displacement control failed to represent adequately the crack pattern, but helps stabilize the solution. In displacement control, it is possible to have different values of displacement corresponding to one value of force, leading to few cracks as compared to force control. Thus, the crack pattern shown below was derived from force control and the remaining of the output was based on displacement control.

Figure 5.5 shows the initiation of cracks for control RC beam. Crack pattern shown in figure 5.6 is as expected for normal reinforced concrete beam where flexural cracks are vertical and flexural-shear cracks are inclined towards the loading points. The state of crack initiation appearing on the control beam corresponds exactly on the stress state shown in figure 5.1.

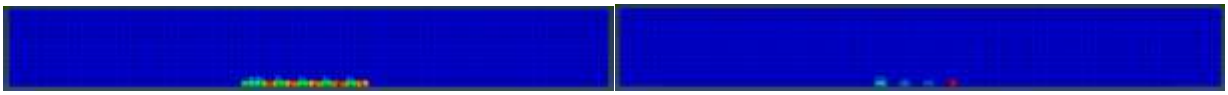

Figure 5.5: Crack initiation: control beam (left), 1300mm-Patch (right)

As it can be seen from figure 5.5, not only the cracking load is different for the control and patch repaired and strengthened beams, but also the initial crack configuration is also different. This was due to the fact that repair has a higher strength and cracks were forced to initiate in the constant bending moment region.

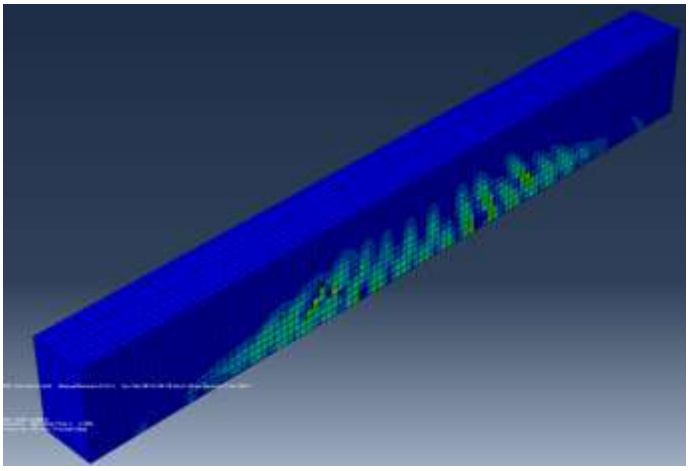

Figure 5.6: Crack distribution: Control RC beam

Beam with 450mm-Patch showed a crack pattern which was far different from that of the control beam.

The beam showed few and widely spaced cracks as compared to control beam cracking. This is attributed to the fact that repair with higher tensile strength was within loading points and cracks were initiating in the constant moment region. That is why the beam also showed another critical crack in that region. However, as compared to control beam critical cracks under loading points were clearly identified. Crack pattern is shown in figure 5.7 below.

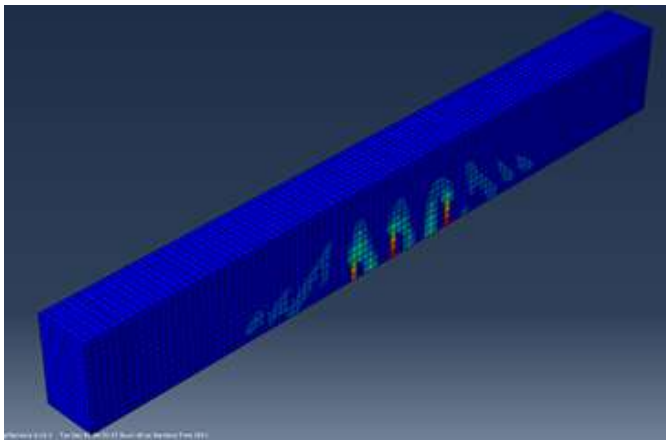

Figure 5.7: Crack pattern for 450mm-Patch repaired beam.

As the patched area was getting larger, the crack pattern was getting uniform like for conventional reinforced concrete beams. Critical cracks were found under loading points and in the constant bending moment region. The use of path repair material made cracks to be widely spaced as compared to control beam. With the increase in patch length more cracks were developed. This was due to the fact that reinforced concrete beams were tending to be made of nearly the same material in the regions that were likely to crack. This can be visualized by comparing crack pattern for RC beams with 800mm, 1300mm and 1800mm patch lengths in figures 5.8and 5.9 below.

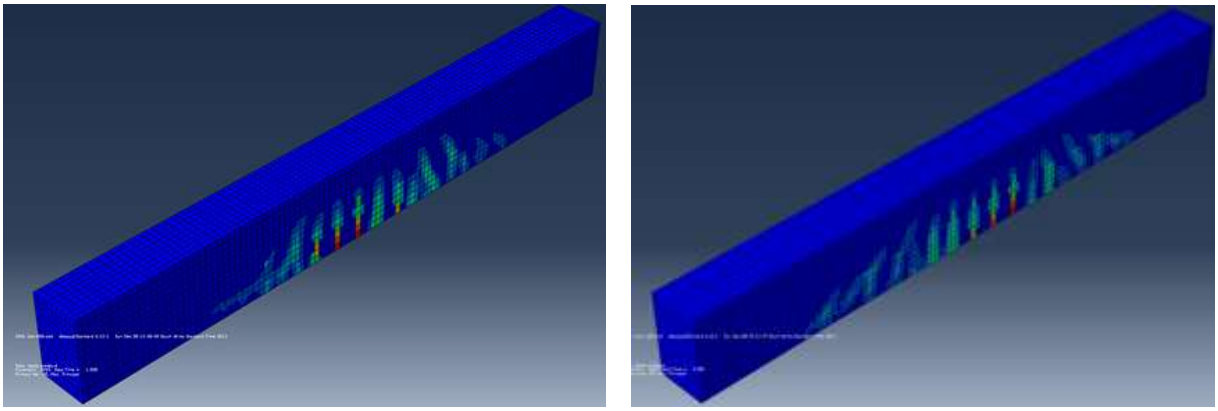

Figure 5.8: Crack distribution: 800mm-Patch (left), 1300mm-Patch (right).

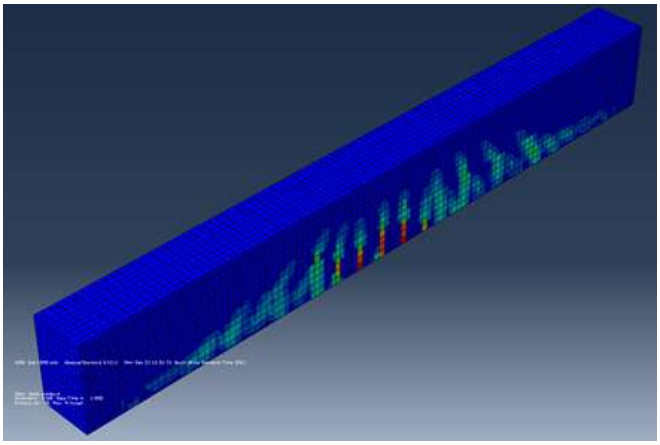

Figure 5.9: Crack distribution: 1800mm-Patched beam.

To assess the effect of repair on crack pattern, two beams were analyzed in terms of cracking. Beam with 450mm-Patch and beam with 1800mm-Patch but without FRP strengthening were loaded with force control of 175KN and 200 KN, respectively. It was seen that cracks were uniformly and widely distributed as was seen for the same beams but with FRP plates. However, critical cracks were not clearly identified. Particularly, more cracks were observed for 450mm-Patched RC beam. Figure 5.10 compares the distribution of cracks for both beams. This means that if we can ensure in practice a good bond between old concrete and the repair material the load carrying capacity of the damaged beam can still be improved through repair to some extent.

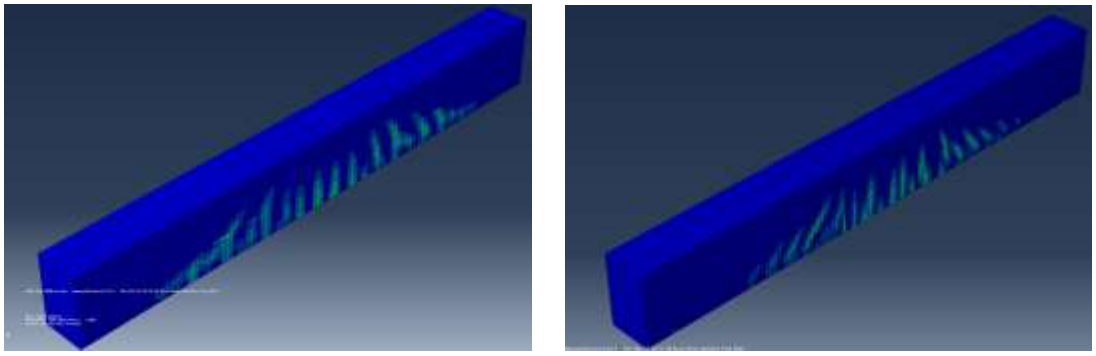

Figure 5.10:Crack pattern for only patch repaired beams: 1800mm-Patch (left), 450mm-Patch right.

Comparing crack pattern for beams in figure 5.7 and 5.10 (right) for 450mm patch and beams in figure 5.9 and 5.10 (left) for 1800mm patch repaired beam, it is seen that the addition of external reinforcement affect structural crack distribution. The distribution is more or less similar to that of control beam. This clearly shows that the reduction in steel cross section due to corrosion may be recovered from higher strength of repair material and from the assumed perfect bond between concrete/repair material and steel.

5.3. Damage and damage energy release rate.

5.3.1. Damage

Damage is defined according to Mazars et al. (1987) as a mode of failure in concrete and other geomaterials due to the propagation and coalescence of microcracks. This phenomenon is also known as strain softening of concrete as discussed in section 4.3.1. According to the same authors, damage may appear as the collapse of microporous structure of the cement matrix or the propagation of the microcracks and is mostly located in the interface transition zone or in the cement matrix. In this study both tensile and compressive damage were considered. Damage parameters were defined to investigate to what extent the elastic stiffness of concrete and repair material will be degraded or damaged when reinforced concrete beams under study are subjected to four points bending loading.

For reinforced concrete under bending, cracking appears before concrete crushing. Thus, tensile damage was of interest even though compressive damage parameters were defined. Figure 5.11 shows tensile damage of the control beam. As can be seen from the figure, when the elastic

properties of concrete get degraded, the first failure will appear as cracking. Therefore tensile damage on concrete stiffness leads to cracking as per definition of damage. This was justified by the fact that tensile damage pattern and flexural cracking all have more or less the same pattern.

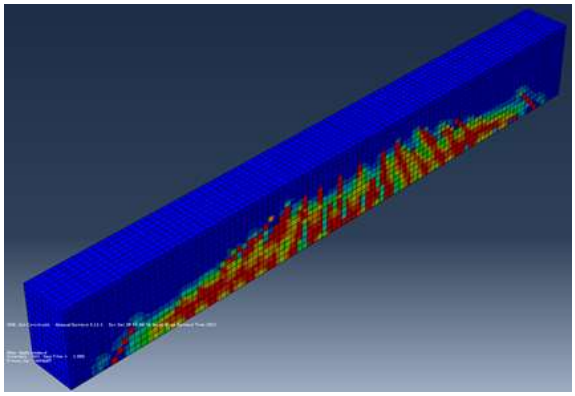

Figure 5.11: Tensile damage for control beam

For patch-repaired beams, concrete and repair material are damaged differently. The reason was the difference in their tensile strength. So, it is clear that concrete with a relatively low tensile strength as compared to that of repair material was severely damaged.

This justifies the reason that repair material must be compatible with existing concrete for effective repair and strengthening of damaged reinforced concrete beams. Figure 5.12 shows how concrete and repair material are damaged due to tension from *a* to *d* showing beams for *450, 800, 1300* and *1800mm* patch. Thus, tensile damage is also a key parameter to identify the likely mode of failure of reinforced concrete beams patch repaired and strengthened with FRP laminates. Observations made from tensile damage show the possibility of flexural or flexural shear crack to propagate horizontally at the level of reinforcement, which may result in concrete cover separation.

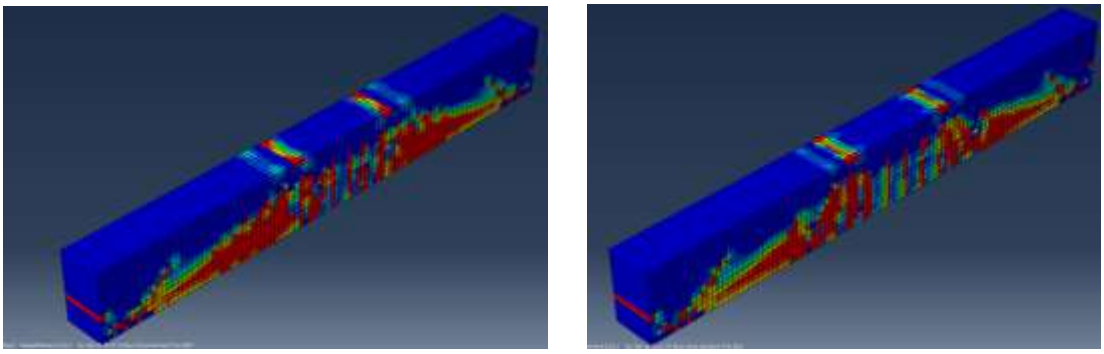

a) b)

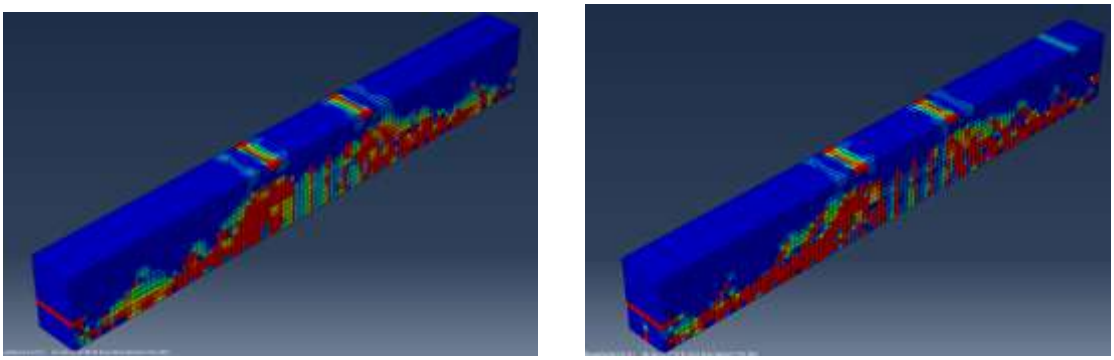

c) d)

Figure 5.12: Tensile damage for patch repaired and strengthened beams.

5.3.2. Damage energy release rate

According to Mazars et al. (1987), permanent strains and damage are irreversible processes leading to the conversion of mechanical energy into heat and surface creation.

Here surface creation stands for cracking. The energy released due to damage is termed as damage energy release rate. This energy is a function of the elastic energy of the system and damage and is always positive. In fact, damage is associated with the propagation of microcracks and there should be energy consumption for it to be possible. Thus, this energy may also be related to fracture energy to some extent, even though damage energy considers the material as a whole and not individual crack. Appendix A shows a sample of Abaqus results in terms of damage energy where cracking loads; i.e. when concrete started to release energy; can be easily visualized.

This energy may also be interpreted as the energy that is dissipated when concrete is undergoing damage failure. It can also be related to the amount of external work required to create new surfaces and hence can be used as measure of the resistance to cracking and thus to total collapse. Figure 5.13 compares the damage energy release rate for all the RC beams analyzed. From the figure, we can see that increasing the patch length implies more energy that would be released. This is because the tensile strength of concrete is also increasing. In addition, from figure 5.13, it can be seen that cracking of concrete highly influences the nonlinear behavior of

concrete. It is clear that after yielding of steel, there is extensive release of energy showing also extensive cracking leading to complete failure. From figure 5.13 it is seen that after yielding there are different trends of energy release rate indicating the effect of patch and that of steel cross section reduction due to corrosion.

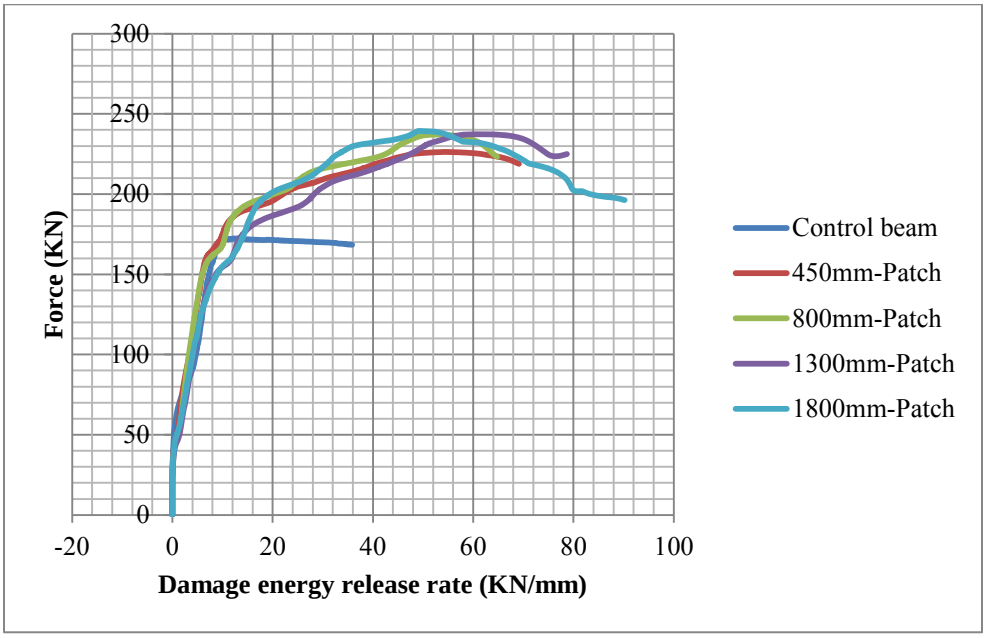

Figure 5.13: Damage energy release rate relationships.

From table 5.1, it was found that the addition of patch material could improve the load carrying capacity of damaged RC beams through measurement of maximum damage energy. The energy required for complete damage was increasing by increasing the patch length. From figure 5.13, it can be seen that the contribution of patch repair to load carrying capacity is less. This is identified by comparing ultimate loads for various patch repaired and FRP strengthened RC beams. Thus, the increase in load carrying capacity is attributed to the provision of external reinforcement, i.e. FRP. As stated previously, the effect of repair is to restore durability, geometry and lost capacity of steel reinforcement due to corrosion.

Table 5.1: Damage energy dissipation for all specimens

RC beam type	Maximum damage dissipation energy (KN/mm)	Percentage increase
Control beam	35.85	0
450mm-Patched beam	64.76	44.65
800mm-Patched beam	69.11	48.13
1300mm-Patched beam	78.69	54.44
1800mm-Patched beam	90.32	60.31

Beam with 1800mm patch length thus showed relatively higher energy. This clearly highlighted the fact that tensile strength of concrete is an important parameter. The salient feature of damage energy is that it could capture accurately the failure stages, i.e. crack initiation, yielding of tensile reinforcement and debonding of FRP. From damage dissipation energy, it could be possible to accurately identify the cracking load, yielding load and the debonding load. This was stated in section 5.2 for cracking loads. Figure 5.14 shows the load-damage dissipation energy for all the beams analyzed in Abaqus using concrete damaged plasticity.

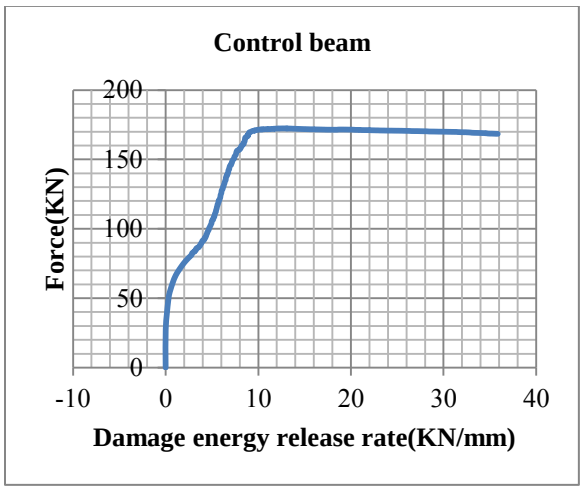

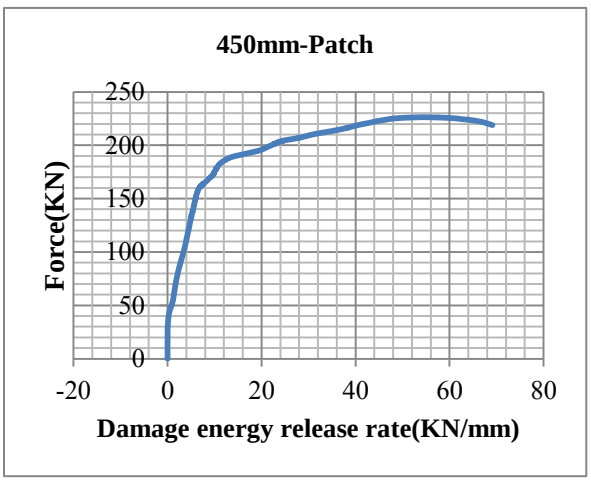

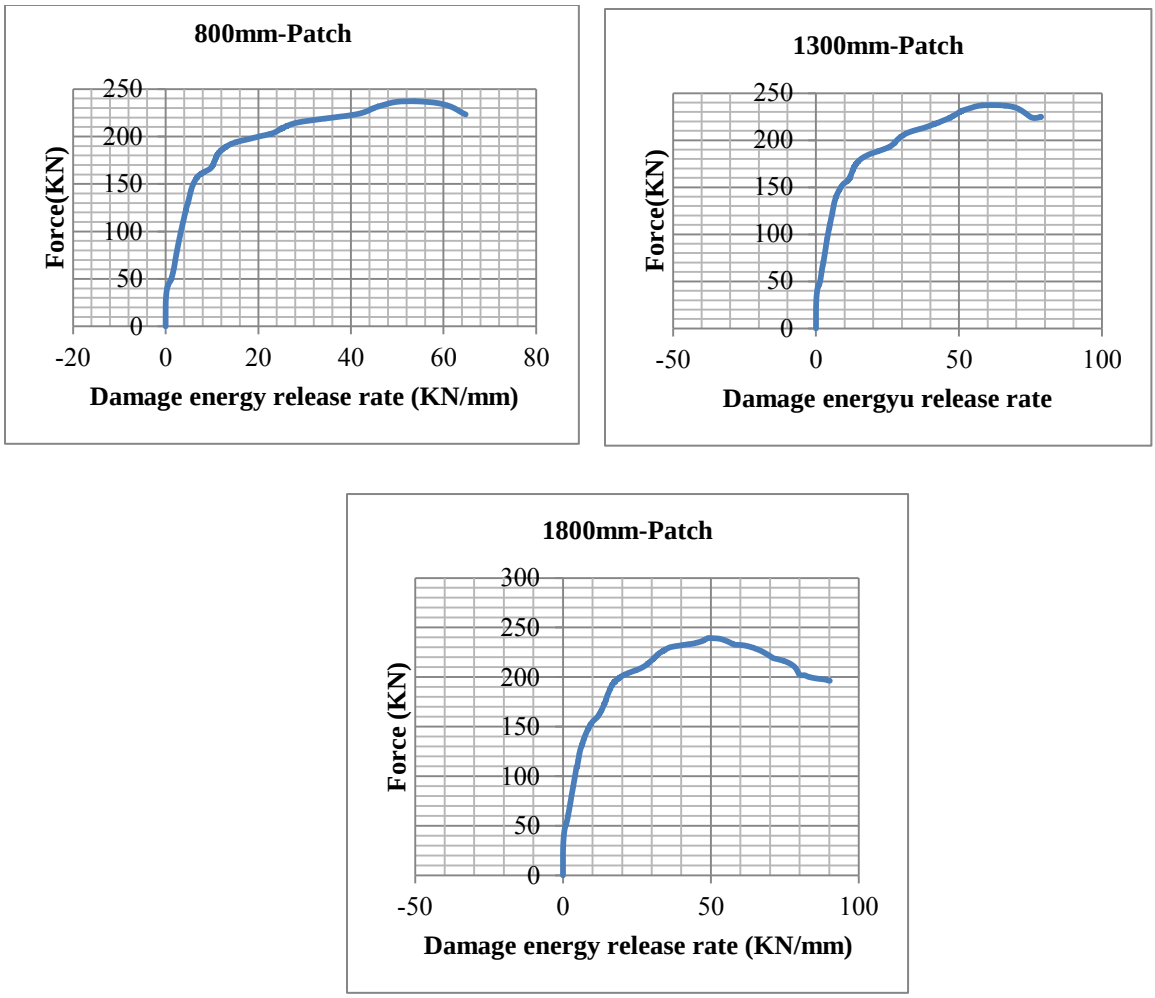

Figure 5.14: Load-Damage energy release rate for each beam.

From the energy point of view, it is observed that the post-yield behavior is not as smooth as revealed by the load deflection curves. This may be attributed to the known behavior of reinforced concrete beams, that when concrete cracks, stress in tensile reinforcement increases. When steel yields stress is constant and if concrete continues to crack the behavior will not be smooth since many cracks will form causing high stress variations in steel.

5.4. Deflection behavior.

One of the parameters used to characterize the behavior of reinforced concrete beams subjected to bending is the load-deflection relationship. The relationship is able to represent different stages of failure as the applied load increases. Generally, those stages include crack initiation, yielding of tensile steel reinforcement and crushing of concrete in compression.

When reinforced concrete beams are flexurally strengthened with FRP plates bonded to their tension face, an additional failure stage corresponding to the plate debonding or plate rupture is also present on the load deflection curve. Each failure stage was characterized by the change in the slope of the curve. In the present study as stated before displacement control was applied and force was requested as history output at the supports. Displacement was also requested in the middle of the span.

It is important to recap that displacement in this case was applied as boundary condition and was specified as a negative value of translational degree of freedom u_2. Figure 5.15 shows a comparison of the load deflection relations for all the beams analyzed in this study.

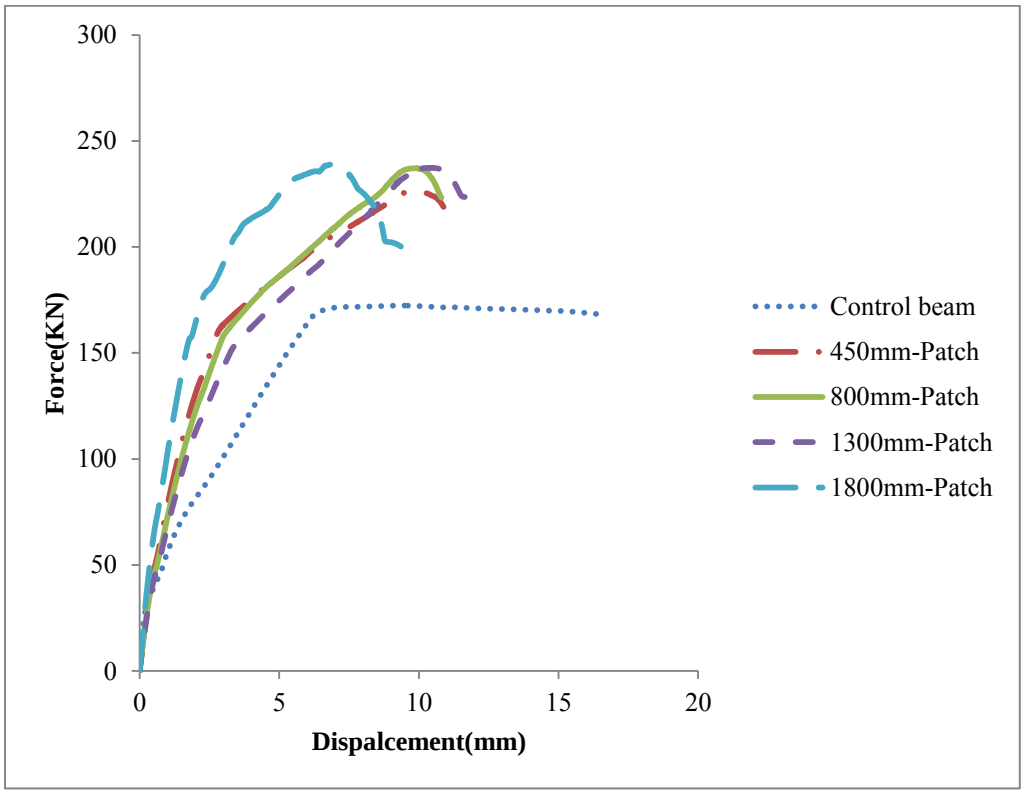

Figure 5.15: Load deflection relationships for all specimens.

From figure, 5.15 above it can be seen that cracking for all beams initiated at nearly the same load as discussed in section 5.2.

This means that the effect of patch repair was to delay crack initiation. For beams repaired over a length of 450mm, 800mm and1300mm the behavior was more or less the same except the differences in yielding and debonding which occurred at different loads and displacement.

Beam with 1800mm length patch repair showed a slightly different load displacement relationship. In comparison with the behavior of other beams, the behavior is relatively more stiff since the debonding load was high but at small deflection as compared to other beams. The reason may probably be attributed to the reduction in tension steel cross section and large size of repair with high tensile strength Figure 5.16 shows the load deflection relationship for each beam analyzed.

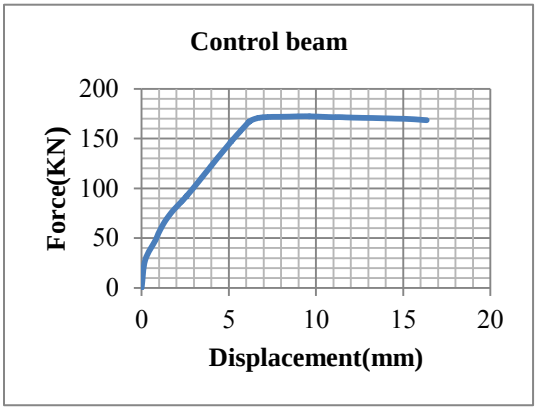

(a)

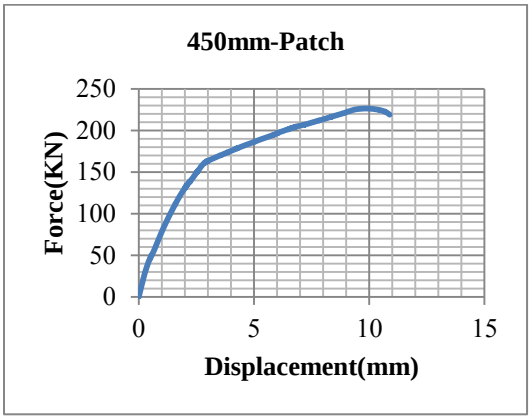

(b)

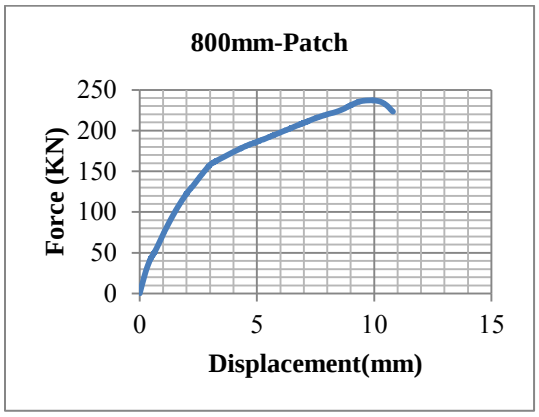

(c)

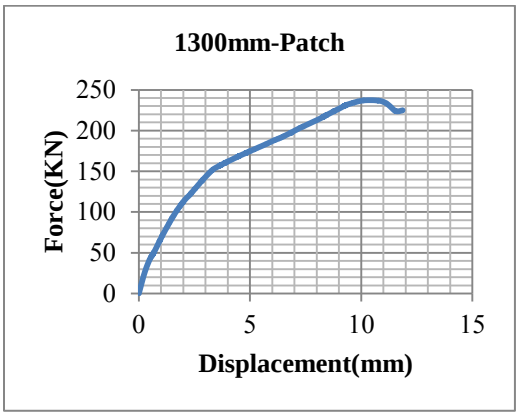

(d)

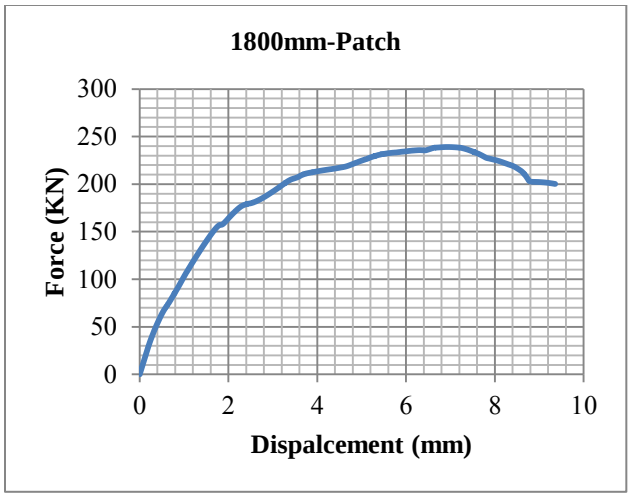

(d)

Figure 5.16: Load deflection for each beam analyzed.

From figure 5.16, it is observed that for control RC beam after yielding of steel no further increment in load carrying capacity was experienced until failure. However, for patch repaired and FRP strengthened beams, this was not the case. This shows that repair and strengthening increase the load carrying capacity of reinforced concrete beams. The debonding loads observed for patch repaired and strengthened RC beams are shown in table 5.2 and are compared with the ultimate load for control beam to assess the effect of the patch and CFRP on the load carrying capacity of the respective RC beams.

Table 5.2: Ultimate loads

Beam type	**Ultimate load (KN)**	**Percentage increase**
Control beam	172.3	0
450mm-Patched beam	226.2	23.8
800mm-Patched beam	236.8	27.2
1300mm-Patched beam	237.3	27.4
1800mm-Patched beam	240.5	28.4

Note that, none of the beams was over-reinforced. All beams showed a ductile behavior. From the observations made, it can be seen that depending on the degree of damage, if the repair can be applied properly and FRP well bonded, a substantial increase in load carrying capacity may be found. However, as stated earlier in the literature, debonding failure prevents full utilization of the FRP, i.e. its use up to rupture. As shown in figure 5.16, concrete damaged plasticity model along with other models for other materials involved was accurate in modeling the behavior of reinforced concrete beams patch repaired and strengthened with FRP. This is true since on each curve, the changes in slope representing the three failure stages may be clearly identified, i.e. crack initiation, yielding of steel reinforcement and debonding failure for strengthened beams and ultimate failure load for control beam.

From the individual load displacement curves, it is clear that yielding load for all the specimens was between 150KN and 200KN. Table 5.3 shows the yielding load for each specimen.

Table 5.3: Yielding loads.

RC beam type	**Yielding load**
Control beam	170KN
450mm-Patched beam	165KN
800mm-Patched beam	160KN
1300mm-Patched beam	155KN
1800mm-Patched beam	155KN

5.5. Strain distribution in FRP plates.

Bonding fiber reinforced polymer materials to the tension face of reinforced concrete beams after patch repairing resulted in increased load carrying capacity as discussed above. However, the failure mode is often associated to debonding of FRP and/or FRP rupture in addition to concrete crushing in compression and tensile steel yielding.

Except debonding of FRP, other failure modes in reinforced concrete beams strengthened with FRP may be controlled. Crushing strain of concrete is known, yielding of tension steel can be measured in the laboratory and FRP rupture can be predicted from rupture strain provided by the manufacturer; but debonding control is still not well understood.

A common measure used to control debonding is to limit the strain in the FRP material to a usable or debonding strain which; when exceeded at some locations; FRP will separates from the beam. Strain in FRP is mostly a governing factor in design of strengthened RC beams. This concept was used in this study. Total strain in FRP increased with increasing in loading. Figure 5.17 shows that the cumulative strain in the middle of the span is about 0.04 for all patch-repaired and strengthened beams.

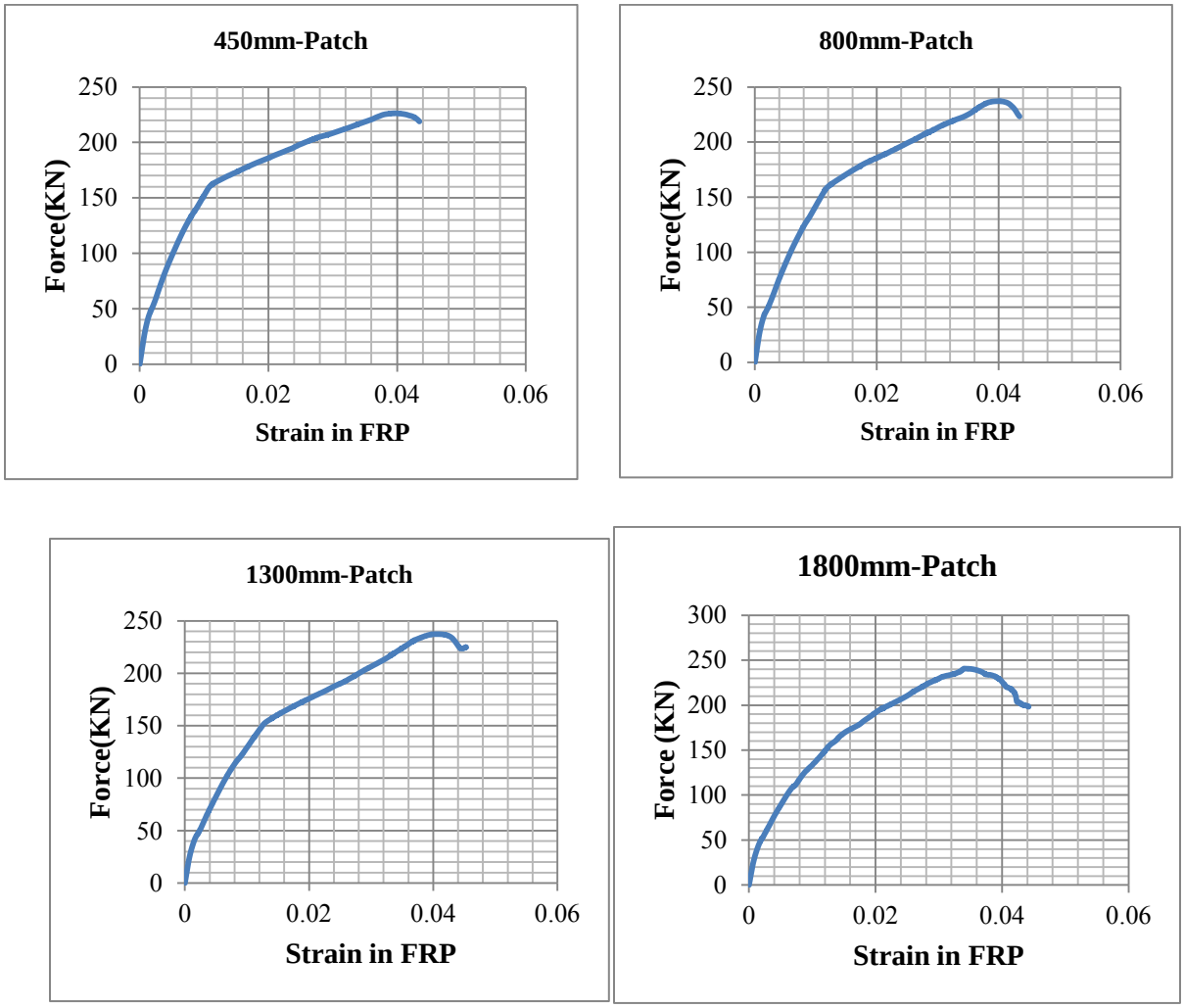

Figure 5.17: Cumulative strain in FRP vs total load.

It is clear from figure 5.17 that the overall response of reinforced concrete beams strengthened with FRP can be predicted through applied load vs. cumulative strain in the FRP. The total cumulative load indicated the corresponding debonding load. Strain distribution in the FRP is shown in figure 5.18 where strain was minimum at the plate end and kept increasing up to debonding strain. The figure shows strain distribution for 800mm-Patch repaired and CFRP strengthened reinforced concrete beam.

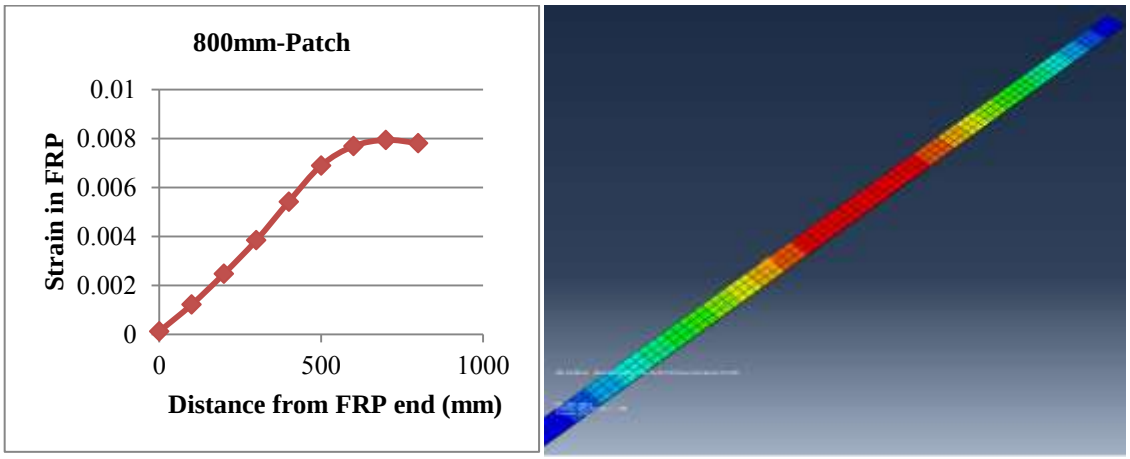

Figure 5.18: Strain distribution in the FRP. (800mm-Patch)

To investigate the effect of the patch repair on the FRP strain distribution and hence on the debonding failure, a comparison of strain distribution for all the cases was made as shown in figure 5.19.

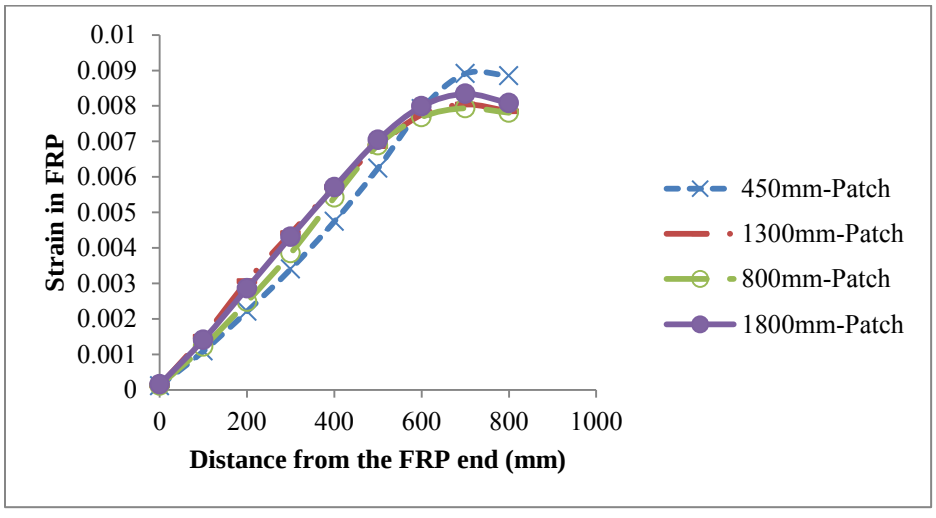

Figure 5.19: Effect of patch length on the strain distribution in FRP.

The strains shown in figure 5.19 are individual strains at different locations along FRP plate. Figure 5.19 shows that the introduction of patch repair affected the strain distribution in FRP material. As the length of the patch was becoming larger, strain distribution in FRP plate was linear up to the peak value. That showed that the discontinuity in the material to which FRP is bonded affect the strain distribution in FRP. It can be seen that beam with 450mm patch showed a nearly non- uniform strain distribution followed by the one with 800mm patch. Clearly, the maximum strain in FRP was in the constant moment region or just under loading points.

5.6. Failure mechanisms.

It has been discussed that the main failure mode of FRP-strengthened beam is debonding of the FRP plate from the main beam. Debonding can take place at the plate end or around flexural or flexural shear cracks. In addition to debonding; like in conventional reinforced concrete beams; other modes of failure like yielding of steel and concrete crushing in compression were experienced. Failure mechanism of control beam was that of conventional reinforced beams. This was illustrated in figure 5.16(a) where yielding was followed by a nearly constant load carrying capacity until crushing of concrete in compression. Note that, as mentioned in section 5.2, the failure mechanisms were analyzed based on displacement control rather than force control as it was the case for crack distribution analysis. Figure 5.20 shows the mode of failure of the control beam. The strain in concrete under loading point was probed and was found to be 0.0065. This was far greater than the ultimate concrete compressive strain. This clearly shows that there has been concrete crushing at failure.

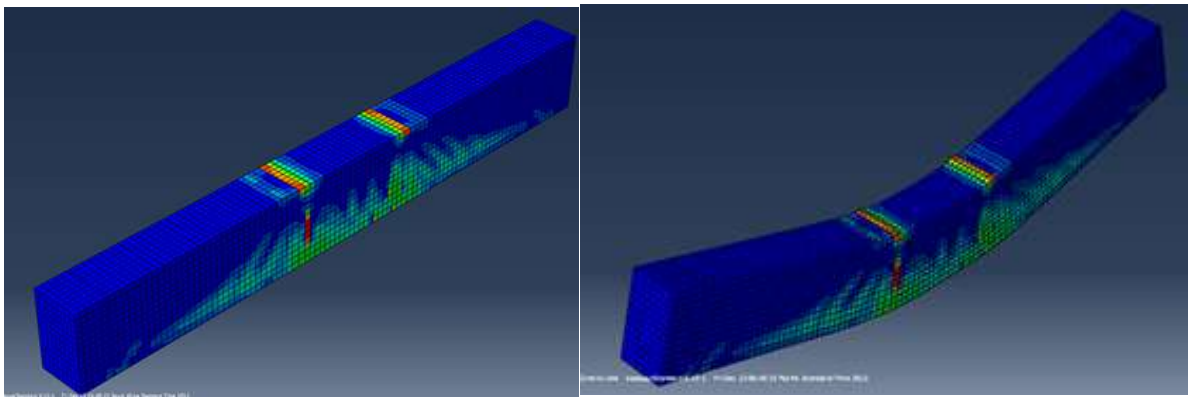

Figure 5.20: Failure mode of the control beam.

The mode of failure observed on FRP-strengthened beams was the yielding of steel followed by debonding of the FRP and concrete crushing in the compression zone under loading points.

Yielding of tensile steel was reported in the previous sections on the load-deflection curves. Debonding failure observed was intermediate crack induced debonding. There was no reason for plate end debonding since all reinforced concrete beams were sufficiently reinforced in shear even though there were no FRP anchors. The intermediate crack induced debonding initiated at or around critical flexural cracks, which were under loading points.

There was possibility for flexural cracks to propagate vertically as well as horizontally. The horizontal propagation speeds up debonding failure. Typically, such mode of failure is shown in figure 5.21 for beam with 1300m patch repair. Propagation of cracks was defined by the maximum principal plastic strain, the direction of which is parallel to the direction of crack. This mode of failure was found for all patch-repaired and FRP strengthened beams.

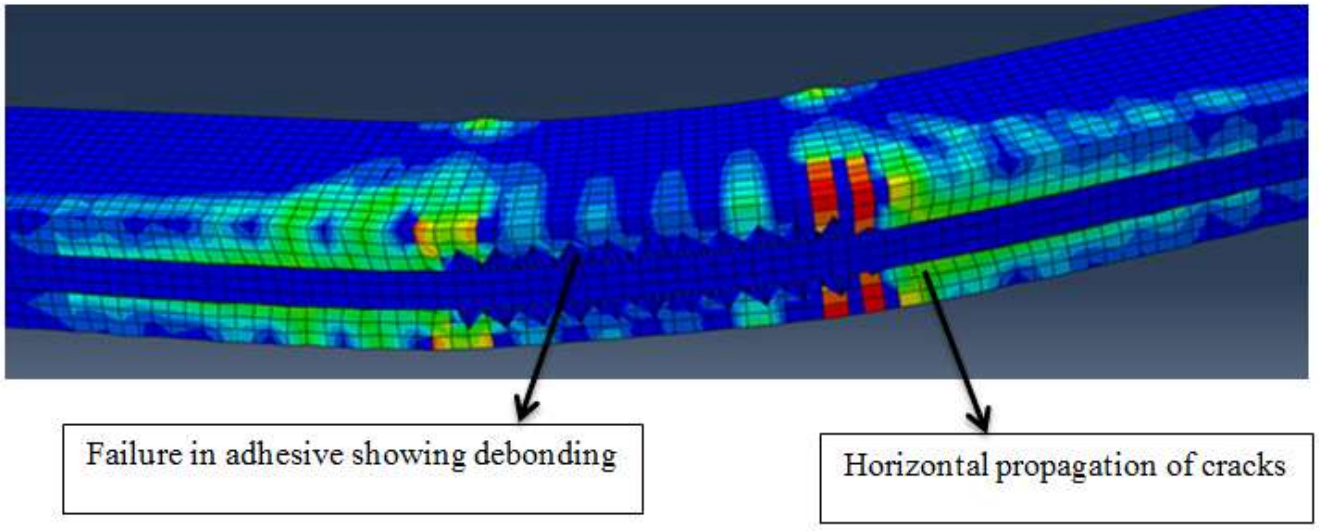

Figure 5.21: Debonding failure

Debonding initiation was also justified by the strain level in FRP as discussed above. The maximum strain in FRP was found to be in the constant bending moment region. This was discussed in section 5.5.

5.7. Validation of the Finite Element Models.

In order to assess the integrity of the finite element model developed in this research thesis and its capability to capture the behavior of reinforced concrete beams patch repaired and strengthened with fiber reinforced polymer materials, three parameters were chosen:

strain in FRP, load displacement relationships and crack distribution along with debonding as observed in the laboratory. In addition a comparison between yield and debonding loads from both FEA and experiments was done.

5.7.1. Strain distribution in FRP

Strain in FRP was chosen because it is often a governing parameter in structural strengthening design. It governs the debonding failure. Thus, its choice covered the overall failure behavior. In finite element models, it was possible to measure strains from the FRP plate end at equally spaced points so that the distribution discussed in section 5.5 could be obtained from which the debonding strain could be identified. The debonding strain so determined from finite element models was compared to that recommended by ACI Committee 440 (2002).

ACI Committee 440 guide recommends that in order to prevent debonding of the FRP laminate, a limitation should be placed on the strain level developed in the laminate. The guide gives an expression for bond-dependent coefficient κ_m which, when multiplied by the ultimate strain gives the debonding or usable strain. The expression is written as:

$$\kappa_m = \begin{cases} \dfrac{1}{60\varepsilon_{fu}}\left(1-\dfrac{nE_f t_f}{360000}\right) \le 0.90 \;\; for \;\; nE_f t_f \le 180000 \\ \dfrac{1}{60\varepsilon_{fu}}\left(\dfrac{90000}{nE_f t_f}\right) \le 0.90 \;\; for \;\; nE_f t_f \prec 180000 \end{cases} \tag{5.1}$$

where E_f is the tensile modulus of elasticity of FRP (MPa), t_f is the nominal thickness of one ply of FRP reinforcement in mm, ε_{fu} is the design rupture strain of FRP in mm/mm and n is the number of plies used.

The FRP material used in this study was having a tensile modulus of elasticity of $165000MPa$, the thickness was $1.2mm$ and the design rupture strain was 1.7% according to the manufacturer. Only one ply was used in this study. Using ACI expression the bond-dependent coefficient was calculated as:

$$\kappa_m = \frac{1}{60x0.017}\left(\frac{90000}{165000x2}\right)$$
$$= 0.45$$

Therefore, the corresponding debonding strain was calculated as $\varepsilon_{fd} = 0.45x0.017 = 0.00765$.

A comparison was made between FEM strain distribution as discussed in section 5.5 and ACI 440.2R-02 predictions. It was found that the debonding strain matched well. Thus, the finite element model used here predicts well the debonding failure of reinforced concrete beams patch-repaired and strengthened with FRP plates.

From the strain distribution predicted by the finite element model it was observed that debonding initiated at a distance of $600mm$ from the FRP plate end which corresponded to the point close to the loading area where debonding initiated from experimental observations. At this location, FE models showed the maximum strain in FRP. Table 5.4 illustrates the comparison.

Table 5.4: Comparison of debonding strain: FEM vs ACI 440.2R-02.

RC beam type	FEM	ACI 440.2R-02	% difference
450mm-Patched beam	0.00792	0.00765	3.4
800mm-Patched beam	0.00768	0.00765	0.4
1300mm-Patched beam	0.00775	0.00765	1.3
1800mm-Patched beam	0.00799	0.00765	4.3

The comparison shown in table 5.4 was done at a distance of 600mm from the FRP plate end. The reason was that considering 0.00765 as the debonding strain, values of the strain in the FRP predicted by FEM were close to 0.00765 at that distance.

5.7.2. Load deflection curves

Load deflection curves obtained from both FEM analysis and laboratory work for control beam and patch repaired and strengthened beams were compared.

As it can be seen from figure 5.17, there is a close agreement between the finite element models used for the analysis of control beam and four patch repaired and FRP strengthened beams with varying the length of the damaged area and 10% reduction in steel cross section due to corrosion.

The comparison in terms of load deflection curves was done up to debonding load since the unloading stage was not of interest in finite element modeling.

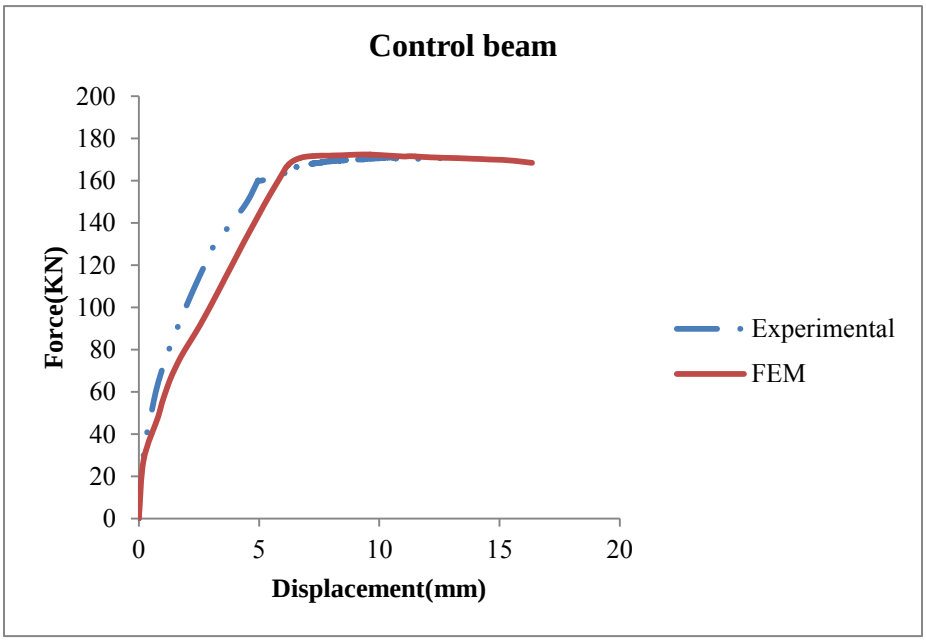

(a)

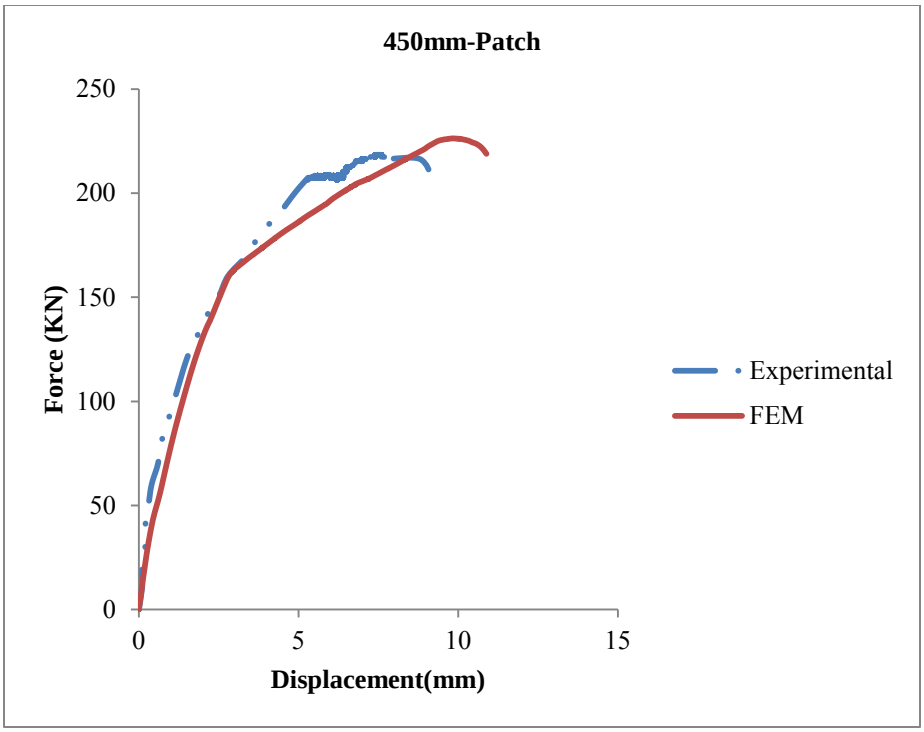
450mm-Patch
250
200
150
100
50
0
Force (KN)
0
5
10
15
Displacement(mm)
Experimental
FEM

(b)

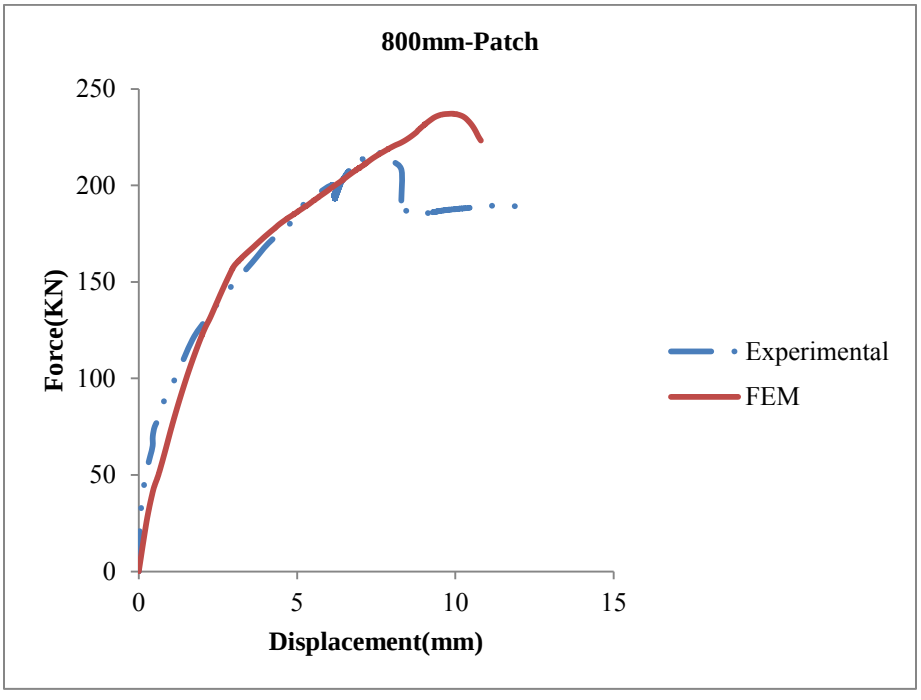
800mm-Patch
250
200
150
100
50
0
Force(KN)
0
5
10
15
Displacement(mm)
Experimental
FEM

(c)

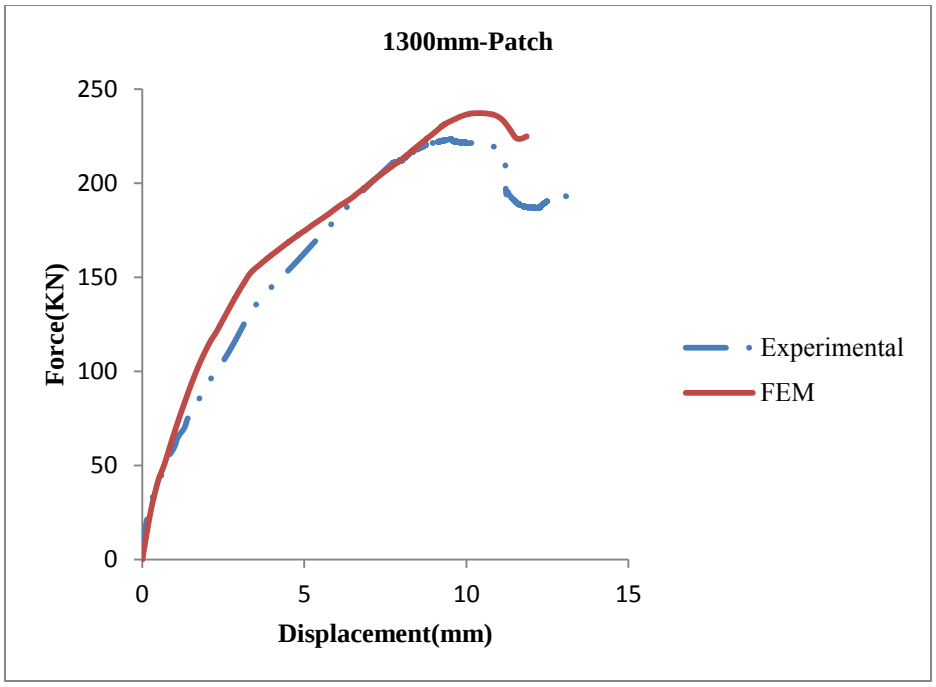

(d)

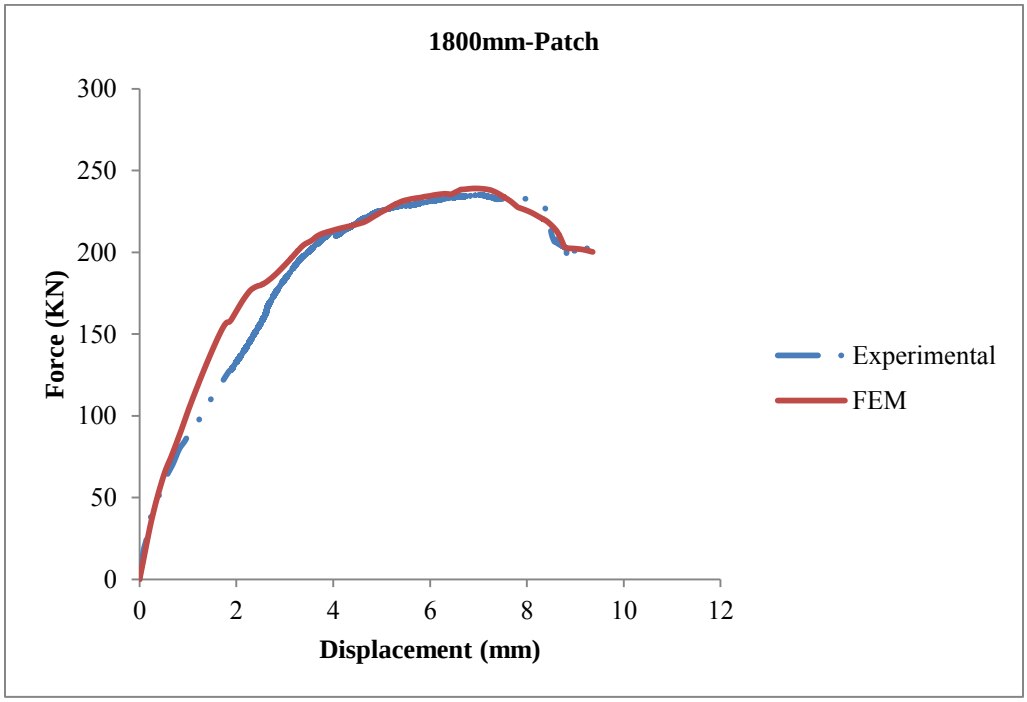

(e)

Figure 5.22: Load deflection curves Experimental vs FEM.

This clearly shows that concrete damaged plasticity model in Abaqus is able to model the overall behavior of reinforced concrete beams patch repaired and strengthened with FRP materials bonded at their interface. However, some differences were identified between experimental and finite elements based analysis.

Those differences were due to the assumptions made in the finite element formulation and the fact that beams were not anchored as in experiment. In addition, as reported by Chaudhari and Cakrabarti (2012), concrete damaged plasticity overestimates the stresses in concrete and this could also be a reason of discrepancies.

5.7.3. Crack distribution and failure mechanisms.

Laboratory investigation was conducted on the same beams. However, FRP strengthened specimens in the lab were anchored with FRP sheets, otherwise other characteristics in terms of materials and geometry were the same as those considered in finite element analysis. Comparison of crack pattern for control beam is shown in figure 5.21 and 5.22.

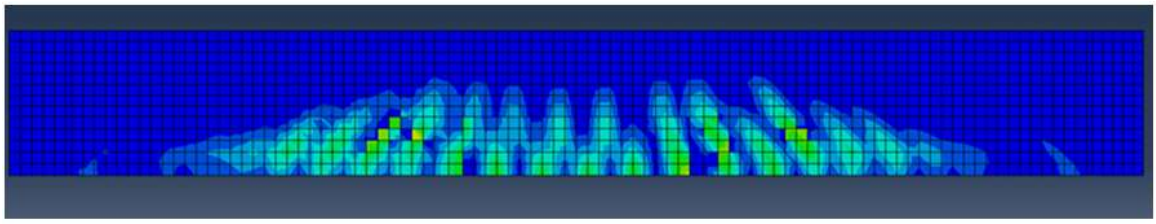

Figure 5.23: Crack pattern for control beam: FE Analysis.

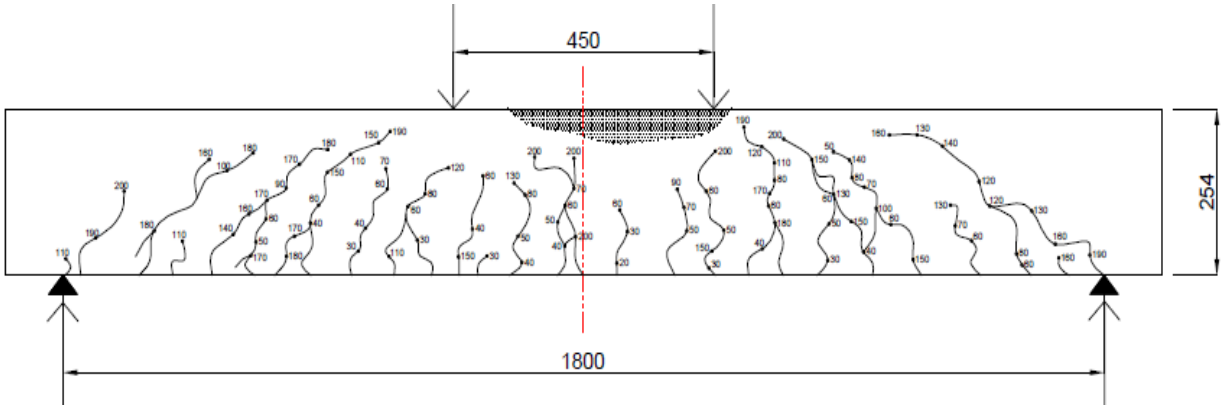

Figure 5.24: Crack pattern for control beam: Experiments.

Even though concrete damaged plasticity model did not capture all the cracks observed in the experiments, figure 5.21 and 5.22 show that the general pattern of crack in both finite elements

analysis and experiments is the same. It is clear that flexural cracks are vertical and flexural/shear cracks are inclined towards loading points. Such differences are due to non-homogeneous distribution of aggregates in concrete that causes cracks such as the one shown in figure 5.23 that could not be captured in numerical analysis. However, these facts do not prevent numerical analysis to be a powerful and reliable tool of analysis as illustrated by the comparison of crack pattern and other aspects between numerical and experimental investigations.

Figure 5.25: Expected crack path in concrete (Baldvin, 2011)

Furthermore, there are such cracks due to shrinkage, concrete settlement or poor placement of concrete. In addition, from experiments cracking load recorded was 30KN which is close to FE prediction where for control beam the cracking load was approximately 27.79KN. This shows that even if concrete damaged plasticity model does not have direct option to consider the transition interface zone and other microstructure properties of concrete, it captures in an excellent manner the overall behavior of reinforced concrete.

As shown in figure 5.20, the failure mode is crushing of concrete following yielding of tensile steel. For the case of CFRP-strengthened reinforced concrete beams, figure 5.24 and 5.25 compares finite element and experiments on beam with 1300mm-Patch repair. From the figures below, it was clear from comparison that the location of critical cracks from FEA where debonding took place was corresponding to experimental observations.

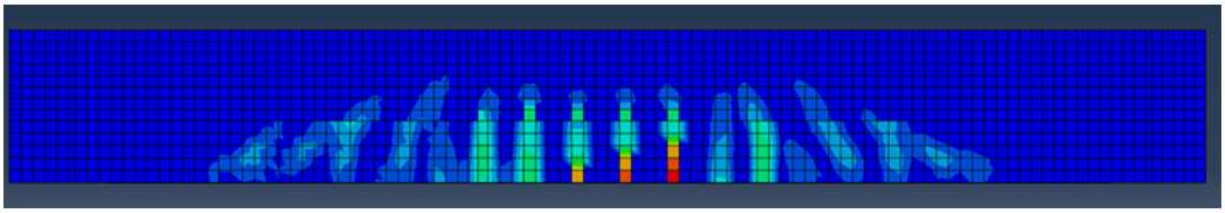

Figure 5.26: Structural crack pattern for 1300mm-Patched beam: FE

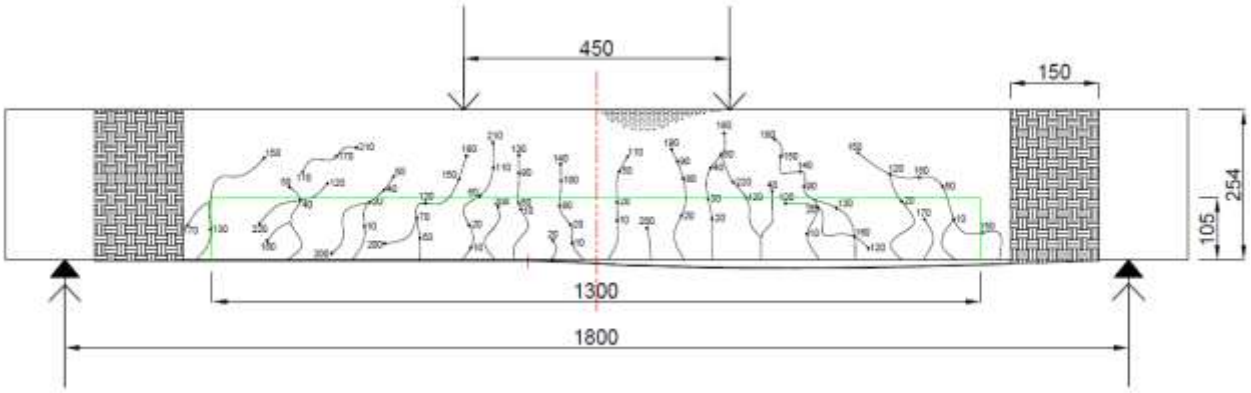

Figure 5.27: Structural rack pattern for 1300mm-Patched beam: Experiments.

From experimental observations, cracking initiated at a load of 10KN but this may be thought as a shrinkage or settlement crack that was widening and not structural cracks. It is also observed that some other cracks initiated at a load of 20KN.

This was in close agreement with finite element predictions where the cracking load for this type of beam was 21.65KN. The failure mode observed from experiments was an intermediate crack induced debonding; where the failure propagated horizontally towards the plate end as seen in figure above. This is in agreement with the failure mode reported from finite element analysis reported in figure 5.21.

Furthermore, the similarity between finite elements method predictions and experimental findings could be traced based on the location of critical cracks. From experimental point of view, crushing of concrete in compression occurred on the right side of the mid axis and debonding took place from this critical cracks. This is in good agreement with the failure mode of the same beam (1300mm-patch repaired and FRP strengthened beam) reported in figure 5.21. This once again shows the integrity of the proposed model to study the behavior of reinforced concrete beams patch repaired and strengthened with FRP laminate.

From the above discussion, a comparison of cracking pattern between finite elements prediction and experimental observations was also done for the remaining of the RC beams patch repaired and strengthened with CFRP plates. This comparison is shown in figures below:

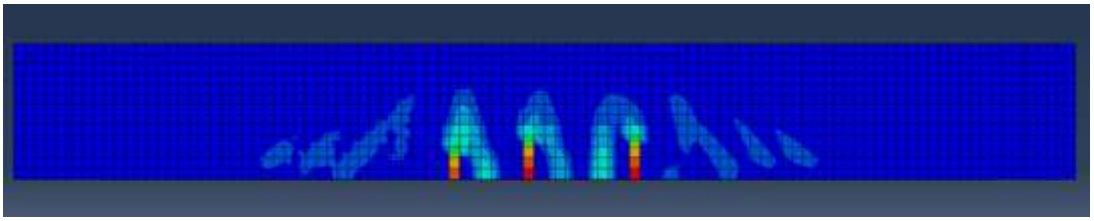

Figure 5.28: Structural crack pattern for 450mm-Patched beam: FE

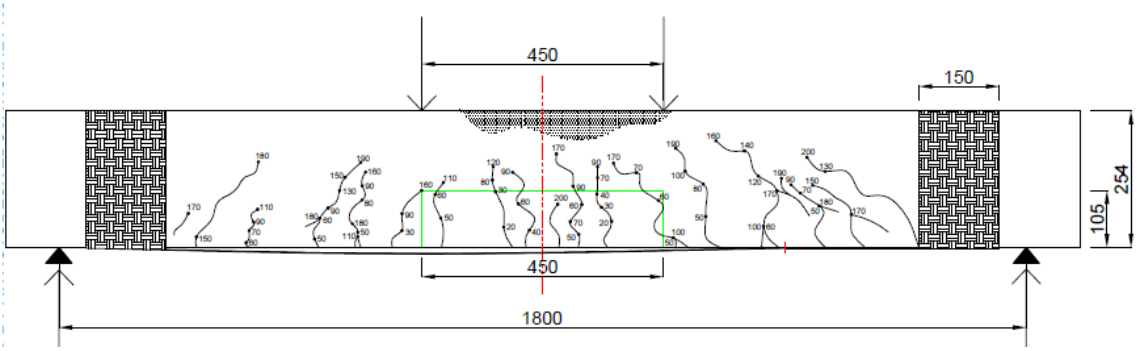

Figure 5.29: Structural rack pattern for 450mm-Patched beam: Experiments.

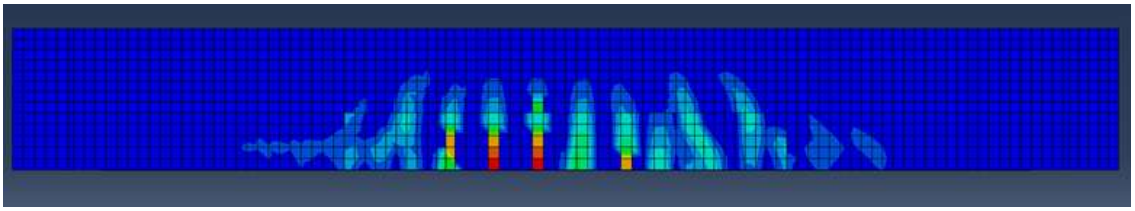

Figure 5.30: Structural crack pattern for 800mm-Patched beam: FE

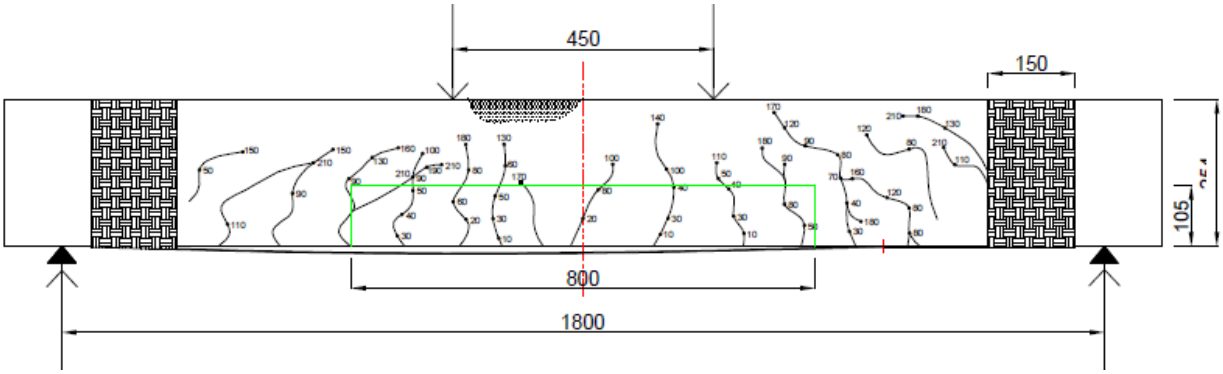

Figure 5.31: Structural rack pattern for 800mm-Patched beam: Experiments.

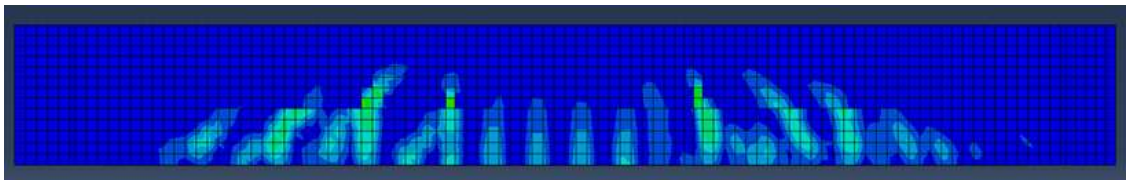

Figure 5.32: Structural crack pattern for 1800mm-Patched beam: FE

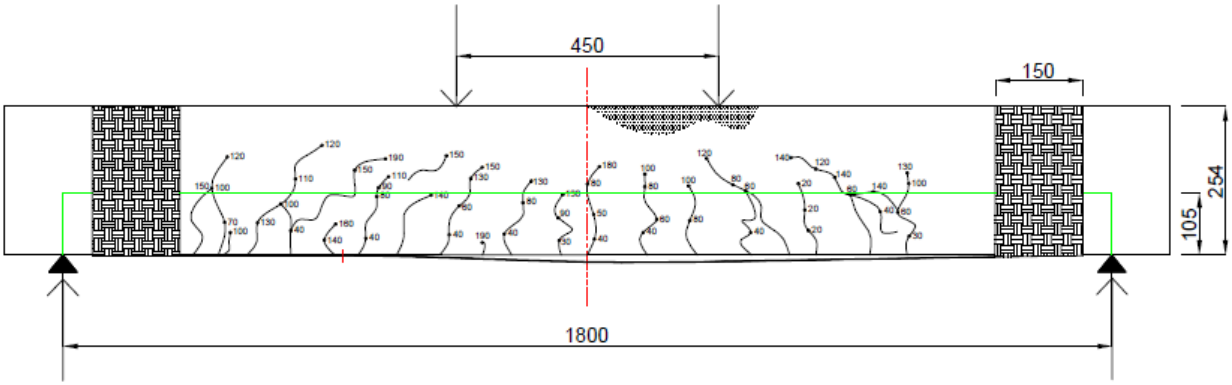

Figure 5.33: Structural rack pattern for 1800mm-Patched beam: Experiments.

5.7.4. Yield and debonding loads

For the purpose of validating the finite elements models developed in this study, a comparison of the yielding and debonding loads predicted by the models and those observed from experiments was done. The results of the comparison are presented in table 5.5. and 5.6. In the experiments, three beams were tested for each set. So the average and the error were calculated.

Table 5.5: Comparison between yielding loads.

RC beam type	FEM	Experiments
Control beam	170KN	171.2±11KN
450mm-Patched beam	160KN	190±10.7KN
800mm-Patched beam	160KN	199.5±12KN
1300mm-Patched beam	155KN	182.3±13.6KN
1800mm-Patched beam	155KN	204±14KN

Results show that the reduction in steel cross section due to corrosion resulted, in general in the reduction of the yielding load. However, in terms of overall load carrying capacity, the lost strength of steel is recovered from patch repair. That may be the reason of slight increase of ultimate loads.

Comparison between numerical findings and lower bound of experimental values gives the percentage difference as 5.7% for control beam, 10.7% for 450mm-Patch repaired beam, 14.7% for 800mm-Patch repaired beam, 8.1% for 1300mm-Patch repaired beam and 10.5 for 1800mm-Patch repaired beam.

Table 5.6: Comparison between debonding loads.

RC beam type	FEM	Experiments
450mm-Patched beam	226.2KN	205±9.7KN
800mm-Patched beam	236.8KN	212.8±12.6KN
1300mm-Patched beam	237.3KN	193.8±17.7KN
1800mm-Patched beam	240.5KN	210.5±11.3KN

The percentage differences from upper bound experimental values are 5.1% for 450mm-Patch repaired beam, 4.8% for 800mm-Patch repaired beam, 10.8% for 13000mm-Patch repaired beam and 7.7% for 1800mm-Patch repaired beam. This shows that the numerical results are within experimental ranges.

Finally, a comparison between cracking loads was also made. Cracking loads were found from crack mapping provided by the experimental observations.

It was assumed that cracks that appeared at a load of 10KN were not structural cracks. Results of the comparison are shown in table 5.7 below:

Table 5.7: Comparison of cracking loads

RC beam type	FEM	Experiments	Percentage difference
Control beam	27.79KN	30KN	7.4
450mm-Patched beam	25.58KN	20KN	21.8
800mm-Patched beam	24.63KN	20KN	18.8
1300mm-Patched beam	21.65KN	20KN	7.6
1800mm-Patched beam	21.57KN	20KN	7.3

5.8. Summary

This chapter presented the results of numerical investigations carried out on one control reinforced concrete beam and four reinforced concrete beams patch-repaired and strengthened with FRP laminates bonded to their tension face using adhesive epoxy.

The results were presented in terms of concrete cracking, strain distribution in the FRP, damage energy release rate and modes of failure. Force control was used for proper presentation of cracking while displacement control was used to capture the failure characteristics of RC beams. Cracking results showed that concrete damaged plasticity model used in this study is able to capture the behavior of reinforced concrete beams, even in the presence of patch material and in the absence of precracking.

However, patch material was found to change the crack pattern as compared to control beam and to delay crack initiation. The cracking loads from experimental and finite elements analyses were close to each other; for example for control beam the cracking load was 30KN from FEM and 28KN from experiments. Cracking pattern predicted by finite elements models matched the crack pattern from experimental results. In addition, the mode of failure was debonding of FRP induced by intermediate flexural crack. Again, the mode of failure was in good agreement with experimental findings.

Strain distribution in FRP; which mostly governs the debonding failure; was varying from minimum at the plate end and kept increasing up to the debonding strain of about 0.077 in or near the constant bending moment region. Its distribution was found to be affected by the length of the patch material. Debonding strain was matching with the ACI 440.2R-02 recommendation.

The load deflection captured the three key points. These are cracking of concrete, yielding of tension steel reinforcement and debonding. The curves from finite elements method were in close agreement with experimental results despite overestimates of debonding load from numerical results. Beam with the largest patched length showed a brittle failure. This could be seen from the damage energy release rate. Damage energy release rate was found to be a good way to represent accurately the cracking load although it also represents the other two characteristic points of the load displacement curves.

Chapter 6

CONCLUSIONS AND RECOMMENDATIONS

6.1. Summary and conclusions

Reinforced concrete beams are structural elements found in a number of structures such as tall buildings, bridges, stadiums, etc. During their service life, reinforced concrete beams may become deficient due to a number of reasons including damage due to steel reinforcement corrosion, poor design and detailing poor workmanship, fire, accidents in case of bridges and earthquake.

To keep serviceable the structure whose structural components such as reinforced concrete beams are damaged, the first option that is widely adopted is to repair and depending on the severity of the damage to strengthen them through bonding external reinforcements. Repair consists of partly removing the damaged concrete, prepare the substrate and apply a repair material that may be concrete or repair mortar in an effort of restoring serviceability and durability. On the other hand strengthening consists of improving the load carrying capacity by introducing additional members or materials. Structural strengthening may also be done when there is a need to change the function of an existing structure which has not shown any sign of damage. This is known as structural retrofitting.

Even though structural repair and strengthening is the most economical solution to improve the serviceability and load carrying capacity of deficient reinforced concrete beams, its effectiveness often becomes compromised. Reasons range from poor workmanship to structural performance. Structural performance being mainly governed by bond mechanisms. The critical issue in repaired and strengthened reinforced concrete beams is related to structural performance where the structure undergoes premature failure of debonding between the strengthening material and the RC beam. This has been an issue over the last years and up to now; it is still attracting the attention of a number of researchers worldwide. Despite the fact that intensive work has been done so far and good results were obtained based on experimental, analytical and numerical approaches, less attention was given to the repair material particularly in numerical investigations.

The main objective of this thesis was to investigate numerically the behavior of reinforced concrete beams patch repaired and strengthened with fiber reinforced polymer (FRP) bonded to their tension face by varying the length of the repair material.

A number of five reinforced concrete beams of *2000*155*254mm* each were analyzed using a finite elements software ABAQUS. The set of beams consisted of control beam (not damaged, hence not repaired and not strengthened) and beams with 450, 800, 1300 and 1800mm patch lengths. Since the beams were not preloaded, the damage modeled was corrosion corresponding to 10% reduction in tensile reinforcement cross section. Cross section was reduced over the length of repair material for respective patch repaired RC beams.

Successful modeling of reinforced concrete beams in finite element software requires the user to provide sound constitutive models to represent the response of various materials when they are subjected to loading. Adequate material constitutive models were used to capture the behavior of concrete and repair in tension and in compression, reinforcing steel, epoxy or interface and FRP material. Concrete used was having a compressive strength of 50MPa while the repair material was having a compressive strength of 70MPa.

Different parts making up the whole system were created in Abaqus/Standard and assembled together. They were assigned material properties that were determined using the material constitutive relations. Interaction between materials, boundary conditions and analysis types were specified and in addition, data outputs of interest were requested. The complete reinforced concrete beam was then discretized into a number of finite elements connected by nodes and solutions for nodal displacement fields were obtained. From nodal outputs other physical quantities such as stresses and strains could also be determined.

Results from the finite elements modeling showed that:

- The adopted material constitutive models, i.e. a concrete damaged plasticity model for both concrete and repair material; a linear elastic perfectly plastic model for steel; a linear elastic model for FRP material and a cohesive model for adhesive are all able to capture accurately the mechanical behavior of the respective materials.

- Cracking of both concrete and repair material initiated at loads close to those observed in the experiments on the same specimens. The difference in percentage of cracking loads between numerical and experimental findings were 7.4%, 21.8%, 18.8%, 7.6% and 7.3% for control beam, 450mm, 800mm, 1300mm and 1800mm-Patched RC beams, respectively. Finite elements models predicted accurately the major crack pattern. (See section 5.1). Cracking loads were accurately measured from the damage energy release rate as that load at which the structural element starts to release the energy.

- Keeping in mind that the strain at yielding of steel is 0.002, yield loads predicted by FEM were in close agreement with those predicted by experimental observation. The comparison showed the following percentage differences for control beam, 450mm, 800mm, 1300mm and 1800mm-Pateched RC beams: 6.5%; 8.4%; 10.3%; 7.5% and 7.2%, respectively.

- Debonding failure was intermediate flexural crack induced followed by concrete crushing in compression. Therefore, all beams failed in a ductile manner thus, meeting the design requirements. See section 5.6.

- Strain distribution in FRP was in good agreement with ACI 440.2R-02 recommendation in regard of debonding strain.

- Force control was used for better representation of crack pattern and displacement control was used capturing failure mechanisms.

- The effect of plate end anchorage is less significant when sufficient shear reinforcements are provided.

6.2. Recommendations

The present study focused on developing a finite element model to investigate the effects of patch repair on the cracking behavior and failure mechanisms of corroded beams patch repaired and strengthened with CFRP composites. Structural repair and strengthening is gaining extensive applications around the world. For the development of some recommendations about repair and strengthening, it is necessary to carry out further numerical and experimental investigations for complete understanding of structural RC elements patch repaired and strengthened with FRP

materials. This section highlights some issues that future research should address for the development of structural strengthening design guidelines.

Based on findings, discussions and conclusions, the following recommendations are made:

- Future researches should address the analytical studies based on the stress analysis and nonlinear material behavior for RC beams patch repaired and strengthened with FRP composites. These studies in addition to finite elements predictions and experimental observations will help in the development of accurate design guidelines.

- Efforts should be made so that finite elements models simulate the practical situations of damaged RC beams, i.e. in service and the fact that stirrups are also corroded. The variation of damaged area in depth should also be considered in future numerical simulations.

- From the results of this study, cracking loads were accurately measured from energy. Future researches should put much effort in the energy approaches to gain better understanding of the behavior of RC beams patch repaired and strengthened with FRP composites.

- For those who will be interested in crack pattern for RC beams, force control is the best choice while displacement control is suited for failure mechanisms capturing since it also considers the descending part of the force relations. In addition, concrete smeared cracking model should be applied to RC beams patch repaired and strengthened with FRP materials and compared with concrete damaged plasticity model in Abaqus. Both models should be compared with experimental findings to assess their effectiveness.

- The bond behavior between both concrete and repair material and both longitudinal and transversal steel should be modeled accurately instead of assuming a perfect bond as done in the present study.

- In addition, much effort should be dedicated to the investigation of the behavior of interface between both concrete and repair material with FRP material. This was found to be highly affected by the patch length.

- Future numerical research should also address the perfect way of determining steel reinforcement yielding load.
- There was a good agreement between numerical results and ACI recommendation about strain distribution in FRP. From this agreement, it is recommended that the ACI provision may undoubtedly be used in practical design of FRP strengthening systems.
- For reinforced concrete beams suffering local corrosion, it is recommended that repair material with relatively higher strength than the parent concrete and higher bond strength be used. This will ensure that the behavior of the resulting system is close to that of undamaged RC beam.

References

Achintha, M. & Burgoyne, C.J. 2008. Fracture mechanics of plate debonding. *Journal of Composites for Construction*. 12(4):396-404.

Achintha, M. & Burgoyne, C.J. 2012. Prediction of FRP debonding using the global energy balance approach. *Magazine of Concrete Research*. 64(11):1033-1044.

American Concrete Institute. Guide for the design and construction of externally bonded FRP systems for strengthening concrete structures. *ACI 440.02R, Detroit*.

Arya, C. & Farmer, N. 2001. Design guidelines for flexural strengthening of concrete members using FRP composites. *Proc., 5th Int. Symp. on Fiber Reinforced Concrete Structures*, Cambridge :167-176.

Asferg, J.L.2006. Modeling of concrete fracture applying the extended finite element method. PhD Thesis. Technical University of Danemark.

Au, C. & Buyukozturk, O. 2006. Debonding of FRP plated concrete: A tri-layer fracture treatment. *Engineering Fracture Mechanics*. 73(3):348-365.

Babu, R.R., Benipal, G.S. & Singh, A.K.2005. Constitutive modeling of concrete: An overview. *Asian Journal of Civil Engineering (Building and Housing).* 6(4):211-246.

Baldvin, J. 2011. Numerical analysis of a reinforced concrete beam in Abaqus 6.10. Master's Thesis. Aalborg University.

Belytischko, T. & Black, T. 1999. Elastic crack growth in finite elements with minimal remeshing. *International Journal for Numerical Methods in Engineering.* 45: 601-620.

Broomfield, J.P.2003. *Corrosion of steel in concrete: understanding, investigating and repair.* Taylor & Francis e-library.

Buyukozturk, O. 1976. Nonlinear analysis of reinforced concrete structures. *Journal of Composites and Structures.* 7: 149-156.

Buyukozturk, O., Gunes,O. & Karaca, E.2004. Progress on understanding debonding problems in reinforced concrete and steel members strengthened using FRP composites. *Journal of Construction and Building materials.* 18: 9-19.

Buyukozturk, O. & Yang Yu, T. 2006. Understanding and assessment of debonding failures in FRP-concrete systems. *Seventh International Congress on Advances in Civil Engineering, October 11-13, 2006, Yildiz Technical University, Istanbul, Turkey.*

Camata, G., Spacone,E. & Zarnic, R. 2007.Experimental and nonlinear finite element studies of RC beams strengthened with FRP plates. *Journal of Composites: Part B.* 38: 277-288.

Casas, J. & Pascual, J. 2007. Debonding of FRP in bending: Simplified model and experimental validation. *Construction and Building Materials*. 21(10):1940-1949.

Carreira, D.J & Chu-Kuang-Han, 1986. Stress-strain relationship for reinforced concrete in tension. *ACI Journal.* 84: 21-28.

Cement and Concrete Institute (C&CI). 2010. Repair of the surface of concrete: Casting defects and minor damage.

Cervera, M. & Chiumenti, M. 2006. Smeared crack approach: back to the original track. *International Journal for Numerical and Analytical Methods in Geomechanics.* 30: 1173-1199.

Chhabra, Y. 2013.Bridge Rehabilitation Techniques. *The DS Brown Company, Singapore.*

Chen, G.M., Teng, J.G., Chen, J.F & Rosenboom, O.A. 2008. Finite element model for intermediate crack debonding in RC beams strengthened with externally bonded FRP reinforcement. *Proceedings of the fourth International Conference on FRP Composites in Civil Engineering.* 22-24 July 2008, Zurich, Switzerland.

Chen, G.M., Teng, J.G. & Chen, J.F. 2011. Finite-element modeling of intermediate crack debonding in FRP-plated RC beams. *Journal of Composites for Construction*. 15(3):339-353.

Chen, W.F. 1982. Plasticity in Reinforced concrete. New York (NY): MC Graw-Hill Book Company.

Chaudhari, S.V & Chakrabarti, M.A. 2012. Modeling of concrete for nonlinear analysis using finite element code ABAQUS. *International Journal of Computer Applications*. 44 (7): 14-18.

Colotti , V., Spadea, G. & Swamy , R.,Narayan. 2004. Structural model to predict the failure behavior of plated reinforced concrete beams. *Journal of Composites Constructions*. 8(2):104-122.

Cornado, C.A. & Lopez, M.M. 2010. Numerical Modeling of Concrete-FRP Debonding Using a Crack Band Approach. *Journal of Composites for Construction*. 14(1):11-21.

Dassault Système Simulia Corp., 2010. *Abaqus/CAE User's Manual.* Providence: Dassault Système.

Daudeville, L., Allix, O. & Ladeveze, P. 1995. Delamination analysis by damage mechanics: Some applications. *Journal of Engineering Composites.* 5(1): 17-24.

Dirk Arend, H.1991. Local approach to fatigue of concrete. PhD Thesis. Technische Universiteit Delfit

Esna Ashari, S. & Mohammadi, S. 2011. Fracture analysis of FRP-reinforced beams by orthotropic XFEM. *Journal of Composite Materials*. 46(11):1367-1389.

Eurocode 2. 2004. Design of concrete structures. Part 1-1: General rules and rules for buildings.

Feenstra, P.H. & Borst, R. 1995. Constitutive model for reinforced concrete. *Journal of Engineering Mechanics.* 12 (5): 587-595.

Gao, B., Leung, K.Y.C. & Kim, J.K. 2005. Prediction of concrete cover separation failure for RC beams strengthened with CFRP strips. *Journal of Engineering Structures.* 27: 177-189.

Grassl, G. & Jirasek, M. 2006. Damage-plastic model for concrete failure. *International Journal of Solids and Structures.* 43: 7166-7196.

Gunes, O. 2004. A fracture based approach to understanding debonding in FRP bonded structural members. Ph.D dissertation, Department of Civil and Environmental Engineering, Massachussets Institute of Technology, Cambridge, Massacussets.

Gunes,O., Buyukozturk, O. & Karaca, E. 2009. A fracture-based model for FRP debonding in strengthened beams. *Journal of Engineering Fracture Mechanics.* 76: 1897-1909.

Hearing, B.P. 2000. Delamination in Reinforced Concrete Retrofitted with Fiber Reinforced Plastics. Ph.D disseltation, Department of Civil and Environmental Engineering, MassachussetsInstitute of Technology, Cambridge, Massachussets.

Hillerborg, A., Modéer, M. & Petersson, P-E. 1976. Analysis of crack formation and crack growth in concrete by means of fracture mechanics and finite elements. *Journal of Cement and Concrete Research.* 6: 773-782.

Hsu, T.C. & Wang, T. 2001. Nonlinear finite element analysis of concrete structures using new constitutive models. *Journal of Computers and Structures.* 79: 2871-2791.

Imran, I. & Pantazopoulou, S.J. 2001. Plasticity model for concrete under triaxial compression. *Journal of Engineering Mechanics.* 127(3): 281-290.

Jansze , W. 1997. Strengthening of RC Members in Bending by Externally Bonded Steel Plates. PhD Thesis. Delft University of Technology.

Jason, L., Huerta, A., Pijaudier, G.C. & Ghavamian, S. 2012. An elastic plastic damage formulation for concrete: application to elementary and structural tests. *Journal of Computer Methods in Applied Mechanics and Engineering.*

Joannes, S. & Renard, J. 2009. Abaqus user element for an accurate modeling of adhesive joints on coarse meshes. *SIMULIA Customer Conference.*

Jumaat, M.Z., Kabir, M.H. & Obaydullah, M. 2006. A review of the repair of reinforced concrete beams. *Journal of Applied Science Research.* 2 (6) : 317-326.

Kmiecik, P., & Kaminski, M. 2001. Modeling of reinforced concrete structures and composite structures with concrete strength degradation taken into consideration. *Journal of Archives of Civil and Mechanical Engineering.* 11 (3) : 623-636.

Kwak, H-G & Filippou, F.C. 1990. Finite element analysis of reinforced concrete structures under monotonic loads. (Report N^0 UCB/SEMM-90/14). *University of Calfornia: Structural Engineering, Mechanics and Materials.*

Lee, H.K., & Hausman, L.R. 2004. Structural repair and strengthening of damaged RC beams with sprayed FRP. *Journal of Composite Structures.* 63: 201-209.

Lee, J. & Fenves, G.L. 1998. Plastic-damage model for cyclic loading of concrete structures. *Journal of Engineering Mechanics.* 124 (8): 892-900.

Lu, X.Z. and others. 2005. Bond-slip models for FRP sheets/plates bonded to concrete. *Engineering Structures*. 27(6):920-937.

Lu, X.Z., Teng, J.G., Ye, L.P. & Jiang, J.J.2005. Intermediate crack debonding in FRP-strengthened RC beams: FE analysis and strength model. *Journal of Composites for Construction.* 11 (2): 161-174.

Lubliner, J., Oliver, J., Oller, S. & Onate, E. 1989. A plastic damage model for concrete. *International Journal of Solids and Structures.* 25(3): 299-326.

Luccioni, B., Oller, S. & Danesi, R. 1996. Coupled plastic-damage model. *Journal of Computer Methods in Applied Mechanics and Engineering.* 129: 81-89.

Malek, A.M., Saadatmanesh, H. & Mohammad, R.E. 1998. Prediction of Fialure Load of R/C Beams Strengthened with FRP Plate Due to Stress Concentration at the Plate End. *ACI Structural Journal*. 95(1):142-152.

Malumbela, G. 2010. Measurable parameters for performance of corroded and repaired RC beams under load. PhD Thesis. University of Cape Town.

Mattys, S. 2000. Structural behavior and design of concrete members strengthened with externally bonded FRP reinforcement. PhD Thesis. Ghent University.

Mazars, J. & Pijaudier-Cabot, G. 1989. Continuum damage theory-Application to concrete. *Journal of Engineering Mechanics.* 115 (2): 345-365.

Mojabeng, T. 2010. Effect of structural repair and strengthening on stiffness and ultimate capacity of corrosion damaged RC beams. Master's Thesis. University of Cape Town.

Motavalli, M. & Czaderski, C. 2007. FRP Composites for retrofitting of existing civil structures in Europe: State-of-the-art review. *American Composites Manufacturers Association,* October 17-19, Tampa, FL USA.

Niu, H. & Wu, Z. 2005. Numerical analysis of debonding mechanisms in FRP- strengthened RC beams. *Journal of Computer-Aided Civil and Infrastructure Engineering.* 20: 354-368.

Niu, H. & Wu, Z. 2007. Analytical modeling on debonding failure of FRP-strengthened RC flexural structures. *Ibaraki University, Japan.*

Nounu, G. & Chaudhary Z-UL-H. 1999. Reinforced concrete repairs in beams. *Journal of Construction and Building Materials.* 13: 195-212.

Obaidat, Y.T., Heyden, S. & Dahlblom, O. 2010. The effect of CFRP and CFRP/concrete interface models when modeling retrofitted RC beams with FEM. *Journal of Composites Structures.* 92: 1391-1398.

Omidi, O. & Lofti, V. 2012. Continuum large cracking in a rate-dependent plastic-damage model for cyclic-loaded concrete structures. *International Journal of Numerical and Analytical Methods in Geomechanics.* 37: 1363-1390.

Rabinovitch, O. 2008. Cohesive Interface Modeling of Debonding Failure in FRP Strengthened Beams. *Journal of Engineering mechanics*. 134(7):578-588.

Rabinovitch, O. & Frostig, Y. 2001. Delamination Failure of RC Beams Strengthened with FRP Strips-A Closed -Form -High Order and Fracture Mechanics Approach. *Journal of Engineering Mechanics*. 127(8):852-861.

Rahman, M.K., Baluch, M.H. & Al-Gadrinkagehib, A.H. 2000. Simulation of shrinkage distress and creep relief in concrete repair. *Journal of Composites: Part B.* 31: 541-553.

Rami, A.H., Mahannad, Z.N. & Jamal, A.A. 2013. Finite element simulation of reinforced concrete beams externally strengthened with short-length CFRP plates. *Journal of Composites: Part B.* 45: 1722-1730.

Rio, O., Andrade, C., Izquierdo, D. & Alonso, C. 2005. Behavior of Patch-repaired concrete structural elements under increasing static loads to flexural failure. *Journal of Materials in Civil Engineering.* 17(2): 168-177.

Roberts, T.M. 1990. Analysis of stress concentrations in the adhesive layer of plated concrete beams. *International Seminar on Structural Repairs/Strengthening by the Plate Bonding Technique, University of Sheffield*.

Roylance, D. 2000. Introduction to composite materials. Massachusetts Institute of Technology.

Saenz, L.P.1964."Discussion of equation for stress-strain curve of concrete " by P. Desayi and S. Krishan. *ACI Journal.* 61(9): 1229-1235.

Salari, M.R., Saeb, S., Patchet, S.J. & Carrasco, R.C. 2004. A coupled elastoplastic damage model for geomaterials. *Journal of Computer Methods in Applied Mechanics and Engineering.* 193 (27-29):2625-2643.

Shastri, A.S. 2010. Computational modeling of conventionally reinforced concrete coupling beams. Master's thesis. Texas A & M University.

Simonelli, G. 2005. Finite element analysis of RC beams retrofitted with fibre reinforced polymers. PhD Thesis. Università degli Studi di Napoli Federico II, London.

Smith, S.T. & Teng, J.G. 2001. Interfacial stresses in plated beams. [*Engineering Structures*]. 23(7):857-877.

Smith, S.T. & Teng, J.G. 2002. FRP-strengthened RC beams. I: review of debonding strength models. *Engineering Structure*]. 24(4):385-395.

Supaviriyakit, T. Pornpongsaro, P. & Pimanmas, A. 2004. Finite element analysis of FRP-strengthened RC beams. *Songklanakarin J. Sci. Technol.* 26 (4): 497-507.

Thabiso, D. 2013. The behavior of patch repaired and strengthened beams: An experimental investigation. Master's Thesis. University of Cape Town.

Teng, J.G., Zhang, J.W. & Smith, S.T. 2002. Interfacial stresses in reinforced concrete beams bonded with a soffit plate: A finite element study. *Construction and Building Materials*. 16(1):1-14.

Teng, J.G., Smith, S.T., Yao, J. & Chen, J.F. 2003. Intermediate crack induced debonding in RC beams and slabs. *Journal of Construction and Building Materials.* 17 (6-7): 447-462.

Teng, J.G. & Chen, J.F. 2009. Mechanics of debonding in FRP-plated RC beams. *Proceedings of the Institution of Civil Engineers, Structures and Buildings*. 162(SB5):335-345.

Teng, J. & Yao, J. 2007a. Plate end debonding in FRP-plated RC beams I: experiments. *Engineering Structures*. 29(10):2457-2471.

Tiiljsten, B. 1996. Strengthening of concrete prisms using the plate-bonding technique. *International Journal of Fracture*. 82:253-266.

United States of America, Department of defense, Guide to concrete repair, 2001. Unified facilities criteria (UFC): Concrete crack and partial depth spall repair.

Vaysburd, A.M. 2006. Holstic system approach to design and implementation of concrete repair. *Journal of Cement and Concrete Composites.* 28: 671-678.

Varastehpour , H. & Hamelin , P. 1997. Strengthening of concrete beams using fiber-reinforced plastics. *Materials and Structures/Materiaux et Constructions*. 30(197):160-166.

Wang , C. & Ling, F. 1998. Prediction model for the debonding failure of cracked RC beams with externally bonded FRP sheets. *Proceedings of the Second International Conference of Composites in Infrastructure (ICCI), Arizona, USA*. :548-562.

Wu, Z. & Niu, H. 2007. Prediction of crack-induced debonding failure in R/C structures flexurally strengthened with externally bonded FRP composites. 63(4):620-639.

Yang, Z.J., Chen, J.F. & Proverbs, D. 2003. Finite element modelling of concrete cover separation failure in FRP plated RC beams. *Construction and Building Materials*. 17(1):3-13.

Yang, Q.S., Peng, X.R. & Kwan, A.K.H. 2004. Finite element analysis of interfacial stresses in FRP-RC hybrid beams. *Journal of Mechanics Research Communications.* 31: 331-340.

Yao, J. 2004. Debonding failures in RC beams and slabs strengthened with FRP plates. PhD Thesis. The Hong Kong Polytechnic University.

Yu, T., Teng, J.G.,Wong, Y.L. & Dong, S.L. 2010. Finite element modeling of confined concrete-II: Plastic-damage model. *Journal of Engineering Structures.* 32: 680-691.

Yu, T., Teng, J.G.,Wong, Y.L. & Dong, S.L. 2010. Finite element modeling of confined concrete-I: Drucker-Prager type plasticity model. *Journal of Engineering Structures.* 32: 665-679.

Zhang, S., Raoof, M. & Wood, L. 1995. Prediction of peeling failure of reinforced concrete beams with externally bonded steel plates. *Structures and Buildings*. 110(3):257-268.

Zhang, L. & Teng, J.G. 2010. Finite element prediction of interfacial stresses in structural members bonded with a thin plate. *Engineering Structures*. 32(2):459-471.

Ziraba, Y. 1995. Combined experimental–numerical approach to characterization of steel–glue–concrete interface. *Materiaux et constructions*. 28(9):518-525.

http://www.theconcreteportal.com/conc_funda.html. Concrete fundamentals.

Appendices

Appendix A: Sample of Damage Energy release rate (Energy vs Load)

	Control beam
Energy (KN/mm)	Load (KN)
0	0
0.00891442	27.79465714
0.28091684	48.20283243
0.449598846	54.55859976
0.824524963	62.26336273

	450mm-Patch
Energy(KN/mm)	Load (KN)
0	0
0	7.432631836
0	14.86526367
0.019055588	25.58917969
0.032718231	28.09073047

	800mm-Patch
Energy (KN/mm)	Load (KN)
0	0
0	7.15851123
0	14.31702246
0.018847837	24.63397461
0.034657513	26.99041406

	1300mm-Patch
Energy (KN/mm)	Load (KN)
0	0
0	7.430692749
0	14.8613855
0	17.64789551
0.008303753	21.65239014
0.053842915	27.06506287

	1800mm-Patch
Energy (KN/mm)	Load (KN)
0	0
0	9.109541345
0	18.21908269
0.002796356	21.57335452
0.025237705	26.22960504